THE UNIVERSITY OF CHICAGO

EXPLOITING TUMOR-INTRINSIC CUES TO ENGINEER INTERLEUKIN-12 FOR CANCER IMMUNOTHERAPY

A DISSERTATION SUBMITTED TO

THE FACULTY OF THE PRITZKER SCHOOL OF MOLECULAR ENGINEERING

IN CANDIDACY FOR THE DEGREE OF

DOCTOR OF PHILOSOPHY

BY

ASLAN MANSUROV

CHICAGO, ILLINOIS

AUGUST 2021

I dedicate this thesis to my parents, Şahin Mansurov and Leyla Mansurova, whose love and support helped me throughout the 8 year academic journey. I cannot imagine how difficult it was to send a 17-year-old boy to U.S. and only being able to see him for a couple months a year. Thank you for being so brave and patient, and I hope this sacrifice was worth it.

“To strive, to seek, to find and not to yield” – From the poem Ulysses of Alfred, Lord Tennyson.

Table of Contents

LIST OF FIGURES

LIST OF TABLES

ACKNOWLEDGMENTS

During my time as a PhD student, I have been extremely fortunate to have gained wonderful mentors, colleagues and friends. Without your support and guidance, this work would not have been possible.

First, I would like to thank my graduate advisor, Jeffrey Hubbell, who took the risk of accepting a student with no prior biology/bionengineering experience in his lab. During our first meeting in October of 2017, he showed me Jun and Ako's matrix-binding CPI paper (which was about to be published), and, to be honest, I understood absolutely nothing (scientifically) from that conversation. Because of my lack of training in biology, I was hoping to join the polymer synthesis side of the lab, but Jeff let me know that he would rather expand the cancer immunotherapy subgroup. This truly exemplifies Jeff as a person who is not afraid of big changes and taking bold steps, a trait that I always admired. Throughout his career, Jeff had tremendous impact on so many fields (hydrogel chemistry, biomaterials for tissue repair, immune tolerance, etc.), demonstrating his never-ending and infectious scientific curiosity. Thank you for believing in me and letting me develop as a bioengineer in your lab, and I hope the risk you took has payed off. It was an honor to be a part of your great team.

Second, I would like to thank "Team Japan", who taught me most of the techniques that I know. Kiyomitsu Katsumata, my first mentor, thank you for being so patient and showing me the simplest things: pipetting and making serial dilutions. Although Kiyo was very laconic, the phrase that stuck with me the most was "Early failure is important". This was one of the guiding principles throughout my PhD. Thank you to Jun and Ako, who had the most profound scientific impact on me. Jun taught me how to work efficiently and approach experiments thoroughly. Thank you for your trust and guidance, and allowing me to collaborate with you on so many projects. I will

cherish those memories forever and hope to catch up with you and your family sometime in London. I would also like to thank the other members of the team: Koichi Sasaki, Risako Miura and Eiji Yuba. Arigato Gozaymas!

I would like to thank the rest of the Hubbell lab, who were always willing to share their expertise and offer help. Thanks to Aaron Alpar, L. Taylor Gray, Elyse Watkins, Tiffany Marchell, Michal Raczy, Erica Budina, Abigail Lauterbach, John-Michael Williford, Suzana Gomes, Priscilla Briquez, Chitavi Maulloo, Rachel Wallace, Marcin Kwissa, Ruyi Wang, D. Scott Wilson, Michael White, Jenni Antane, Lisa Volpatti, Joe Reda, Shijie Cao and Nick Mitrousis.

I would also like to thank Prof. Melody Swartz and the members of her lab for creating such a collaborative environment between the two groups. Particularly, I would like to thank Peyman Hosseinchi, for being a great friend and collaborator. I will always remember fondly the times we played tennis, went out and ordered deep dish (with pineapple?) for late night sac days. At the time that this is being written, Peyman is back home after being away for more than 6 years, so I hope you are having a great time with your family and friends, you truly deserved this! Thanks to Lambert Potin and Lea Maillat, who were so supportive and helpful in my early days as a graduate student. Thanks to Shann Yu, who then transitioned into becoming the scientific director of CIIC and has helped us with several grant applications.

I would like to thank my thesis committee, Juan Mendoza and Nicolas Chevrier, who have been extremely insightful during our meetings. I am very grateful to Juan and his lab for collaborating with us on the masked IL-12 project. I would like to thank Mustafa Guler, whose classes I enjoyed and TA'ed.

Thanks to the University of Chicago staff, particularly Ani Solanki from the Animal Resources Center, who has done countless tail-vein injections and helped with all the *in vivo* work. I would also like to thank David Leclerc from the flow cytometry core, who take care of all the equipment and helped us with multiplex assays.

ABSTRACT

The overall goal of this thesis is to use recombinant engineering to improve the therapeutic index of cytokine immunotherapies. The model cytokine that we used was interleukin-12 (IL-12), which had displayed intolerable toxicity in clinical trials when administered in its native form.

Chapter 1 introduces the pathophysiological aspects of solid tumors, namely vascular remodeling, abnormal deposition of extracellular matrix and overexpression of proteases. We then discuss the role of the immune system in cancer progression and mention the key players of the immune system that either facilitate or impede tumor growth. We also provide a brief survey of various immunotherapy strategies that are currently employed in the clinic. Last, we introduce cytokines as potential immunotherapeutics, predominantly focusing on IL-12.

Chapter 2 describes the collagen-targeting technology that we applied to IL-12. Because collagen is overexpressed in solid tumors and is abberantly exposed to the bloodstream, we decided to engineer a fusion protein consisting of a collagen-binding domain (CBD) and IL-12 to target the tumor matrix. We confirmed that CBD-IL-12 fusion protein was bioactive *in vitro* and displayed high affinity to collagen. We showed that CBD-IL-12 exerted superior antitumor efficacy compared to unmodified IL-12 in various solid tumor models. We also demonstrated that CBD-IL-12 induces less systemic side effects in tumor-bearing and healthy mice. Finally, we showed that CBD-IL-12 strongly synergizes with checkpoint inhibitor (CPI) antibodies in aggressive transplantable melanoma as well as in autochthonous melanoma.

Chapter 3 describes the masking technology that we applied to IL-12. A masking domain, which inhibits the interaction between IL-12 and its endogenous receptor, was fused to IL-12 via a protease-cleavable linker. Upon cleavage by tumor-associated proteases, the masking domain

dissociates, yielding bioactive IL-12 which activates the immune cells locally. In the periphery, due to lack of proteases, the masking domain prevents IL-12 from binding to its receptor, eliminating any off-target effects. We first confirmed that masked IL-12 displayed ~80-fold less bioactivity than unmodified IL-12, whereas treatment with recombinant proteases fully restored the bioactivity. We then demonstrated that masked IL-12 induced potent antitumor efficacy in various tumor models and potentiated CPI therapy. Last, we showed that masked IL-12 significantly decreased the incidence of adverse events, boosting the therapeutic index of IL-12.

In Chapter 4, we discuss potential limitations of each technology and offer potential strategies to overcome these limitations. We also comment on how IL-12 can be used in the clinic, given its complex biology and restricted expression of its receptor.

CHAPTER 1: INTRODUCTION

According to the Center of Disease Control and Progression, cancer is the second leading cause of death in the United States. Historically, cancer therapy consisted of three main approaches: chemotherapy, radiotherapy, and surgery. These modalities have been the most commonly pursued approaches throughout the 20th century. Chemotherapy relies on the usage of small molecules that penetrate the cell membrane and nonspecifically kill actively dividing cells, usually by interfering with cell division and/or DNA repair mechanisms. Radiotherapy involves the use of an ionizing radiation to kill or inhibit the growth of cancers and is localized to a particular area in the body. Surgery is performed on most cancer patients bearing solid tumors and it offers the best chance of eliminating the disease, particularly when the tumor has not yet spread to distant parts of the body. In the last three decades, a new form cancer therapy, termed immunotherapy, has become an important therapeutic alternative, and is now the first choice in many indications. Immunotherapy harnesses the power of our immune system, teaching it to recognize and kill tumors. In this chapter, we review the pathophysiology of solid tumors, their interaction with the immune system and current immunotherapy strategies with a particular focus on cytokines.

1.1 Pathophysiology of the Tumor Microenvironment

Cancer is a dynamic disease caused by dysregulated cells within a tissue that proliferate at abnormal rates. The etiology of the disease is complex, ranging from environmental stimuli (radiation, pollution, unhealthy diet) to hereditary factors (mutations in proto-oncogenes). However, once the formation of the tumor is initiated, several common pathophysiological characteristics within the tumor microenvironment (TME) govern the dynamics of cancer growth. In this section, we discuss the key principles underlying the pathophysiology of solid tumors.

1.1.1 Tumor Angiogenesis

Cancer cells constantly require sustenance in the form of nutrients and oxygen in order to support their growth. As the tumor mass increases in size, its growing demands activate the "angiogenic switch", which leads to the formation of new blood vessels, a process termed neovascularization[1]. Tumor-associated neovascularization is a feature of rapidly growing tumors, and not of dormant tumors[2]. In healthy tissues, the balance between pro-angiogenic and anti-angiogenic factors maintains vascular quiescence and controls endothelial cell proliferation[3]. However, during tumor progression, pro-angiogenic factors, such as vascular endothelial growth factor (VEGF)[4] and platelet-derived growth factor (PDGF)[5], become upregulated, leading to dysregulated blood vessel formation and increased interstitial pressure[6]. Formation of the disordered neovasculature, alongside lymphangiogenesis and tumor cell-derived macrovesicles, pave the way for the establishment of pre-metastatic niche at later stages of cancer growth[7]. Hypoxia, which stems from an imbalance between oxygen consumption and oxygen transport, is another result of abnormal vasculature[8]. Hypoxia plays a key role in dissemination of cancer cells by priming distal organs such as lung and bone for metastatic colonization via the recruitment of bone-marrow derived cells[9,10] and secretion of tumor-homing chemokines[11].

The observation that tumors possess a disordered vasculature was exploited to enhance the delivery of small molecule cancer therapeutics via the use of nanoparticles. In 1986, Maeda *et al.* coined the term "enhanced permeability and retention (EPR) effect"[12], which gave rise to the field of nanomedicine and tumor targeting. The idea behind the EPR effect is that, due to irregular angiogenesis, tumor vasculature is hyperpermeable to macromolecules and nanoparticles[13]. Vascular leakiness, combined with poor lymphatic drainage, results in passive accumulation of the intravenously- (i.v.)-administered nanoparticles inside the tumor[14]. This strategy led to the

approval of liposomal nanoparticle encapsulating doxorubicin (Doxil) in various solid tumors in 1995[15]. Yet, over the past decade, the widespread use of chemotherapeutic-encapsulating nanoparticles was not achieved due to their low tumor penetration, as only 0.7% of nanoparticles are delivered to a solid tumor[16].

1.1.2 Remodeling of the Extracellular Matrix During Tumor Growth

Extracellular matrix (ECM), the three-dimensional scaffold in which cells are residing, plays a profound role in tumor formation. The ECM can be divided into two main structures: the interstitial matrix and the basement membrane. The interstitial matrix is primarily composed of collagen types I, III, V, etc., elastin and fibronectin[17], whereas the basement membrane consists of collagen IV and laminins[18]. Many solid tumors tend to express high levels of ECM proteins[19], comprising nearly 60% of the total tumor mass. The invasiveness of the solid tumors also correlates with increased density of ECM proteins, which leads to resistance to therapies and poor prognosis[20,21].

Collagen, being the most abundant protein in the body, is one of the most essential tumor ECM proteins, preserving the structural integrity of the tissue and regulating cell motility. Collagen expression, similar to other ECM proteins, is upregulated during cancer development[22,23]. Secreted collagen is a supramolecular fibrillar network, formation of which depends on several collagen-processing enzymes, such as lysyl oxidases[24] and lysyl hydroxylases and prolyl hydrolases[25], which are overexpressed as well. Although tumor cells themselves exhibit increased collagen I and III expression, other producers of interstitial matrix proteins are myofibroblasts, which are generated in the presence of chronic inflammation and transforming growth factor β (TGF-β)[26]. Collagen can also impact cancer cells directly and promote their growth and metastasis[27]. For example, the binding between collagen I and α2 integrin decreases E-cadherin levels (known as

"suppressor of invasion"[28]), elicits epithelial-mesenchymal transition- (EMT)-like changes and increases "stemness" of cancer cells[29]. Since collagen plays a central role in tumor growth and metastasis, and its density limits the penetration of drugs, several direct and indirect collagen-targeting therapies have been investigated. Preclinically, systemic treatment with collagenase improves the penetration of monoclonal antibodies in xenograft models by increasing transcapillary pressure gradient[30]. EN3835, a purified collagenase *Clostridium histolyticum*, was tested in a phase I trial in patients with uterine leiomyoma and exhibited marginal efficacy (NCT02889848). Although some other strategies aimed at degrading/depleting collagen are pursued, somewhat conflicting and confusing results suggest complex functions of collagen in tumor growth.

1.1.3 Degradation of Tumor Extracellular Matrix by Tumor-associated Proteases

Proteolysis is another marked feature of almost all solid cancers. Description of the proteolytic nature of cancers can be traced back to 1946, when Fisher described that proteolysis of cancer cells is, in part, responsible for their malignant properties[31]. Extensive literature exists suggesting that proteases, such as matrix metalloproteinases (MMPs)[32] and serine proteases[33,34], are overexpressed in TME, and are involved in tissue remodeling during tumor growth and metastasis. The source of these proteases are cancer cells and stromal cells such as bone-marrow derived cells[32,35]. Secreted MMPs drive tumor angiogenesis[36] and lymphangiogenesis[37], which allows for dissemination of cancer cells into secondary organs via blood and lymphatic vessels. Further degradation of dense collagenous networks and the basement membrane facilitates metastatic processes. For example, levels of secreted MMP-2 and MMP-9 are significantly higher in the tumor than in adjacent normal tissue (ANT) in breast cancer patients[38]. MMP-2, MMP-9 and urokinase-type plasminogen activator (uPA, a serine protease) are elevated significantly in

advanced ovarian tumors and at metastatic sites but not in benign tumors[39]. In a study of 147 non-small cell lung cancer cases, uPA levels were 6.5-fold higher in the tumor tissue than in lung parenchyma[40]. Certain proteases are membrane-bound, such as membrane type 1-MMP (MT1-MMP or MMP14), which allows proteolysis to occur directly on cancer cell surface[41]. MMP-14 overexpression is associated with advanced tumor stage and lower overall survival in colorectal cancer patients[42]. MMPs have been considered as potential targets in cancer therapy, with many synthetic MMP inhibitors being tested in clinical trials from the 1990s to early 2000s. Despite encouraging preclinical data, the results of clinical trials were disappointing, as MMP inhibitors did not demonstrate therapeutic benefit and produced severe side effects[43].

Collectively, abnormal angiogenesis, increased ECM deposition and elevated degradation of ECM molecules represent key features of aggressive solid tumors, and enhance the ability of cancer cells to migrate to distal sites (Figure 1).

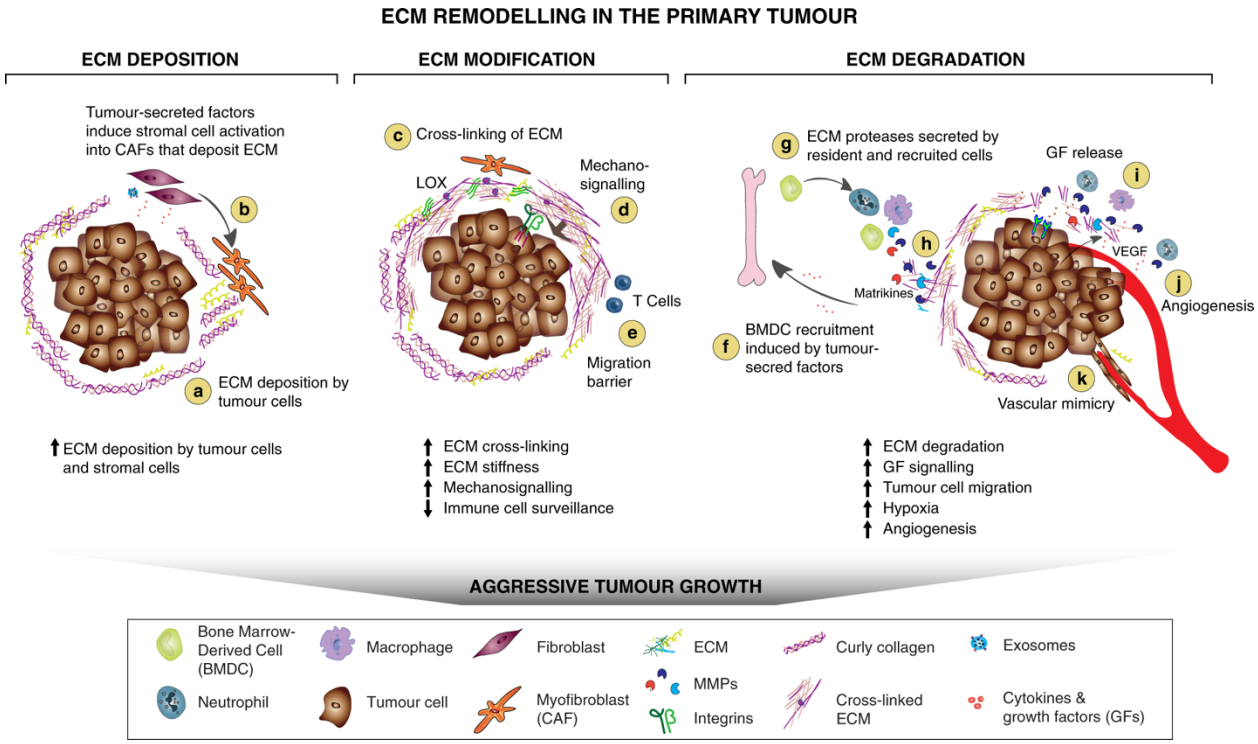

Figure 1. Schematic of the pathophysiological aspects of the tumor microenvironment. Adapted from Winkler *et al.* [35]

1.2 The Role of the Immune System in Cancer

Our immune system has evolved to recognize potential threats, such as viral or bacterial infections, and mount an inflammatory response against these threats. In that sense, in the "eyes of our immune system", cancer is no different than a viral infection, since cancer cells display altered (mutated) antigens. Interestingly, one of the first ever clinical applications of immunotherapy was performed by William Coley in 1890s, when he administered a mix of heat-killed streptococcus and *Serratia* marcescens intratumorally (i.t.) to induce local inflammation[44]. This bacterial infection led to regression of large sarcomas and a complete cure rate of about 10% of patients[45]. "Coley's toxins" illustrate the interplay between cancer and our immune system: cancer always tries to evade the recognition by our immune cells, yet once recognized, our immune system is capable of mounting a strong inflammatory response and eliminating even the well-established tumors. In this section, we discuss the cancer-immunity cycle by highlighting the important players of the immune system, mechanisms of cancer cell recognition and destruction, and ways in which cancer cells can evade the detection by our immune cells.

1.2.1 Cancer-Immunity Cycle: Key Players

The immune system can be broadly divided into two subsets, the innate immunity and the adaptive immunity. Innate immune cells are comprised of dendritic cells (DCs), monocytes/macrophages, granulocytes, and natural killer (NK) cells. The innate cells express germline-encoded pattern recognition receptors (PRRs) that are able to sense "danger signals", such as lipopolysaccharide (LPS) or CpG DNA motifs and are the first responders in the case of any potential threat. Activation of the PRRs leads to a cascade of intracellular events resulting in secretion of proinflammatory cytokines and additional recruitment of leukocytes. Among the innate immune cells, DCs and macrophages are known as professional antigen presenting cells

(APCs)[46], and are pivotal in presentation of tumor-associated antigens. The adaptive immunity consists of T cells and B cells, which express specific, high affinity T cell receptors (TCRs) and B cell receptors (BCRs), respectively. Unlike PRRs of the innate cells, these receptors are generated as a result of random rearrangement of gene segments, yielding highly diverse receptor pools. The adaptive immune cells play a fundamental role in the progression of tumors. This section will largely focus on the interactions between APCs and T cells, as these interactions are instrumental for the induction of potent antitumor immunity. Although the role of B cells in cancer has been overlooked for many years, their influence on antitumor immunity has been gaining interest recently[47]. However, the contribution of B cells to anticancer immunity is not discussed here.

APCs represent the interface between the innate and adaptive immune systems, because they can present endogenous antigens as well as cross-present exogenous antigens to T cells. Antigens are loaded on major histocompatibility complex (MHC) class I or II molecules for presentation to the TCRs of $CD8^+$ T cells (cytotoxic T lymphocytes) or $CD4^+$ T cells (T helper cells), respectively. The stimulation of the TCR by MHC molecules is known as the "signal 1" of the APC-T cell interplay. In order to achieve T cell activation, co-stimulatory ligands on APCs (CD80, CD86, CD137L) need to engage co-stimulatory receptors on T cell surface (CD28 and CD137), a process known as "signal 2". The expression of CD80/86 co-stimulatory molecules is crucial, since stimulation of the TCR without "signal 2" can lead to T cell anergy or apoptosis[48]; this would be detrimental in the case of cancer antigen-specific T cells, as these cells would become deleted (inactivated). Engagement of the TCR-MHC and co-stimulatory molecules, alongside a soluble cytokine-mediated communication ("signal 3") can dictate the fate of the naïve $CD4^+$ T cells, which can differentiate into T helper 1 (Th_1) or Th_2 effector cells. APC-produced proinflammatory cytokines, such as interleukin-12 (IL-12), drive the Th_1 program, whereas IL-4

production supports Th_2 differentiation[49]. Induction of strong Th_1 immunity is essential for elimination of cancers, both in preclinical models[50] and humans[51], as infiltration of these cells is correlated with prolonged survival[52].

DCs are potent APCs capable of migrating to the tumor, cross-presenting tumor antigens and secreting inflammatory factors for further recruitment of immune cells. DCs can be divided into two subsets, conventional DCs (cDCs) and plasmacytoid DCs (pDCs). cDCs are further subdivided into $XCR1^+$ DCs (cDC1) and $CD11b^+$ DCs (cDC2)[53]. Within the cDC1 subset, migratory $CD103^+$ DCs are particularly important in antitumor immunity[54,55], as these cells can traffic intact antigens to the tumor-draining lymph nodes and cross-present to $CD8^+$ T cells[56], and secrete T cell-recruiting chemokines such as C-X-C motif ligand-9 (CXCL9) and CXCL10[57]. pDCs are able to secrete proinflammatory type I interferons (IFNs) and activate $CD8^+$ T cells[58,59], yet in the presence of immunosuppressive mediators, pDCs may hinder antitumor immunity and their infiltration has been associated with poor clinical outcome in some tumors[60].

Macrophages constitute a major fraction of myeloid cells present within the tumors[61]. Most of the tumor-associated macrophages (TAMs) are differentiated from circulating monocytes, which are recruited to the tumors via the CCL2 chemokine[62]. Depending on the environmental stimuli, TAMs can be reprogrammed into proinflammatory "M1" TAMs or protumorigenic "M2" TAMs. M1 macrophages are induced by IFNγ and tumor necrosis factor-α (TNFα) and are characterized by $IL\text{-}12^{high}/IL\text{-}10^{low}$ cytokine profile, whereas M2 macrophages are induced by IL-4 and IL-13, and display $IL\text{-}12^{low}/IL\text{-}10^{high}$ phenotype[63]. Activated M1 TAMs express high levels of MHC molecules, are able to directly kill cancer cells via secretion of cytotoxic molecules and orchestrate Th_1-biased immunity[64]. M2 macrophages play an important role in wound healing, as they support neovascularization, ECM remodeling via secretion of VEGF and TGF-β[65], and induce

direct suppression of T cell activity[66]. These characteristics make M2 macrophages detrimental during tumor progression and are associated with poor clinical outcome[67]. It also needs to be noted that the M1 versus M2 representation of macrophages is overly simplistic, since the markers that are used to delineate the subpopulations were mostly derived from *in vitro* studies[68] and, in some cases, are not as easily applicable to *in vivo* scenarios[69].

Another important component of the innate immunity are NK cells, which can mount a potent and rapid cytolytic response against transformed cells[70]. NK cells express an array of stimulatory and inhibitory receptors on their cell surface and the final activation status of the cell is determined by the balance of these stimulatory/inhibitory signals. For example, cancer cells tend to downregulate MHC expression, which is recognized as a "missing self" signal, and triggers NK cells[71]. Activated NK cells secrete cytolytic granules, such as granzyme and perforin, directly leading to tumor cell death[72] and proinflammatory cytokines (IFNγ, TNFα) resulting in recruitment of T cells[73].

1.2.2 Cancer-Immunity Cycle: Adaptive Attack

T cells are the second most frequent immune cell type found within tumors after TAMs[74]. Their role in tumor progression has been extensively studied, as these cells are the major orchestrators and effectors of the adaptive immunity. Approximately 4×10^{11} T cells circulate in the human body[75], with each cell expressing several TCRs that are (ideally) unreactive against self-antigens. As mentioned, TCRs are generated as a result of random rearrangement of gene segments (VDJ recombination) that could theoretically yield a TCR diversity of about 10^{15}. Yet the actual number of TCR clonotypes is between 10^6-10^8 *in vivo*[76,77]. Such broad diversity gives T cells a chance to recognize mutated self-antigens (neoantigens or oncoantigens), which arise as a

consequence of oncogenesis. Dying cancer cells release neoantigens which are picked up and processed by DCs in an inflammatory context. DCs expressing neoantigen:MHC complexes along with co-stimulatory molecules are able to prime and activate effector T cell responses against cancer-specific antigens[78]. Classically, this process is thought to happen primarily in the tumor-draining lymph node[79], yet recently, tertiary lymphoid structures have been described in the tumor itself[80], suggesting that antigen presentation may happen within the tumor bed. Nevertheless, $CD8^+$ T cell clones that are successfully activated by DCs can infiltrate the tumor and engage cancer cells expressing neoantigens on their MHC-I molecules. This leads to cancer cell death via the secretion of perforins and granzymes by $CD8^+$ T cells[81]. Killing of cancer cells releases even more tumor-associated antigens in the TME that are picked up by cross-presenting APCs, which in turn recruit and prime naive $CD8^+$ T cells. This creates a positive feedback loop, increasing the breadth and magnitude of the systemic antitumor response driven by effector $CD8^+$ T cells.

The role of Th_1 cells is of significance this cycle, as these cells are able to produce proinflammatory cytokines such as IL-2, TNFα, and IFNγ, which promote not only $CD8^+$ T cell priming, but also activate phagocytic phenotype of macrophages, cytotoxic functions of NK cells and increase MHC expression on tumor cells[82,83]. $CD4^+$ T cells are also required in generating memory $CD8^+$ T cells[84], which is essential for establishing potent systemic anticancer immunity[85]. As mentioned, $CD4^+$ T cells recognize antigens in the context of MHC-II, which are predominantly expressed by professional APCs; however, a subset of tumor cells are also able to express MHC-II molecules[86,87], which is associated with superior clinical outcome[88,89]. These observations further stress the importance of Th_1 cells in antitumor immunity, in addition $CD8^+$ T cells.

1.2.3 Cancer-Immunity Cycle: Immune Evasion

In a fraction of cancer patients, the cancer-immunity cycle is impaired, due to the presence of certain immunoregulatory mechanisms, which are meant to protect our body from autoimmunity during homeostasis. These immunosuppressive mechanisms involve cell-cell as well as soluble interactions that lead to T cell dysfunction, anergy and exhaustion.

Several immunosuppressive cell populations are present in the TME, which are either recruited to or differentiated within the tumors. One of the most potent immunoregulatory cells are regulatory T (T_{reg}) cells which are $CD4^+CD25^+$ and express forkhead box protein P3 (FOXP3) transcription factor[90]. These cells inhibit the functional maturation of tumor antigen-specific $CD8^+$ T cells and diminish their cytolytic abilities via the secretion of TGF-β [91]. T_{reg} cells constitutively express high levels of CD25, which is the high-affinity receptor for IL-2, and thus, act as a sink for IL-2[92]. T_{reg} cells can also secrete IL-10, which is considered to be an strong immunoregulatory cytokine[93]. In fact, the ratio of effector $CD8^+$ T cells to T_{reg} cells in the tumor is the most critical parameter in predicting the outcome of the patients[94,95].

Presence of suppressive or tolerogenic APCs, such as M2 TAMs impairs the antitumor immunity. These cells display low levels of co-stimulatory ligands CD80/86, which results in deactivation of effector T cells[96]. Furthermore, myeloid-derived suppressor cells (MDSCs) contribute to T cell dysfunction by secreting suppressive metabolites such as indoleamine-2,3-deoxygenase (IDO)[97] and arginase 1[98].

One of the central pathways of peripheral immune tolerance is immune checkpoints. These molecules are expressed on activated T cells to prevent them from killing harmless cells. Cytotoxic T lymphocyte antigen-4 (CTLA-4), a homologue of CD28, is expressed on activated or exhausted

T cells[99]. CTLA-4 binds to CD80/86 molecules with a higher affinity and avidity than does CD28, thereby limiting T cell activation[100]. CTLA-4 is also constitutively expressed on T_{reg} cells, allowing them to compete for CD80/86 co-stimulatory molecules[101]. Binding of CTLA-4 to CD80/86 molecules induces recruitment of phosphatases to the cytoplasmic tail of CTLA-4, which leads to reduced activation of essential transcription factors such as nuclear factor of activated T cells (NFAT) and nuclear factor-κB (NF-κB)[102,103].

Another crucial checkpoint is programmed cell death-1 (PD-1), which is a receptor for programmed cell death ligand-1 (PD-L1). PD-1 is expressed on T cells upon TCR activation, whereas its ligand is constitutively expressed on APCs and can be expressed by non-hemopoietic cells in the presence of proinflammatory cytokines[104]. The interaction of PD-1 with its ligand leads to dephosphorylated of CD28[105], which induces T cell exhaustion or apoptosis, depending on the context[106]. PD-L1 can be expressed by tumor cells as well, especially in the presence of proinflammatory cytokines such as IFNγ[107,108]. Hence, PD-L1 expression on tumor cells is indicative of prior immune inflammation, which is beneficial for patients receiving checkpoint-targeting therapies (covered in Section 1.3).

Some tumor types are poorly immunogenic, with minimal mutational burden (few neoantigens) and low expression of IFNγ signature and thus, are not infiltrated with T cells. These so-called “cold” tumors are more aggressive than their “hot” counterparts and represent a major therapeutic challenge. For example, active Wnt/β-catenin signaling within the TME results in exclusion of T cells from the tumor[109]. These tumors are often heavily infiltrated with suppressive myeloid-derived cells and lack cross-presenting Batf3-dependent DCs, major producers of T cell-recruiting chemokines CXCL9 and CXCL10[110].

1.3 Overview of Current Immunotherapy Strategies

As discussed in the previous sections, the immune system plays a pivotal role in the development of cancers. In this section, we introduce major immunotherapy strategies that are pursued clinically. Some of the mentioned therapeutics are already approved by the Food and Drug Administration (FDA). Therapeutics that are mentioned here do not represent the full list of actively investigated drugs but rather are highlights of the most commonly pursued approaches. It is important to note that the combinations of these approaches are also currently tested in the clinic and some of them are noted here.

1.3.1 Checkpoint Inhibitor Antibodies

Checkpoint inhibitor (CPI) antibodies are the most widely used class of immunotherapy. Upon binding to their target antigens, they inhibit the receptor-ligand interactions that normally induce apoptosis or deactivation of T or NK cells. In 2011, the FDA approved ipilimumab (Yervoy, Bristol-Myers Squibb), an anti-CTLA-4 antibody, in patients with metastatic melanoma[111]. This was followed by the approval of two anti-PD-1 antibodies, pembrolizumab (Keytruda, Merck & Co) and nivolumab (Opdivo, Bristol-Myers Squibb), for melanoma patients in 2014[112]. PD-L1 blocking antibodies, atezolizumab (Tecentriq, Roche), durvalumab (Imfinzi, AstraZeneca) and avelumab (Bavencio, EMD Serono) were approved for the treatment of non-small cell lung cancer (NSCLC), bladder cancer and Merkel cell carcinoma[113]. Currently, more than a dozen major cancer types are treated using CPI antibodies, becoming the standard-of-care therapy, especially in advanced, inoperable malignancies. However, blockade of these immunoregulatory pathways also leads to immune-related adverse events (irAEs), with 10-15% of patients developing grade 3-5 irAEs[114]. The most common cause of death as a result of irAE for patients receiving ipilimumab is colitis, whereas fatalities in patients receiving anti-PD-1/L1 are mostly due to pneumonitis,

hepatitis and neurotoxic effects[115]. In some indications, combination of anti-CTLA-4 and anti-PD-1 is an approved therapy, and the incidence and severity of irAEs increases as a result of blocking two nonredundant pathways[116]. Some next-generation CPI antibodies, such as anti-TIGIT, anti-TIM-3 and anti-LAG-3, are also evaluated in numerous clinical trials, whether as single agents or in combination with approved CPI antibodies[117].

1.3.2 Recombinant Cytokine Therapies

Cytokine therapy is one of the earliest forms of the FDA-approved immunotherapy. IL-2, which is a growth factor T and NK cells, and IFN-alpha, an anti-tumor cytokine, were approved for treating various types of advanced cancers. High-dose recombinant IL-2 (aldesleukin, Proleukin) was approved for the treatment of advanced renal cell carcinoma in 1992[118] and metastatic melanoma in 1998[119], and IFN-alpha (Intron-A) was approved for the treatment of hairy cell leukemia[120] and Kaposi's sarcoma in patients with acquired immunodeficiency syndrome, both in 1986[121]. These results were one of the first demonstrations that shifting the immunological balance towards a pro-inflammatory phenotype can lead to robust regression of established tumors in the clinic. In recent years, other cytokines have entered clinical trials, including IL-12 (covered in Section 1.4), IL-15, and IL-7[122] but, to date, none of them are approved by the FDA, either due to limited efficacy or intolerable toxicity[123]. Despite the excitement around using cytokines in cancer therapy, which was based on convincing results in animal models, further translation of recombinant antitumor cytokines was halted. Due to severe adverse events in patients, such as capillary leak syndrome and cytokine storm[124], high-dose IL-2 therapy is now less commonly used, especially after the advent of CPIs.

1.3.3 Alternate Clinical Strategies

Besides CPI antibodies and recombinant cytokines, alternate approaches are also pursued within the context of cancer immunotherapy and some of the most widely pursued strategies are mentioned here. Agonistic antibodies are a class of therapeutics that activate the immune cells and upregulate their effector functions upon binding to the co-stimulatory molecules. Urelumab is an anti-CD137 (also known as anti-4-1BB) agonistic antibody, which primes activated T and NK cells resulting in secretion of proinflammatory cytokines (IL-2 and IFNγ)[125,126]. Administration of urelumab to patients with various advanced cancers resulted in severe irAEs, most common one being hepatotoxicity[127].

Another class of immunotherapeutics that is widely used in the clinic are antitumor antibodies. Antitumor antibodies bind to antigens that are specifically (over)expressed on tumor cells and not on healthy cells. Although initially they were not perceived as immunotherapeutics, since their primary objective was to block oncogenic pathways, the immunostimulatory effects contribute to their efficacy. These antibodies, via their Fc portions, recruit innate immune cells and induce antibody-dependent cellular cytotoxicity (ADCC) or complement-dependent cytotoxicity of tumor cells[128]. Examples include cetuximab (Erbitux, Eli Lilly and Co.), which blocks epidermal growth factor receptor (EGFR) and trastuzumab (Herceptin, Genentech), which binds to human epidermal growth factor receptor 2 (HER-2/neu)[129]. Cetuximab is approved for EGFR-positive colon, and also for head and neck cancer, and trastuzumab is approved for HER-2/neu-positive breast cancer.

Adoptive transfer of T cells is another successful immunotherapy approach, particularly in liquid tumors. This approach relies on either *ex vivo* expansion of autologous T cells[130] or engineering of these T cells to express chimeric antigen receptors (CARs)[131]. CAR-T cells

expressing the receptor for CD19 (CTL-019, Kymriah, Novartis) were approved by the FDA in 2017 in patients with B cell acute lymphoblastic leukemia. Despite achieving durable remissions in hematological malignancies, major irAEs, such as cytokine release syndrome (CRS) and neurologic toxicity, and cost of production limit their widespread use[132].

1.4 Interleukin-12 as a Potential Antitumor Therapeutic Cytokine

Cytokines are soluble molecular messengers that allow cells to communicate in paracrine and autocrine fashion, resulting in a coordinated response to various threats. Secreted cytokines mediate signaling by binding to a cytokine-specific receptor complex with high affinity, leading to phosphorylation of signal transducer and activator of transcription (STAT) transcription factors[133]. Activated STATs dimerize and bind to the promoters of responsive genes in the DNA, which ultimately determines cell fate[134]. Effects induced by cytokines are generally short-lived and tightly regulated due to rapid clearance from the bloodstream and localized production. Most cytokines are below the threshold of renal clearance (<40 kDa[135]) and lack recycling mechanisms (such as neonatal Fc receptor, FcRn), causing their rapid clearance.

Cytokines are divided into families, such as ILs, IFNs, chemokines, TGFs, TNFs and colony-stimulating factors (CSFs) based on their biological properties. Certain cytokines can exert similar immunological effects, causing some degree of redundancy in the cytokines, yet the spectrum of responses and the dependence on concentration of the cytokine can vary. Cytokines can also induce antagonistic effects, adding to the complexity of understanding the network of cytokine responses. This makes the relative concentration and localization of cytokines, as well as their timing, important parameters.

In this section, the focus is on immunological functions of IL-12, one of the most promising cytokines for cancer immunotherapy. Challenges in its translation as a recombinant protein therapeutic as well as potential engineering solutions are also discussed.

1.4.1 Biological Properties of Interleukin 12

IL-12, a heterodimeric cytokine consisting of disulfide-linked p35 and p40 subunits, is one of the most potent proinflammatory cytokines. IL-12 was first discovered as an NK cell stimulatory factor by Giorgio Trinchieri's laboratory in 1989[136]. It was found that IL-12 also induces activation of naïve T cells and skews them towards Th_1 fate[137], highlighting its role in triggering inflammatory responses of both innate and adaptive immunity[138]. IL-12 family also includes IL-23, IL-27, and IL-35, of which IL-23 is pro-inflammatory[139], IL-35 is anti-inflammatory[140], whereas IL-27 has both pro- and anti-inflammatory roles[141].

IL-12 binds to a heterodimeric receptor complex (IL-12R) consisting of IL-12Rβ1 and IL-12Rβ2[142], the former being constitutively expressed by T cells[143], whereas the latter is expressed upon activation and is a marker of Th_1 cells[144]. Interestingly, resting NK cells can express the heterodimeric receptor complex[145], suggesting that these cells can respond to IL-12 without pre-activation. Upon binding to IL-12R, IL-12 causes phosphorylation of STAT4, which dimerizes and translocates into the nucleus to regulate gene expression[146]. IL-12 can also act on cells of myeloid origin, such as dendritic cells[147,148], and directly augment MHC-II expression. The main mediator of pro-inflammatory and antitumor effects of IL-12 is IFNγ[149], which is secreted by T and NK cells. IFNγ induces expression of CXCL9 and CXCL10, chemokines that are important for immune cells recruitment[57] and inhibition of angiogenesis of the tumors[150]. These chemokines can be secreted by tumor cells themselves, as it was observed that the expression of IFNγ receptor

on tumor cells was crucial for IL-12-mediated tumor control[151,152]. Interestingly, antitumor effects of IL-12 are diminished, but not abolished, in immune-incompetent mice as well[153], suggesting that T/NK cell-mediated IFNγ secretion is not the only antitumor mechanism. In fact, $NKp46^+$ lymphoid tissue-inducer (LTi) cells were reported to be the initiators of tumor rejection upon IL-12 therapy[154], further confirming the important actions of IL-12 on innate and adaptive immunity. Certain cytokines, such as IL-10[155] and TGF-β1[156], can exert regulatory effects on IL-12 by suppressing the transcription of the p40 subunit.

1.4.2 Clinical Trials Using Recombinant Human IL-12

Early preclinical studies conducted in the 1990s demonstrated potent antitumor activity of recombinant IL-12 administered systemically to mice bearing primary and metastatic tumors[157]. These results prompted the initiation of a phase I clinical trial in patients with advanced malignancies (melanoma and renal cell carcinoma), in which the maximum tolerated dose (MTD) of 500 ng/kg/day was established[123]. Recombinant IL-12 was administered by bolus i.v. injection once as a test dose, followed by a 2-week rest period, and then 5 times a week, every 3 weeks. In the follow-up trial at this dose, IL-12 caused deaths of two patients and induced severe side effects in 12 out of 17 patients, resulting in temporary discontinuation of clinical trials using recombinant IL-12. The marked difference between the two clinical trials was caused by the use of a priming dose of IL-12 14 days prior to daily treatment in the phase I trial, contrasted with the absence of it in the phase II trial[158]. Such a protective effect of the pre-dose was also observed in mice[159,160], which was associated with decreased levels of systemic IFNγ production after subsequent IL-12 administrations. Repeated administration of IL-12 leads to reduced IFNγ production capacity through specific downregulation of phosphorylated STAT4 protein[161]. Systemic IFNγ is the main contributor to the side effects of IL-12 therapy. Experiments with mice lacking the IFNγ receptor

revealed that most of the side effects are due to IL-12-induced IFNγ[162]. Likewise, administration of neutralizing antibodies against IFNγ abrogate IL-12-induced body weight lost in mice[159,160]. Despite this, IFNγ is crucial for antitumor effect of IL-12 therapy. Solving this dilemma may require an engineered IL-12 that can localize its proinflammatory effects to the tumor site, while sparing the healthy organs and limiting systemic inflammation (engineering strategies for IL-12 are discussed in Section 1.4.3). Careful design of the dosing regimen and determining the optimal route of administration will be key factors in IL-12 therapy.

Since the premature termination of the phase II trial, several clinical trials were launched with less frequent dosing (twice or three times a week) and subcutaneous (s.c.) or i.t. route of administration in order to mitigate the side effects. In head and neck squamous cell carcinoma patients, once a week i.t. administration of IL-12 at 300 ng/kg still produced grade 3 liver toxicity, and the dose had to be decreased to 100 ng/kg for some patients[163]. In this trial, mRNA expression of IFNγ in peripheral blood mononuclear cells (PBMCs) was drastically increased as compared to control patients. Enlargement of lymph nodes, increased infiltration and activation of B cells, as well as IgG subclass switch towards IgG1 and IgG4 was noted[164]. Currently, preferred administration route for human IL-12 is s.c., as several clinical trials demonstrated that IL-12 at 300-500 ng/kg (MTD) can be given s.c. two or three times a week, with manageable toxicity[165-168]. At this dose, IL-12 alone does not produce any significant clinical benefit, and thus several trials were launched evaluating this agent in combination with other drugs, such as recombinant IL-2[169] and IFNα-2b[170]. In these trials, clinical activity was only observed at or above the MTD and thus were not followed up in phase II trials. Recently, a clinical trial evaluating the combination of s.c. IL-12 and pembrolizumab (αPD-1) was launched (NCT03030378), the results of which have not been published yet.

1.4.3 Engineering of Recombinant IL-12

Given the low therapeutic index of recombinant wild-type IL-12, several protein engineering strategies have been applied to IL-12 to mitigate the side effects and facilitate its clinical translation. Dario Neri's group has fused IL-12 to a single-chain variable fragment (scFv) (the fusion referred to as IL12-L19) recognizing the extra domain B (EDB) splice variant of fibronectin isoform, which is a marker of neovasculature and is overexpressed in a variety of solid tumors[171]. It was shown that i.v. injected IL-12 targeting EDB fibronectin resulted in slower tumor growth compared to IL-12 targeting an irrelevant protein. In a lung metastasis model, IL12-L19 outperformed an equimolar dose of unmodified IL-12, demonstrating that targeting subendothelial extra-cellular matrix (ECM) is viable in a metastatic model. Dario Neri and colleagues developed another fusion of IL-12 and an scFv, termed IL12-F8, that targets EDA fibronectin and demonstrated additive therapeutic effect between the engineered IL-12 and paclitaxel[172]. A similar approach has also been employed to target mesothelin, a glycoprotein highly overexpressed in mesothelioma[173].

Another immunocytokine, comprising two molecules of IL-12 fused to a full immunoglobin G (IgG) recognizing DNA/histone to target tumor necrosis, was developed by the National Cancer Institute[174]. This immunocytokine (referred to as NHS-IL12) has an increased half-life due to Fc portion of the antibody, yet its specific bioactivity is markedly decreased compared to a wild-type IL-12. NHS-IL12 was tested in a phase I clinical trial in patients with metastatic solid tumors[175]. NHS-IL12 was dosed once every 4 weeks and the MTD was 16.8 mg/kg. Although antitumor responses need to be investigated in the follow-up trial, 5 patients had durable stable disease. This drug is currently being evaluated as a monotherapy in a phase I/II as

well as in combination with M7824[176] (a bifunctional protein blocking PD-L1 and TGF-b) in patients with advanced Kaposi sarcoma (NCT04303117).

huBC1-IL12 (AS1409) is another immunocytokine, structurally similar to NHS-IL12, that was engineered to target the EDB-containing fibronectin isoform[177]. This molecule was studied in a phase I clinical trial in patients (n = 13) with malignant melanoma (n = 11) and renal cell carcinoma (n = 2), in which an MTD of 15 mg/kg weekly was determined[178]. Stable disease was seen in 6 patients and partial response was seen in one patient.

Fusion of IL-12 and Fc portion has been made to increase its half-life and limit the number of injections to decrease IL-12-mediated toxicity[179]. This molecule, in contrast to full IgG-fused IL-12 variants, demonstrated a similar specific bioactivity compared to wild-type IL-12. IL12-Fc exhibited long serum half-life, resulting in superior antitumor efficacy in several syngeneic tumor models. Head-to-head comparison of toxicity between IL-12 and IL12-Fc was not made in this study.

For intratumoral injection use, IL-12 has recently been fused with lumican, a collagen-binding protein, and mouse serum albumin (IL12-MSA-Lumican), which can be localized within the tumor matrix upon intratumoral injection[180]. This construct was less toxic upon intratumoral injection, as evidenced by body weight loss, than IL12-MSA, while antitumor efficacy was comparable between the two constructs.

Besides recombinant approaches, there are several IL-12 gene therapies under development, such as plasmid electroporation (in development by OncoSec Medical, Inc.)[181], lipid nanoparticle formulated mRNA (Moderna, Inc.)[182], and adenovirus-mediated delivery (Ziopharm Oncology, Inc.)[183]. These approaches, however, rely solely on i.t. administration.

CHAPTER 2:

COLLAGEN-BINDING IL-12 ENHANCES TUMOR INFLAMMATION AND DRIVES THE COMPLETE REMISSION OF ESTABLISHED, IMMUNOLOGICALLY COLD TUMORS

2.1 Abstract

CPI immunotherapy has achieved remarkable clinical success, yet its efficacy in 'immunologically cold' tumors has been modest. IL-12 is a powerful cytokine that activates the innate and adaptive arms of the immune system, yet its administration has been associated with immune-related adverse events. Here, we show that the intravenous administration of a collagen-binding domain fused to IL-12 (CBD–IL-12) in mice bearing aggressive murine tumors accumulates in the tumour stroma, owing to exposed collagen in the disordered tumor vasculature. In comparison with the administration of unmodified IL-12, CBD–IL-12 induced sustained intratumoral levels of IFNγ, markedly reduced its systemic levels as well as organ damage, and led to superior anticancer efficacy, eliciting complete regression of CPI-unresponsive breast tumors. Furthermore, CBD–IL-12 potently synergized with CPI to eradicate large established melanoma, induced antigen-specific immunological memory, and controlled tumor growth in a genetically engineered mouse model of melanoma. CBD–IL-12 may potentiate CPI immunotherapy for immunologically cold tumors.

2.2 Introduction

Immunotherapy is a promising approach for treating cancer patients. Although CPI therapies, such as αCTLA-4 and αPD-1 antibodies, have achieved clinical success, these antibodies fail to induce regression of established tumors in a majority of patients, keeping the complete response (CR) rates low[184]. CPI therapy inherently relies on pre-existing antitumor immunity, which is absent in poorly immunogenic, so called "cold" tumors[185]. To trigger immunologic destruction of advanced, cold tumors, sufficient numbers of effector immune cells capable of recognizing tumor antigens with high avidity must infiltrate the tumor stroma[186]. A strategy that aims to convert immune-excluded tumors into immune-infiltrated tumors would be a major advancement in cancer care.

IL-12 is considered to be an attractive antitumor therapeutic cytokine as it can activate both the innate and the adaptive arms of the immune system[138], and is able to elicit antigen-specific immune responses[187,188]. IL-12 promotes Th1 polarization, results in IFNγ secretion by effector cells such as $CD8^+$ T cells[189], and stimulates antigen presentation[190]. Despite encouraging preclinical findings, systemic administration of recombinant human IL-12 showed unsatisfactory outcomes in clinical trials due to intolerable irAEs, resulting in discontinuation of trials with systemic IL-12[191]. A major barrier in recombinant IL-12 therapy stems from the inability to reach sufficiently high local concentrations within the TME[192], thus motivating the development of tumor-targeted IL-12 therapy to unleash the full therapeutic potential of this cytokine. In this regard, IL-12 has recently been fused with lumican, a collagen-binding protein, which can be retained within the tumor matrix upon intratumoral injection[180]. An approach that would enable i.v. administration could further extend the translatability of IL-12 therapy to non-superficial and metastatic tumors.

We have recently reported that the A3 collagen-binding domain (CBD) of von Willebrand factor (VWF) can be retained within solid tumors upon i.v. administration due to exposure of collagen within the tumor stroma associated with vascular leakiness[193]. Chemical conjugation of CBD protein to CPI antibodies and recombinant fusion to IL-2 resulted in enhanced antitumor efficacy compared to their unmodified forms, but the efficacy was insufficiently strong to show CRs in aggressive models such as B16F10 melanoma and the immune-excluded EMT6 mammary carcinoma. Here, we have focused our attention on a cytokine more likely to induce tumor inflammation, with the objective to make cold tumors inflamed and thus more responsive to CPI therapy, installing collagen affinity to IL-12 to enhance its efficacy and overcome safety challenges that have hindered its clinical translation.

2.3 Results

2.3.1 CBD-IL-12 Binds to Collagen I and III with High Affinity

We exploited the heterodimeric structure of IL-12 and fused one CBD molecule to each of the subunits to install high affinity to collagen (Fig. 2a). CBD-IL-12 exhibited slightly reduced bioactivity compared to IL-12 as assessed by STAT4 phosphorylation (Fig. 2b) and splenocyte activation (Fig. 3a). We further characterized the molecular weights of IL-12 and CBD-IL-12 by SDS-polyacrylamide gel electrophoresis (SDS-PAGE) (Fig. 3b) and matrix-assisted laser desorption/ionization time-of-flight (MALDI-TOF) spectrometry (Fig. 3c,d). According to MALDI-TOF spectra, the molecular weights of IL-12 and CBD-IL-12 were 62.8 kDa and 106.6 kDa, respectively. We determined the equilibrium dissociation constants of CBD-IL-12 against collagen I and III using surface plasmon resonance (SPR), which were 3.6 and 6.2 nM, respectively (Fig. 2c,d). Such high binding affinity can be partially attributed to the avidity effect caused by two CBD molecules fused to IL-12, since monoCBD-IL-12 exhibited weaker binding to collagen

I (Fig. 3e). Unmodified IL-12 did not bind to collagen I, as confirmed by SPR (Fig. 3f). CBD-IL-12, but not unmodified IL-12, bound to human melanoma cryosections and localized around the blood vessels, where collagen is particularly enriched (Fig. 2e,f). These data show that CBD-IL-12 is functional as we have designed it, capable of activating cells *in vitro* and binding to collagens I and III with high affinity.

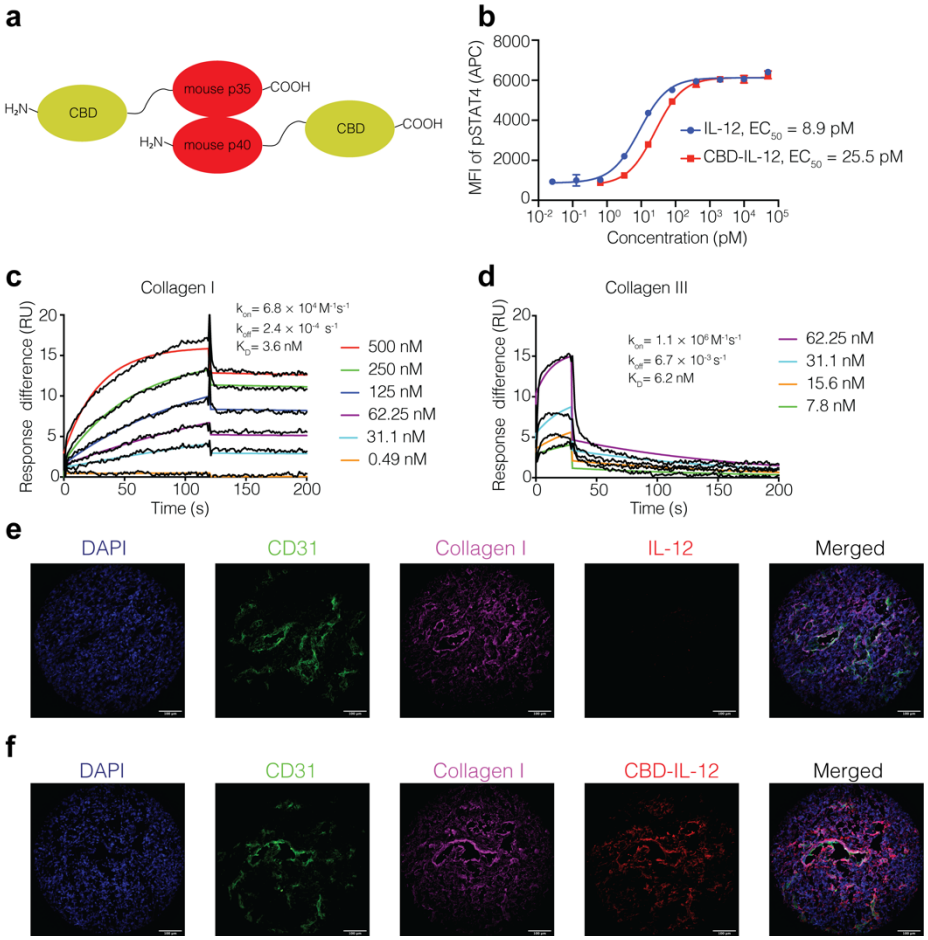

Figure 2. CBD-IL-12 binds to collagen with high affinity while retaining bioactivity. a, Schematic illustrating the fusion sites of the von Willebrand factor A3 CBD to murine p35 and p40 subunits. CBD was fused to each of the subunits via a $(G_3S)_2$ linker. b, Dose-response relationship of phosphorylated STAT4 with IL-12 and CBD-IL-12 in preactivated primary mouse $CD8^+$ T cells (n=3, mean ± SD). c,d, Affinity (K_D values are shown) of CBD-IL-12 against collagen I (c) and collagen III (d) as measured by SPR. CBD-IL-12 was flown over over the chips at indicated concentrations. Curves represent the specific responses (in resonance units, RU) to CBD-IL-12. Experimental curves were fitted with 1:1 Langmuir model. Dissociation constants (K_D) and rate constants (k_{on} and k_{off}) determined from the fitted curves are shown. e,f, Binding of unmodified IL-12 (e) or CBD-IL-12 (f) to human melanoma cryosections was imaged by fluorescence microscopy. Scale bars, 100 µm. Experiments were performed twice (b,c,d,e,f), with similar results. Representative data are shown.

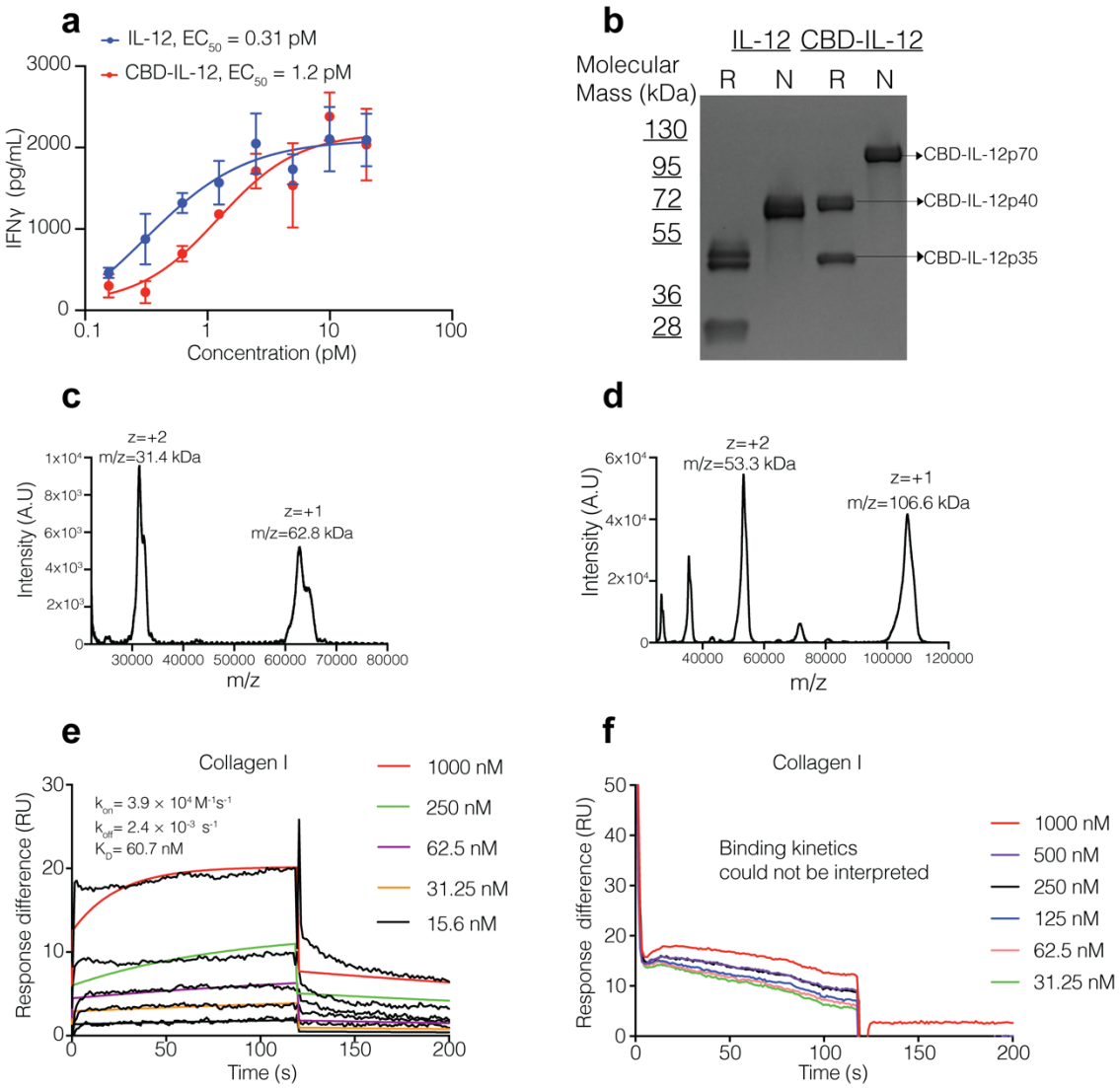

Figure 3. Biophysical characterization of IL-12 and CBD-IL-12. a, Splenocytes were cultured in the presence of 10 ng/mL IL-2 and indicated amounts of IL-12 or CBD-IL-12 (n = 3). IFNγ in the supernatant was measured using ELISA. Data are mean ± SEM. b, SDS-PAGE for IL-12 and CBD-IL-12 under reducing (R) and non-reducing (N) conditions. As expected, two bands appear under reducing conditions for IL-12, corresponding to the p35 and p40 subunits. Under reducing conditions, these bands were shifted by ~20 kDa in the case for CBD-IL-12, indicating that one CBD molecule was fused to each subunit. c,d, MALDI-TOF linear positive mode spectra of IL-12 (c) and CBD-IL-12 (d). The single and double charged molecular ions are indicated for each molecule with a corresponding m/z value. e, SPR analysis of monoCBD-IL-12 (where CBD protein is only fused to the p40 subunit) binding to collagen I. f, SPR analysis of IL-12 binding to collagen I. Binding kinetics was not determined. All experiments were performed twice, with similar results.

2.3.2 CBD-IL-12 is More Efficacious than Unmodified IL-12 in Melanoma and Breast Cancer

IL-12 has been tested clinically, both alone and in combination, in patients with advanced melanoma and breast cancer[123,194,195]. We first examined the antitumor activity of CBD-IL-12 in the aggressive B16F10 melanoma model (Fig. 4a,b). Mice bearing day 7 B16F10 tumours (~60 mm^3 at the start of therapy) were treated once with either PBS, IL-12 or equimolar CBD-IL-12. We administered the cytokines either peritumorally (p.t.) or i.v. to determine the most efficacious injection route. Systemic administration of CBD-IL-12 resulted in robust regression of B16F10 melanoma, as opposed to both p.t.- and i.v.-administered unmodified IL-12, which delayed the tumor growth compared to treatment with PBS. Interestingly, although p.t. injection of CBD-IL-12 was still more favorable than either route of unmodified IL-12, its antitumor efficacy was inferior to i.v. administration of CBD-IL-12. A single i.v. injection of CBD-IL-12 resulted in 10 CR out of 15 treated mice (67%).

We then tested the efficacy of CBD-IL-12 in the triple negative, immune-excluded EMT6 breast cancer model[193,196] (Fig. 4c,d). CBD-IL-12 administered i.v. once on day 7 resulted in 13 CR out of 15 mice (87%), whereas unmodified IL-12 resulted in 6 CR out of 15 mice (40%). Importantly, CBD-IL-12-treated mice that were tumor-free developed systemic immunological memory, as 12 mice out of 13 rejected rechallenge with the EMT6 tumor cells in their contralateral mammary fat pad (Fig. 4e). These data indicate that CBD fusion to IL-12 greatly improves the antitumor responses and results in complete tumour remissions of moderately-sized B16F10 melanoma and EMT6 mammary carcinoma in the majority of mice when used as a single agent.

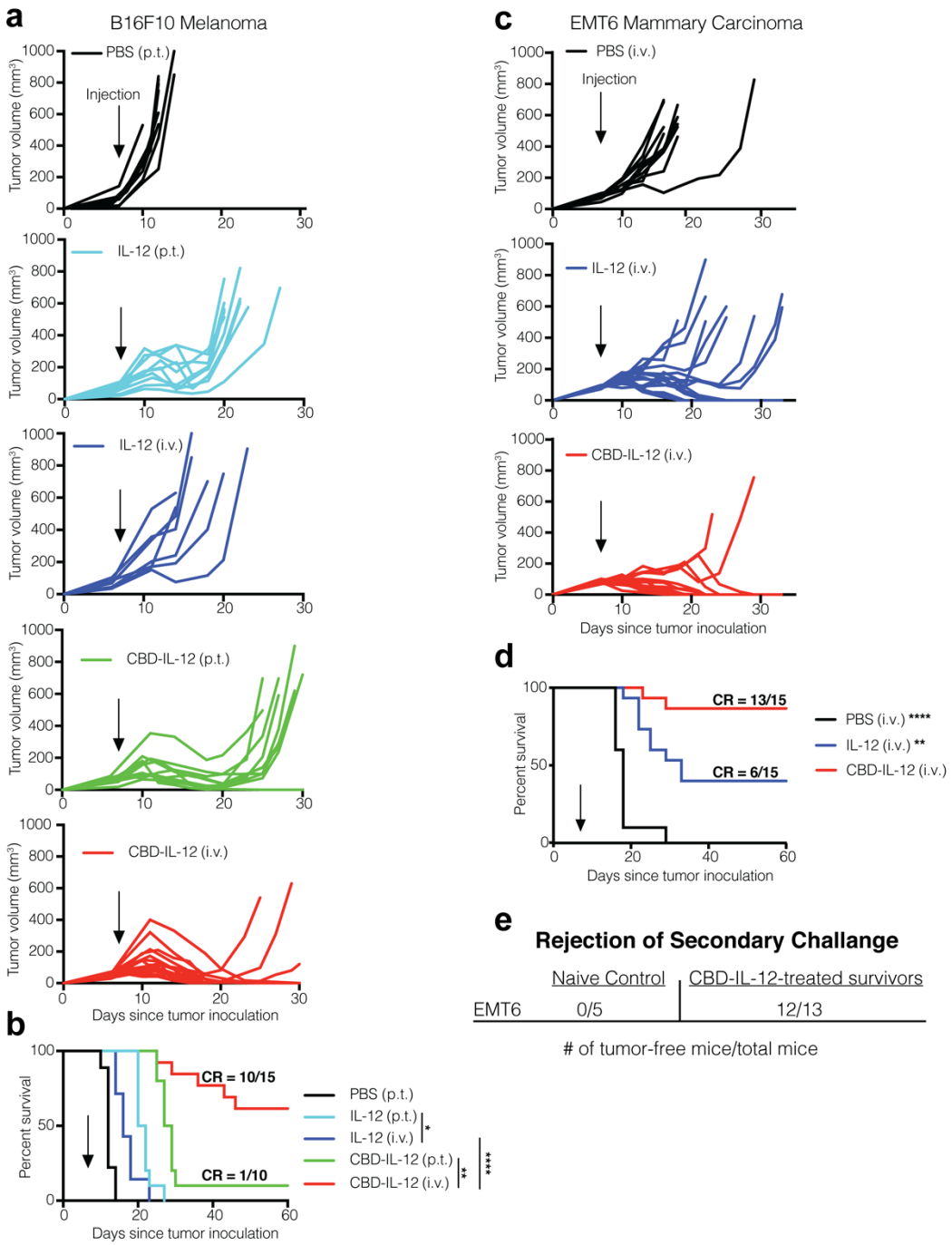

Figure 4. CBD-IL-12 induces regression of B16F10 melanoma and EMT6 mammary carcinoma. a,b, 5×10^5 B16F10 melanoma cells were inoculated intradermally on back skin and mice were treated with either PBS (p.t., n = 9), 25 µg IL-12 (p.t., n = 10), 25 µg IL-12 (i.v., n = 7), equimolar CBD-IL-12 (p.t., n = 10), or equimolar CBD-IL-12 (i.v., n = 15) once on day 7. Individual tumor curves (a) and survival curves (b) are shown. c,d, 5×10^5 EMT6 mammary carcinoma cells were inoculated into the left mammary fat pad and mice were treated i.v. with either PBS (n = 7), 25 µg IL-12 (n = 15) or equimolar CBD-IL-12 (n = 15) once on day 7. Individual tumor curves (c) and survival curves (d) are shown. Data are compiled from two independent experiments. Statistical analyses were done using log-rank (Mantel-Cox) test.

2.3.3 CBD-IL-12 Demonstrates Increased Accumulation in Tumors and Decreased Systemic Circulation and Causes Profound Changes in the Tumor Microenvironment

Recombinant CBD efficiently accumulates within tumors following i.v. administration[193]. To confirm that CBD-fused IL-12 targets the tumor, EMT6-bearing mice were injected with fluorescently labelled IL-12 or CBD-IL-12. As expected, CBD-IL-12 had significantly greater accumulation in the tumor compared to unmodified IL-12 (Fig. 5a). Increasing the molecular weight of a cytokine can alter its circulation half-life, which can potentially contribute to increased toxicity[197]. CBD-IL-12 exhibited much shorter serum half-life compared to the unmodified IL-12, despite having a larger molecular weight (Fig. 5b).

EMT6 tumours are characterized by very sparse $CD8^+$ T cell infiltration[193], a property that is shared among many human immune-excluded tumor types[198]. To visualize how the TME is re-shaped upon treatment with CBD-IL-12, we analyzed $CD8^+$ T cell infiltration by immunohistochemistry (Fig. 5c). CBD-IL-12 therapy induced extensive infiltration of $CD8^+$ T cells into the EMT6 tumor stroma, converting an immunologically cold tumor into a more inflamed one.

In melanoma patients treated with rhIL-12, the ability to maintain a robust and prolonged elevation of IFNγ is associated with positive clinical response[199] and expression of IFNγ-responsive genes in the tumor predicts clinical response to immunotherapy[200]. Treatment with CBD-IL-12 but not unmodified IL-12 induced sustained levels of B16F10 intratumoral IFNγ, the main mediator of antitumor activity of IL-12, for at least 4 days following treatment (Fig. 5d). On day 4 after treatment, the amount of intratumoral IFNγ was about 4 times higher in the CBD-IL-12-treated cohort compared to equimolar IL-12 (Fig. 5e).

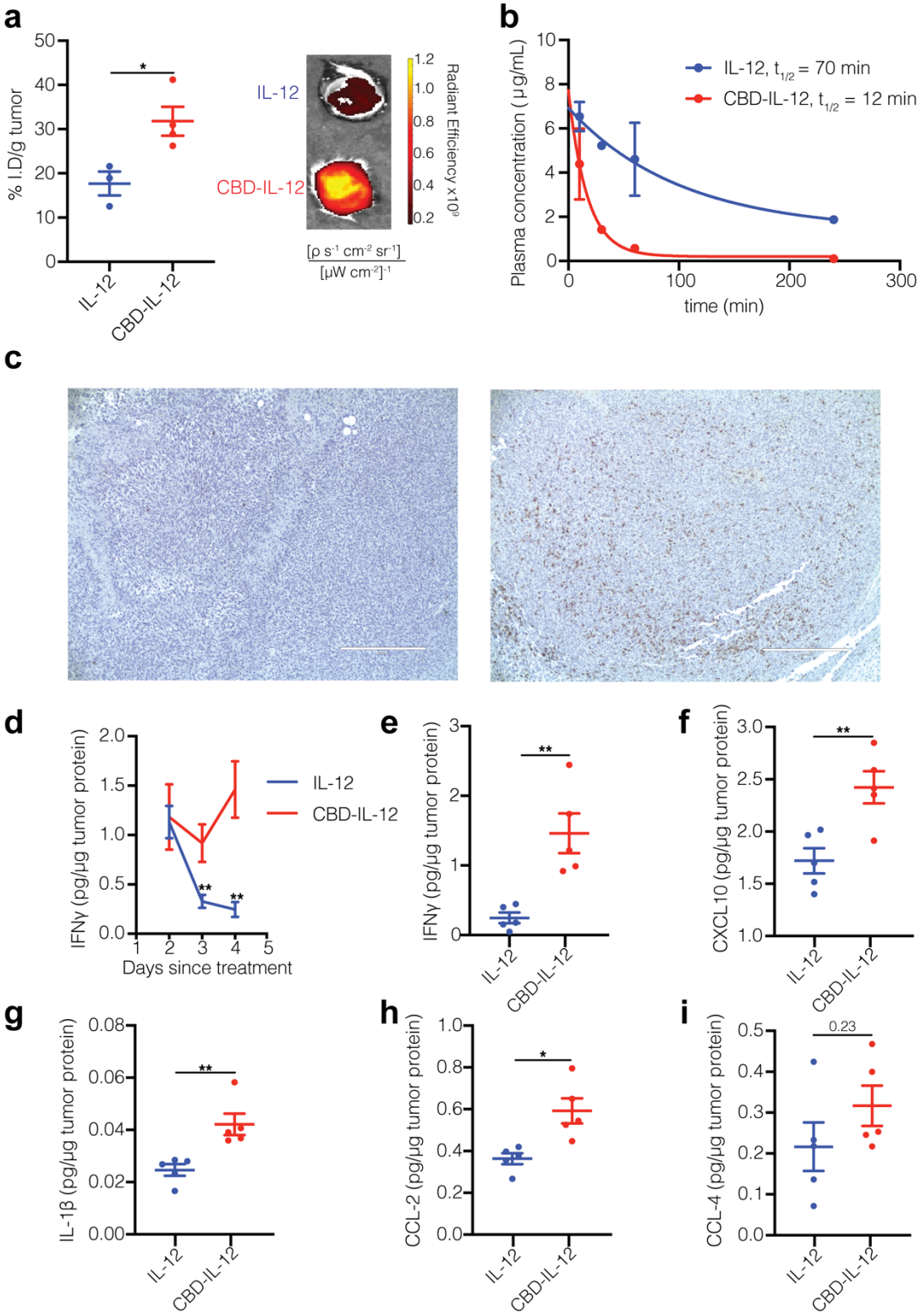

Figure 5. CBD-IL-12 induces intratumoral inflammation by rapidly localizing into the tumor. a, Mice bearing EMT6 tumors were injected i.v. with 25 μg of DyLight 650-labeled IL-12 (n = 3) or CBD-IL-12 (n = 4). Fluorescence intensity in each tumor was measured using IVIS 1 hr post injection and normalized to the weight of the tumor. (Continued on the following page.)

Figure 5, continued. CBD-IL-12 induces intratumoral inflammation by rapidly localizing into the tumor. b, Naïve C57BL/6 mice were administered 25 μg IL-12 (n = 3) or equimolar CBD-IL-12 (n = 3) via i.v. injection. Blood was collected at the indicated time points, plasma was separated and analyzed for IL-12p70 concentration via ELISA. c, Mice bearing established EMT6 tumors were injected i.v. with either PBS (left, n = 3) or 25 μg CBD-IL-12 (IL-12 molar eq., right, n = 3) and 3 days after injection, tumors were, fixed and stained with H&E and anti-mouse CD8 (brown). Scale bar = 400 μm. d, B16F10 melanoma-bearing mice were treated with either 25 μg IL-12 or equimolar CBD-IL-12 i.v. once on day 7 and tumors were harvested 2, 3 and 4 days after treatment. Tumors were homogenized for protein extraction and IFNγ levels were quantified using ELISA and normalized by total tumor protein content. For day 2, n = 9. For day 3, n = 10. For day 4, n = 5. f-i, Luminex assay was performed on day 4 tumor lysates and analyzed for indicated cytokines/chemokines (n = 5). Data are mean ± SEM. Experiments in a,b,c were performed twice, with similar results. Representative data are shown. In d, data were compiled from two independent experiments. Luminex assay was performed once on independent biological samples. Statistical analyses were done using unpaired, two-tailed t-test with Welch correction for a,f,g,h and two-tailed Mann-Whitney test for d,e,i due to nonparametric data.

Additionally, CBD-fused IL-12 increased intratumoral levels of various proinflammatory cytokines/chemokines, such as CXCL10, a chemokine that is important for effector T cell recruitment[57] and anti-angiogenesis[150], and IL-1β, a cytokine required for priming of IFNγ-producing, antigen-specific $CD8^+$ T cells[201] (Fig. 5f-i). We also quantified tumor-infiltrating lymphocytes and identified IFNγ-producing immune cells by *in vivo* injection of brefeldin A (BFA)[202] in B16F10 melanoma model (Fig. 6). Treatment with CBD-IL-12 led to increases in $CD8^+$ T cell-to-Treg ratio (Fig. 6d) and $IFN\gamma^+$ immune cells (Fig. 6g). IFNγ-producing $CD8^+$ T cells (Fig. 6h) constituted the majority of total IFNγ production (Fig. 6m).

2.3.4 CBD Fusion to IL-12 Decreases Systemic Toxicity

One of the major hurdles in clinical translation of recombinant IL-12 therapy is the toxicity induced by this cytokine[123]. Systemic IFNγ is the main contributor to the irAEs of IL-12. Experiments with $IFN\gamma R^{-/-}$ mice revealed that most of the side effects are due to IL-12-induced IFNγ[162]. Thus, we tested if CBD fusion can decrease the amount of IFNγ in circulation in tumor-

bearing mice. Serum IFNγ peaked on day 2 after treatment (Fig. 7a, left). CBD fusion significantly decreased systemic IFNγ levels across a broad range of doses (Fig. 7a, right). Notably, 50 μg of CBD-IL-12 (IL-12 molar basis) induced similar levels of serum IFNγ as did 10 μg of unmodified IL-12.

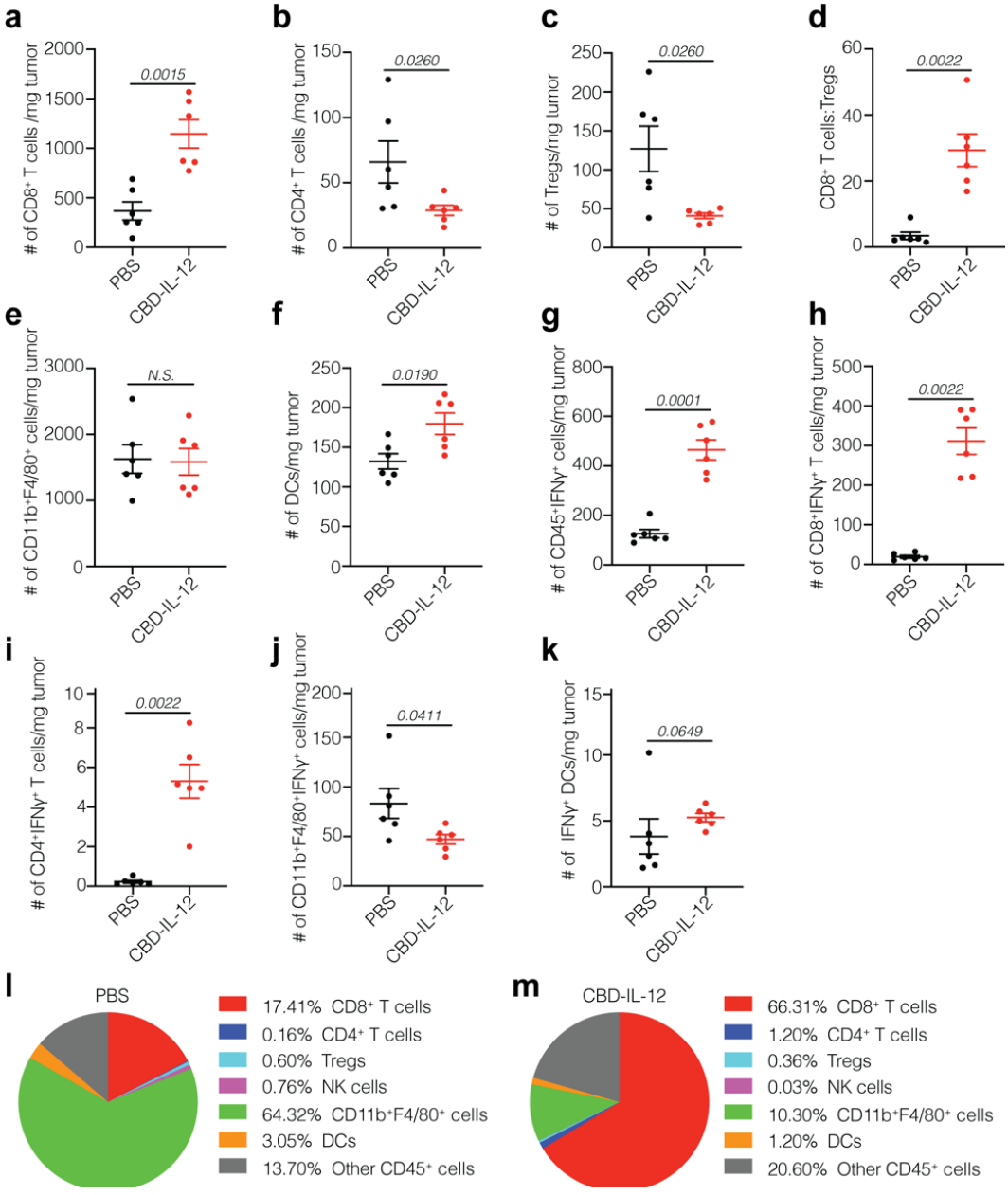

Figure 6. CD8⁺ T cells in the tumor are major producers of IFNγ upon CBD-IL-12 therapy. a-m, 5×10^5 B16F10 melanoma cells were inoculated intradermally on back skin and mice were treated with either PBS or CBD-IL-12 once on day 6 (n = 6 per group). On day 10, 250 μg of brefeldin A (BFA) was injected i.p. and tumors were collected 5 hr post BFA injection. (Continued on the following page.)

Figure 6, continued. $CD8^+$ T cells in the tumor are major producers of IFNγ upon CBD-IL-12 therapy. Tumors were processed and stained for flow cytometric analysis. Counts of $CD3^+CD8^+$ T cells (a), $CD3^+CD4^+$ T cells (b), $CD3^+CD4^+Foxp3^+$ Tregs (c) per mg of tumor. Ratio of $CD8^+$ T cells to Tregs (d). Counts of $CD11b^+F4/80^+$ cells (e) and $CD11c^+MHCII^+$ DCs (f) per mg tumor. g-k, Counts of $IFN\gamma^+CD45^+$ immune cells (g), $IFN\gamma^+CD8^+$ T cells (h), $IFN\gamma^+CD4^+$ T cells (i), $IFN\gamma^+CD11b^+F4/80^+$ cells (j) and $IFN\gamma^+$ DCs (k) per mg tumor. l,m, Pie chart representing percentages of $IFN\gamma^+$ cells within total $CD45^+$ cells after treatment with PBS (l) or CBD-IL-12 (m). Experiment was performed twice with similar results. Representative data are shown. Data are mean ± SEM. Statistical analyses were performed using unpaired, two-tailed t-test with Welch correction for a,e,f,g and a two-tailed Mann-Whitney test for b,c,d,h,i,j,k due to nonparametric data.

To further characterize the toxicity induced by cytokine treatment, we performed blood chemistry analysis on day 3 after treatment in tumor-bearing animals. Alanine aminotransferase (ALT), a liver damage marker, is upregulated in patients treated with rhIL-12[123]. In our mouse model, serum ALT activity peaked 3 days after administration of IL-12 (Fig. 7b, left). In accord with our systemic IFNγ measurements, ALT activity levels were also reduced upon CBD fusion at doses of 10 μg and 25 μg (Fig. 7b, right). We found that the toxicity of CBD-IL-12, as indicated by serum IFNγ and ALT activity, was diminished in tumor-free animals as well (Fig. 7c,d), likely due to much shorter serum half-life of CBD-IL-12[197,203] and slightly decreased bioactivity. We also found that upon treatment with unmodified IL-12, but not CBD-IL-12, amylase and lipase levels were significantly elevated, suggesting reduced pancreatic damage (Fig. 8a,b). Total serum protein levels were significantly decreased in IL-12-treated mice, indicating potential liver and kidney disorder, whereas this was not observed in the CBD-IL-12-treated cohort (Fig. 8c). No significant changes in total bilirubin, creatinine and blood urea nitrogen levels were detected at this time point (Fig. 8d-f). We did not observe tissue damage based on histology sections of lungs

and kidneys (Fig. 8g). CBD-IL-12 did not induce body weight loss upon treatment (Fig. 8h). Together, these data suggest that systemic toxicity of IL-12 is markedly reduced by CBD fusion.

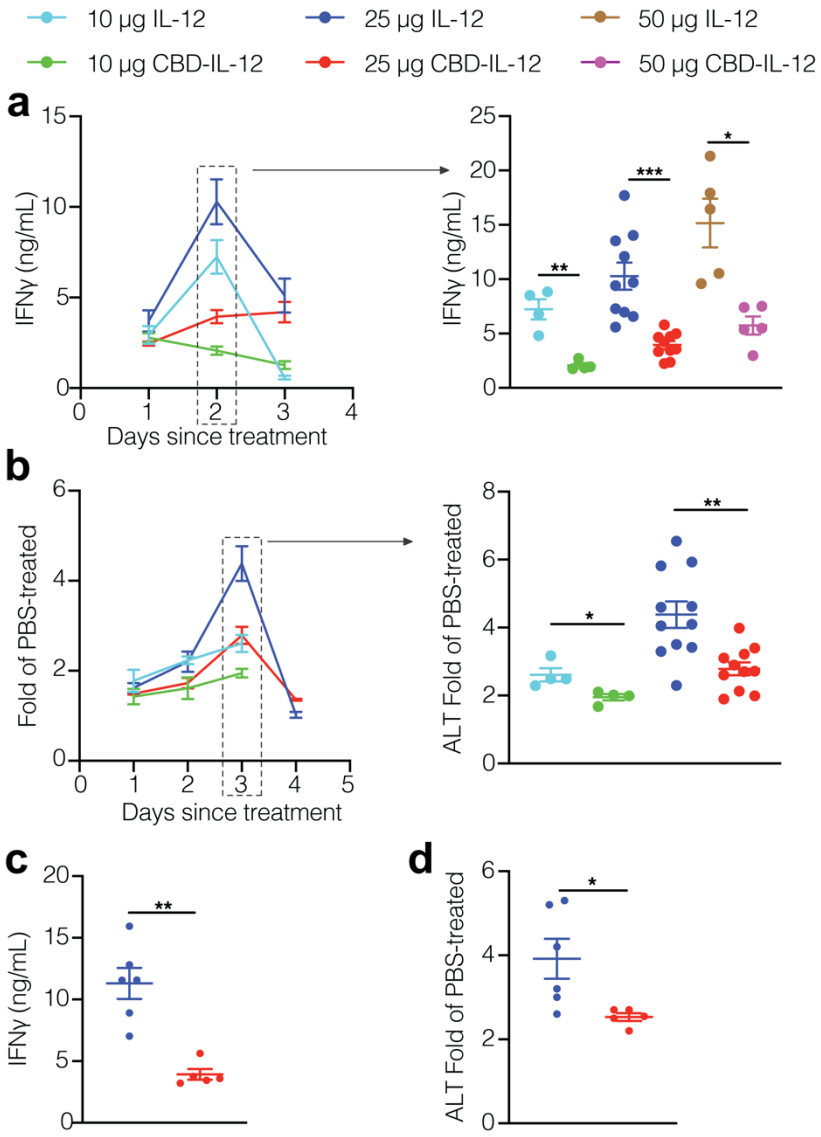

Figure 7. CBD-IL-12 minimizes irAEs in tumour-bearing and non-tumour-bearing mice. a,b, 7 days before cytokine treatment, 5×10^5 B16F10 melanoma cells were inoculated and mice were treated i.v. with either 10, 25, 50 µg IL-12 or with either 10, 25 or 50 µg CBD-IL-12 (IL-12 molar eq.) once on day 0. a, Kinetics of IFNγ levels (left) and day 2 comparison (right) in the serum are shown. b, Kinetics of serum ALT activity (left) and day 3 comparison (right) are shown. Data are represented as fold of PBS-treated. For 10 µg groups, n = 4. For 25 µg groups, n = 11. For 50 µg groups, n = 5. c,d, Naïve C57BL/6 mice received either 25 µg IL-12 or 25 µg CBD-IL-12 (IL-12 molar eq.) once on day 0 and bled on days 2 and 3 for IFNγ and ALT activity measurements, respectively. n = 5 per group. Data are mean ± SEM. Data are compiled from three independent experiments. Statistical analyses between two groups were done using unpaired, two-tailed t-test with Welch correction.

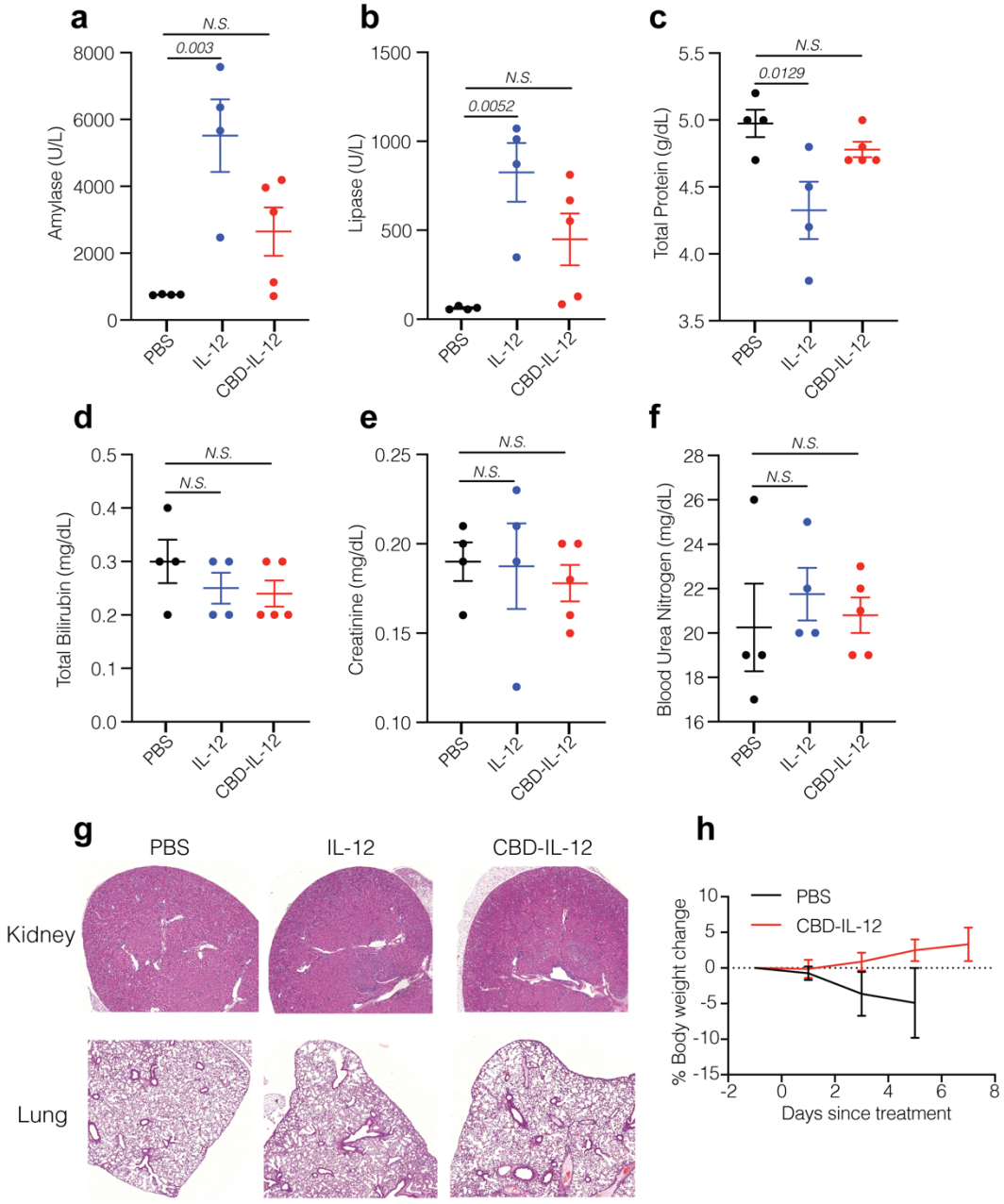

Figure 8. CBD-IL-12 decreases pancreatic damage and does not cause lung and kidney damage. a-g, B16F10-tumor bearing mice received either PBS (n = 4), 25 µg IL-12 (n = 4) or 25 µg CBD-IL-12 (IL-12 molar eq., n = 5) via i.v. injection. a-f, 3 days after treatment, serum was collected and analyzed for indicated damage markers using Vet Axcel Clinical Chemistry Analyzer. Amylase (a) and lipase (b) indicate pancreas damage. Total protein (c) and total bilirubin (d) indicate liver damage. Creatinine (e) and blood urea nitrogen (f) indicate kidney damage. g, 3 days after treatment, kidneys and lungs from mice were harvested, fixed and stained with H&E. Representative images are shown. h, Body weight change of B16F10 melanoma-bearing mice treated with PBS (n = 5) or 25 µg CBD-IL-12 (IL-12 molar eq., n = 7) via i.v. injection. Lines represent mean ± SEM. Statistical analyses were done using ordinary one-way ANOVA with Dunnett's multiple comparison test. Experiments were performed twice with similar results.

2.3.5 CBD-IL-12 Triggers Activation of Innate and Adaptive Immunity in a Metastatic Model

The advantage of CBD-IL-12 is accumulating in the tumor matrix after systemic administration, enabling treatment of both primary and metastatic tumors, including tumors in inaccessible tissues. We, thus, compared the antitumor efficacy of IL-12 and CBD-IL-12 in a B16F10 experimental lung metastasis model. 8 days after i.v. injection of B16F10 cells, metastatic nodules were visible in the lungs (Fig. 9). After treatment with IL-12 or equimolar CBD-IL-12 on day 8, lungs were harvested on day 17 for quantification of metastatic burden. A single injection of CBD-IL-12 reduced the metastatic burden ~2-fold compared with unmodified IL-12 (Fig. 9, Fig. 10a). We then investigated the immune cell infiltrates upon CBD-IL-12 therapy using flow cytometry. CBD-IL-12 treatment significantly increased the numbers of total T cells and $CD8^+$ T cells and decreased the frequency of T_{reg} cells within $CD45^+$ cells compared to unmodified IL-12 (Fig. 10b,c and Fig. 11a). Furthermore, the percentage of effector-memory $CD8^+$ T cells was significantly increased in the CBD-IL-12-treated group (Fig. 10d). The ratio of effector $CD8^+$ T cells to T_{reg}s, an indicator of successful immunotherapy, was significantly elevated in the lungs of CBD-IL-12-treated mice (Fig. 10e). Although the total number of $CD4^+$ T cells was similar across the groups, the proportion of effector $CD4^+$ T cells was enriched in the CBD-IL-12-treated group (Fig. 11b,c). We did not observe any differences in NK cells (Fig. 11d) at this time point.

IL-12 plays a key role in activating the antigen presentation pathways of professional APCs through IFNγ-dependent mechanisms[204]. Treatment with CBD-IL-12 significantly increased the numbers of dendritic cells (DCs) (Fig. 10f), including cross-presenting migratory $CD103^+$ DCs (Fig. 10g) and $CD11b^+$ DCs (Fig. 10h). Furthermore, treatment with CBD-IL-12 led to an increase in the fraction of proinflammatory $CD80^+MHCII^+$ macrophages within total macrophages (Fig. 10i)[205,206].

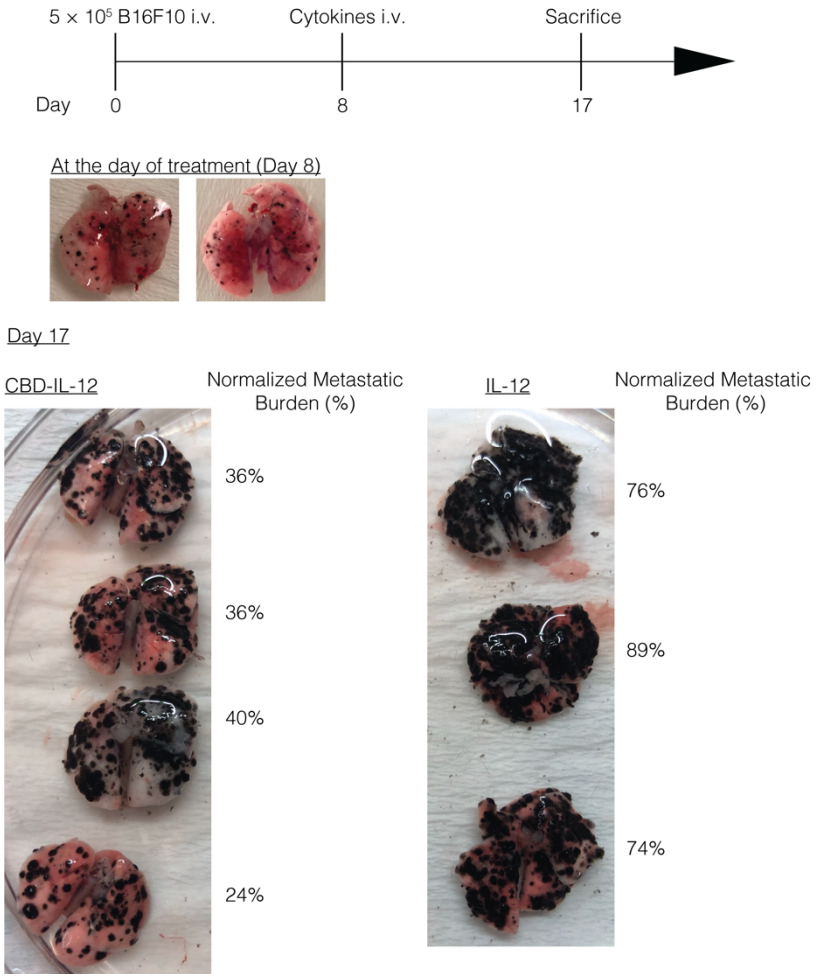

Figure 9. CBD-IL-12 decreases metastatic burden in the lungs. 5×10^5 B16F10 cells were injected i.v. on day 0. 25 µg of IL-12. (n = 3) or equimolar CBD-IL-12 (n = 4) was administered 8 days after B16F10 inoculation, when metastatic nodules were visible. Data shown in Fig. 10a are depicted. Experiment was performed twice, with similar results.

Despite similar numbers of lung-infiltrating B cells, phenotypically these cells were more proinflammatory in the CBD-IL-12 group, as they expressed significantly higher levels of MHCII and CD86 (Fig. 11e, f). Collectively, the enhanced antitumor efficacy of CBD-IL-12 in a lung metastasis model indicates that our matrix-binding technology can be applied effectively to small, disseminated nodules, in addition to primary tumours, evoking a multifaceted immune reaction.

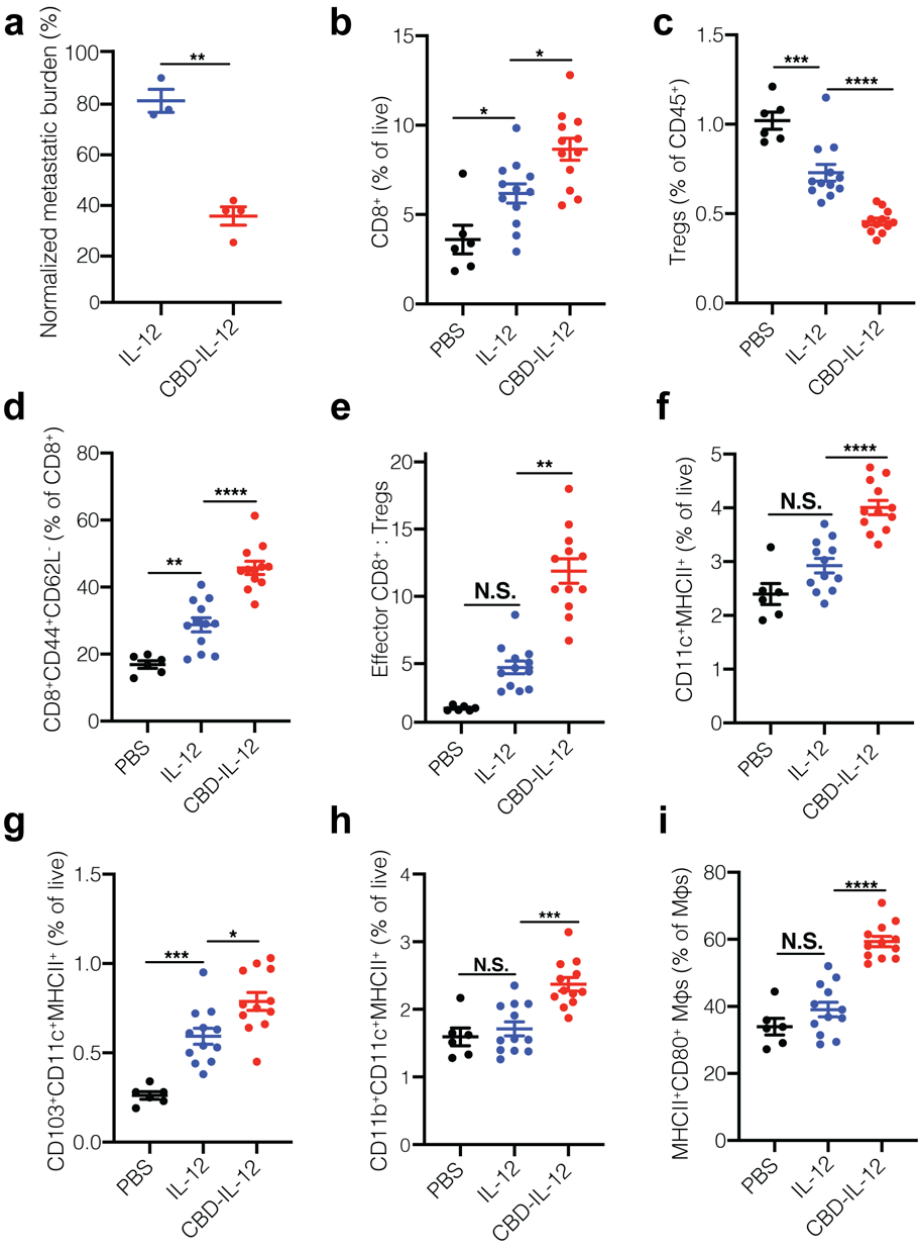

Figure 10. CBD-IL-12 decreases metastatic tumour burden by triggering activation of innate and adaptive compartments of the immune system in the pulmonary metastatic model of B16F10 melanoma. a, 5×10^5 B16F10 cells were injected i.v. on day 0. Mice were treated with either 25 µg IL-12 (n = 3) or with equimolar CBD-IL-12 (n = 4) i.v. once on day 8 and sacrificed on day 17. Metastatic burden was quantified using ImageJ software and normalized by total area of the lung. b-i, 2.5×10^5 B16F10 cells were injected i.v. on day 0. Mice were treated with either PBS (n = 6), 25 µg IL-12 (n = 12) or with equimolar CBD-IL-12 (n = 12) i.v. once on day 9 and lungs were collected on day 18. 2×10^6 live cells/well were plated for flow cytometric analysis. b, Percentages of $CD3^+CD8^+$ T cells within live cells. c, Frequency of $CD3^+CD4^+CD25^+Foxp3^+$ Tregs within lung-infiltrating immune cells (% of $CD45^+$). d, Frequency of $CD3^+CD8^+CD44^+CD62L^-$ effector $CD8^+$ T cells within total $CD8^+$ T cells. e, Ratio of effector $CD8^+$ T cells to Tregs. (Continued on the following page.)

Figure 10, continued. CBD-IL-12 decreases metastatic tumour burden by triggering activation of innate and adaptive compartments of the immune system in the pulmonary metastatic model of B16F10 melanoma. f-h, Percentages of DCs ($CD11c^+MHCII^+F4/80^-$) (f), $CD103^+$ DCs (g), and $CD11b^+$ DCs (h) within live cells. i, Frequency of $MHCII^+CD80^+$ macrophages within total macrophages (defined as $CD11b^+F4/80^+$). Lines represent mean ± SEM. Antitumor efficacy experiment (a) was performed twice, with similar results. Flow analysis was performed once on independent biological samples. Statistical analyses were done using unpaired, two-tailed t-test with Welch's correction (a), ordinary one-way ANOVA with Tukey's test for parametric data (b,c,d,f,g,h,i) and Kruskal-Wallis test followed by Dunn's multiple comparison for nonparametric data (e).

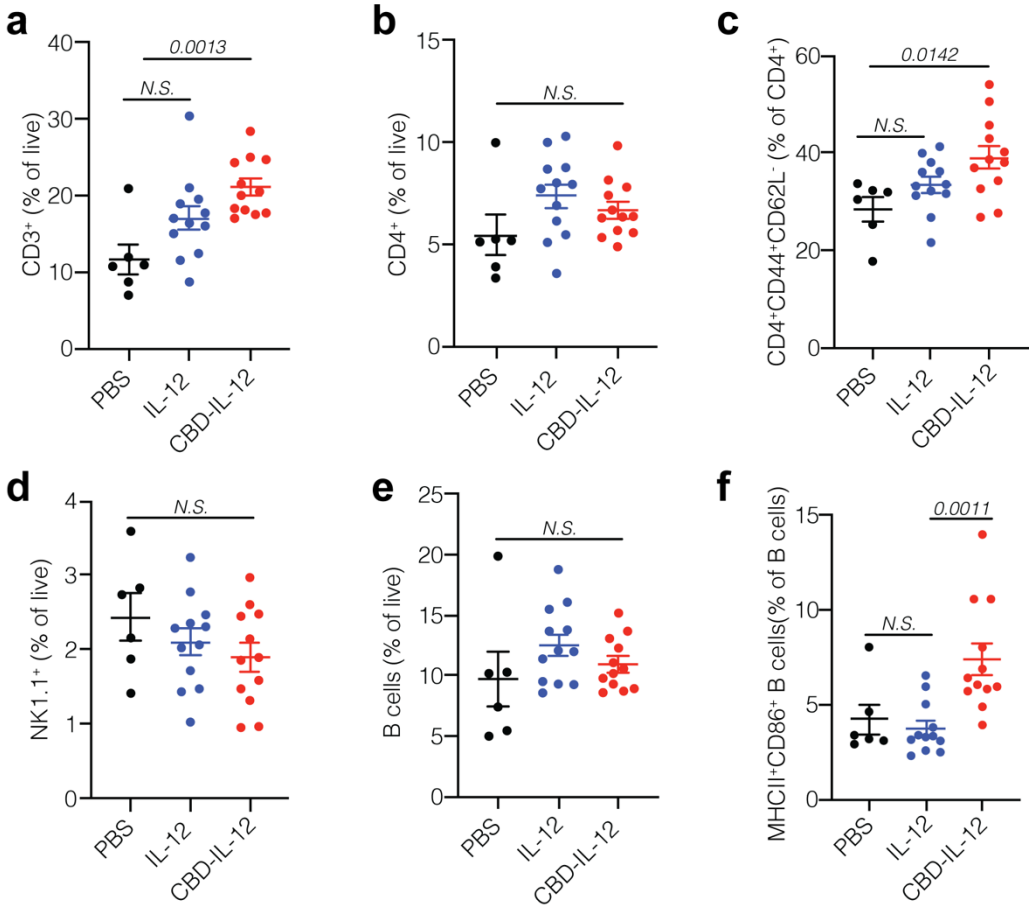

Figure 11. Immune cell infiltration in the lungs of B16F10 metastases-bearing mice. a-f, 2.5×10^5 B16F10 cells were injected i.v. on day 0. Mice were treated with either PBS (n = 6), 25 µg IL-12 (n = 12) or with 25 µg CBD-IL-12 (IL-12 molar eq., n = 12) i.v. once on day 9 and lungs were collected on day 18. 2×10^6 live cells/well were plated for flow cytometric analysis. a, Percentages of $CD3^+$ T cells within live cells. b, Percentages of $CD4^+CD3^+$ T cells within live cells. c, Frequency of $CD3^+CD4^+CD44^+CD62L^-$ effector $CD4^+$ T cells within total $CD4^+$ T cells. d, Percentages of $NK1.1^+$ cells within live cells. e, Percentages of $CD45^+CD19^+$ cells within live cells. f, Frequency of $MHCII^+CD86^+$ B cells within total B cells (defined as $CD45^+CD19^+$). Lines represent mean ± SEM. Statistical analyses were done using ordinary one-way ANOVA with Tukey's test for parametric data. For nonparametric data (f), Kruskal-Wallis test followed by Dunn's multiple comparison was used.

To determine which cell subtypes play important roles in reduced metastatic burden in this model, we conducted a correlation analysis using the data from the flow cytometry analysis and tumor burden in individual animals (Fig. 12). Antitumor efficacy correlated with higher levels of total T cell infiltration, $CD8^+$ T cell infiltration and decreased numbers of Tregs (Fig. 12a-c). Decreased metastatic burden did not correlate with increased numbers of lung-infiltrating NK cells (Fig. 12d). Effector $CD8^+$ T cell-to-T_{reg} ratio correlated strongly with diminished metastatic burden (Fig. 12e). The total number of DCs and $CD103^+$ DCs, but not $CD11b^+$ DCs, correlated with less tumor burden (Fig. 12f-h). Mice that had a higher proportion of $CD80^+MHCII^+$ macrophages had reduced metastatic burden, whereas an increased fraction of $CD86^+MHCII^+$ B cells did not correlate with improved antitumor activity in this model (Fig. 12i,j).

2.3.6 CBD-IL-12 Synergizes with CPI therapy and Elicits an Antigen-specific Immune Response

CPI therapy has revolutionized the treatment of melanoma patients, yet the majority of patients cannot achieve durable responses upon CPI immunotherapy. B16F10 melanoma responds poorly to CPI therapy[207], likely due to impaired T cell infiltration and antigen presentation. Therefore, we examined if CBD-IL-12 can synergize with CPI therapy to treat large, established B16F10 tumors. Mice bearing day 9 tumours that sized around 120 mm^3 were treated twice with either PBS, CPI (αCTLA-4 + αPD-1), CBD-IL-12, or CBD-IL-12 + CPI (Fig. 13a,b). As expected, CPI alone had little effect on the growth of B16F10 tumors. Although CBD-IL-12 alone initially induced tumor regression, no curative responses were observed in these more established tumors, in contrast to our observation in the less established (~60 mm^3) tumors. CBD-IL-12 in combination with CPI, on the other hand, elicited a more long-lasting antitumor response, resulting in 7 CR out of 12 treated mice (58%).

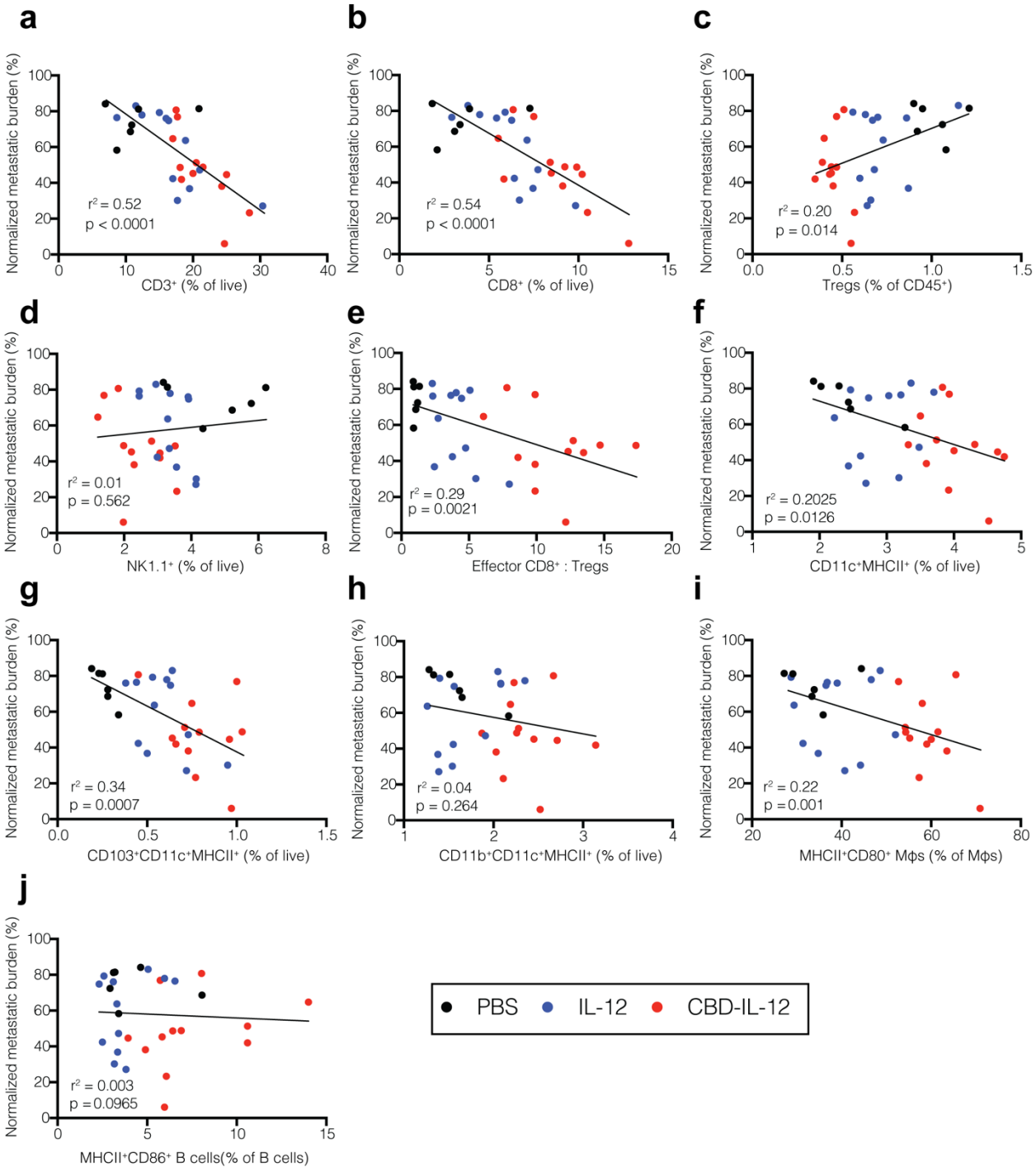

Figure 12. Correlation analysis between various immune cell infiltrates and metastatic burden. a-j, Simple linear regression analysis was performed using data presented in Fig. 10b-i and Fig. 11a-f. Mice were treated as described in Fig. 10b-i. PBS, n = 6. IL-12, n = 12. CBD-IL-12, n = 12. Metastatic burden was quantified using ImageJ software and normalized by the total area of the lung. Immune cell subsets are defined in Fig. 10 and in Fig. 11.

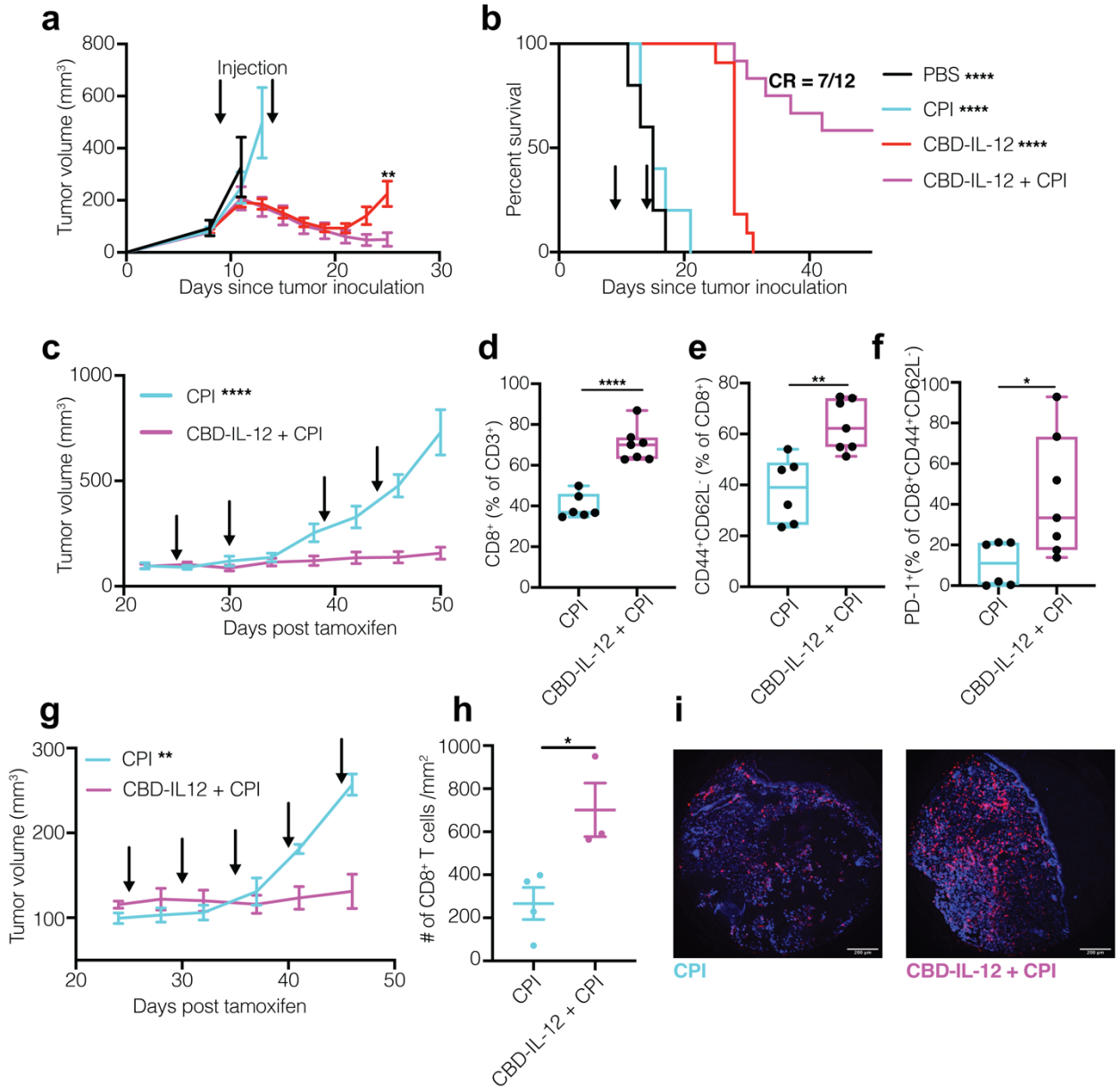

Figure 13. CBD-IL-12 synergizes with CPI and elicits tumor antigen-specific response. a,b, 5 × 10^5 B16F10 cells were inoculated intradermally on day 0. PBS (n = 5), α-PD-1 + α-CTLA-4 (CPI, 100 µg each; n = 5), 25 µg CBD-IL-12 (IL-12 molar eq., n = 11) or CBD-IL-12 + CPI (n = 12) were administered on days 9 and 14. CBD-IL-12 was administered i.v. and CPI was administered i.p. Tumour growth curves (a) and survival curves (b) are shown. c-f, *Tyr:Cre-ER*$^+$*/LSL-Braf*^{V600E}*/PTEN*$^{fl/fl}$ mice received 50 µg of 4-OH-tamoxifen on their back. Mice were treated with CPI (n = 6) or CBD-IL-12 + CPI (n = 7) on days 25, 30, 39 and 44 post tamoxifen application. d-f, On day 50, mice were bled for the analysis of circulating T cells. Box plots (median, min to max) for total CD8$^+$ T cells (% of CD3$^+$) (d), effector CD8$^+$ T cells (% of CD8$^+$ T cells) (e), and PD-1$^+$ cells (% of effector CD8$^+$ T cells) (f) are shown. g-i, *Tyr:Cre-ER*$^+$*/LSL-Braf*^{V600E}*/PTEN*$^{fl/fl}$*/βCat*^{STA} mice received 50 µg of 4-OH-tamoxifen on their back. Mice were treated with CPI (n = 4) or CBD-IL-12 + CPI (n = 4) on days 25, 30, 35, 40, 45 post tamoxifen application. (Continued on the following page.)

Figure 13, continued. CBD-IL-12 synergizes with CPI and elicits tumour antigen-specific response. h,i, On day 50, tumours from CPI (n = 4) and CBD-IL-12 + CPI (n = 3) were excised, fixed and stained with DAPI (blue) and anti-mouse CD8 (purple). For each tumor sample, $CD8^+$ T cells were counted within two different fields and average was calculated (mean ± SEM). Representative images (i) are shown. Scale bars, 200 μm. Tumor curves are represented as mean ± SEM. Experiments in a,b, were performed twice, with similar results. $Braf^{V600E}/PTEN^{fl/fl}$ and $Braf^{V600E}/PTEN^{fl/fl}/\beta Cat^{STA}$ experiments were performed once on distinct biological samples. Statistical analysis for a,c,d,e,g,h was done using unpaired, two-tailed t-test with Welch correction. For f, two-tailed Mann-Whitney test was applied due to nonparametric data. Statistical analysis for survival curve was done using log-rank test.

Our combination immunotherapy did not involve any antigen-specific approaches, such as antitumor antibodies (e.g., TA99[208]) or vaccines comprising melanoma specific antigens (e.g., Trp1, Trp2, gp100), yet it resulted in regression of large B16F10 tumors. We hypothesized that mice whose B16F10 tumors were completely eradicated by CBD-IL-12 + CPI therapy developed a strong, antigen-specific immunological memory against melanoma antigens. To test this, we performed antigen restimulation of splenocytes from these mice. On day 60 post B16F10 challenge, splenocytes were isolated from CBD-IL-12 + CPI-treated survivor mice and stimulated with several B16F10 antigens *in vitro.* Besides common B16F10 antigens (Trp1, Trp2 and gp100), we included recently reported B16F10 neoantigens[209], kif18b and cps3fl, as well as melanocyte protein (pMel) and even B16F10 exosomes to further diversify the antigenic repertoire. After splenocyte culture in the presence of the indicated antigens, supernatants were analyzed for IFNγ and IL-2 secretion by ELISA (Fig. 14 and Fig. 15). Our results demonstrate that CBD-IL-12 + CPI immunotherapy generated a broad antigen-specific response. For instance, we observed notable IFNγ responses from Trp2- and pMel-stimulated splenocytes (Fig. 14c,d), and IL-2 responses from Trp1- and B16F10 exosome-stimulated splenocytes (Fig. 15b,g).

We then assessed the efficacy of CBD-IL-12 + CPI in the autochthonous genetically engineered $Braf^{V600E}/PTEN^{fl/fl}$ melanoma model[210], which is partially responsive to CPI therapy[211]. CBD-IL-12 + CPI combination therapy elicited a robust control of established $Braf^{V600E}/PTEN^{fl/fl}$ melanoma growth, highlighting its strong efficacy in an induced autochthonous tumor model (Fig. 6c). On day 50 post tamoxifen application, mice were bled for immune profiling of circulating $CD8^+$ T cells (Fig. 13d-f). Mice treated with CBD-IL-12 + CPI combination experienced a 2-fold increase in circulating $CD8^+$ T cells compared to CPI treatment alone within the $CD3^+$ compartment (Fig. 13d).

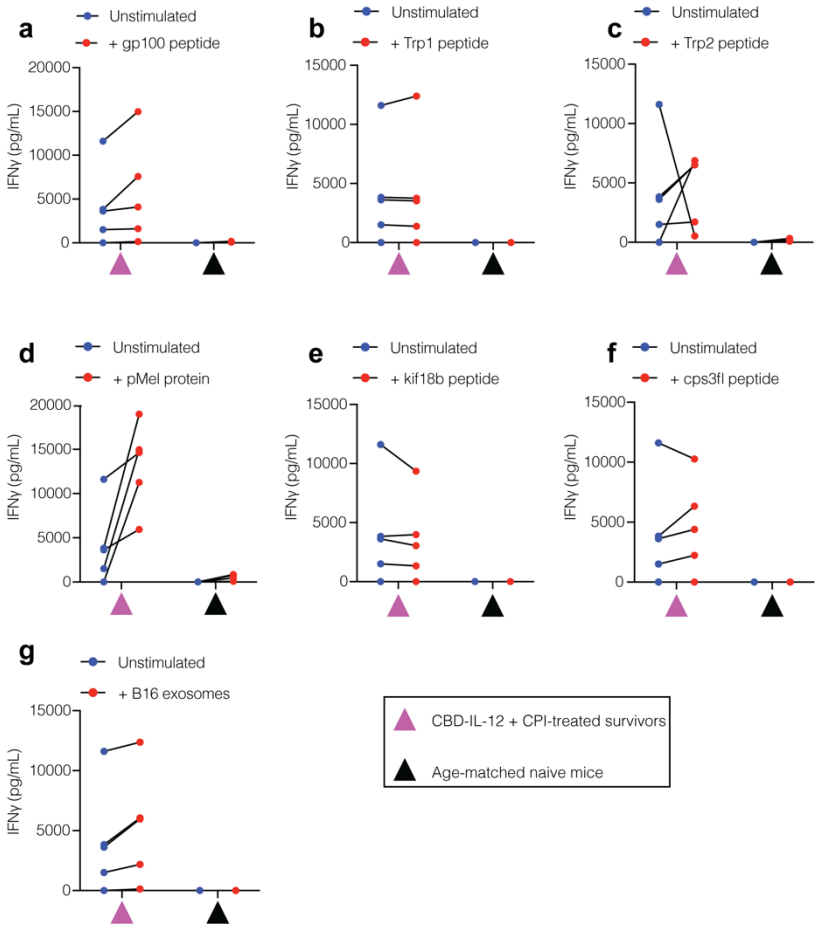

Figure 14. IFNγ secretion of splenocytes from CBD-IL-12 + CPI-treated survivors and age-matched naïve mice upon antigen restimulation. a-g, Mice were treated as described in Fig. 13a,b. Spleens from surviving mice (n = 5) or age-matched naïve mice (n = 5) were harvested and stimulated with indicated antigens. IFNγ secretion from the supernatants was detected by ELISA. Experiment was performed twice, with similar results.

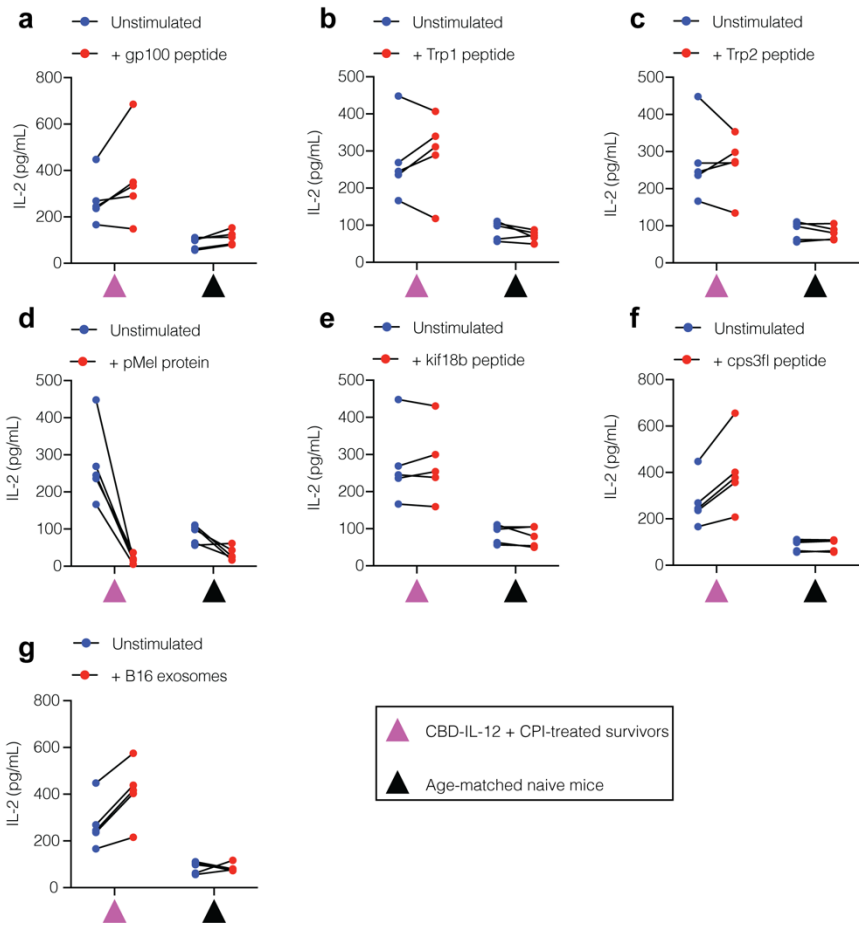

Figure 15. IL-2 secretion of splenocytes from CBD-IL-12 + CPI-treated survivors and age-matched naïve mice upon antigen restimulation. a-g, Mice were treated as described in Fig. 13a,b. Spleens from surviving mice (n = 5) or age-matched naïve mice (n = 5) were harvested and stimulated with indicated antigens. IL-2 secretion from the supernatants was detected by ELISA. Experiment was performed twice, with similar results.

Nearly 60% of circulating $CD8^+$ T cells were effector cells (Fig. 13e). $CD8^+CD44^+$ T cells expressed high levels of PD-1 (Fig. 13f), indicating that these T cells are antigen-experienced, suggesting tumor reactivity[212]. We further tested the efficacy of our combination therapy in an immune-desert, $Braf^{V600E}/PTEN^{fl/fl}/\beta Cat^{STA}$ melanoma, which overexpresses β-catenin, rendering the tumor resistant to CPI therapy[213]. In this autochthonous model, combination of CBD-IL-12 and CPI resulted in strong antitumor control (Fig. 13g) and 3-fold more $CD8^+$ T cell infiltration into the tumor compared to CPI alone. Together, these results demonstrate that the combination

of CBD-IL-12 with CPI is highly effective in both transplantable and cold, autochthonous tumor models, eliciting an effective, antigen-specific immune response.

2.4 Discussion

Immunotherapy has already shifted the paradigm of cancer treatment, yet improvement of the response rate and reduction of irAE frequency remains a major challenge[214], driving exploration of other approaches. For example, in murine models, complete remission of large established tumors treated with the combination of antitumor cell antibody, IL-2, α-PD-1, and vaccination (AIPV) has been recently reported[215]. While effective, this method restricts generality, in that tumor cell type-specific therapeutics (the antibody and vaccine antigen components) are needed. Thus, development of alternative therapies that are tumor type-agnostic and well-tolerated are being sought.

IL-12 is an attractive cytokine for activating multiple pathways of immunity. CBD-IL-12 efficiently accumulated in the tumor upon i.v. administration, resulting in increased and sustained production of intratumoral IFNγ. Elevated levels of intratumoral IFNγ accompanied by decreased systemic IFNγ suggests tumor-specific immune activation guided by CBD fusion. Prolonged induction of intratumoral IFNγ results in activation of APCs, a key step in the priming of antitumor immunity, leading to strong $CD8^+$ T cell responses[216]. This explains the durable antitumor response of CBD-IL-12 compared to unmodified IL-12. In the B16F10 melanoma model, CBD-IL-12 was much more effective than equimolar CBD-IL-2, our variant of another cytokine being explored in immunotherapy[193].

CBD-IL-12 treatment recruited $CD8^+$ T cells into EMT6 tumors, likely due to chemokine upregulation upon intratumoral IFNγ induction[217], turning an immune-excluded tumor into an

inflamed one. Because T cell recruitment is a critical challenge for immunotherapy, this suggests CBD-IL-12 can synergize with other immunotherapies. Indeed, we showed that a strong synergy exists between CBD-IL-12 and CPI therapy. This highlights the possibility to improve CPI therapy in the clinic by combination with CBD-IL-12, as means to recruit immune cells into poorly inflamed tumours.

The CBD-based tumour targeting approach relies on accessible collagen in the tumour matrix and subsequent retention of the CBD-comprising agent in the tumour stroma. Exposed collagen around the blood vessels is a result of defective vasculature formation, a phenomenon that has been observed in human cancers[218]. We explored the targeting capability of CBD fusions in multiple tumor models with varying degrees of leakiness and inflammation. For example, primary B16F10 melanoma grows very rapidly, meaning that the vasculature in this model could potentially be very disordered. To explore response in smaller, metastatic lesions, where vascular remodelling is slower, we examined the pulmonary metastatic B16F10 model, in which CBD-IL-12 was also more efficacious than the untargeted IL-12. We also showed favourable efficacy in two autochthonous models, where tumor growth is even slower, and one displays very low inflammation, boding well for the translatability of our matrix-targeting approach to human patients.

Clinical trials using systemic rhIL-12 were terminated due to intolerable irAEs[123,160]. The main toxicities observed in these clinical trials were cytokine storm (particularly, high levels of serum IFNγ) and grade 3 hepatotoxicity, defined as more than 5-fold increase of ALT over normal levels[219]. In our study, we demonstrate that CBD fusion to IL-12 significantly decreases serum IFNγ and hepatic and pancreatic damage markers and does not cause any apparent histological damage in the kidneys and lungs. This, again, suggests that CBD-IL-12 activates antitumor

immunity rather than autoimmunity in healthy tissues. The beneficial effect on toxicity is not only due to sequestration of CBD-IL-12 in the tumor, since CBD fusion to IL-12 also decreased toxicity in non-tumour-bearing mice. Decreased toxicity in tumor-free mice can be explained by slightly reduced EC_{50} and the substantially shorter serum half-life of CBD-IL-12 compared to IL-12. The faster systemic clearance may be due to binding to matrix in the liver and kidney, in which the endothelium is fenestrated, as we have previously observed[193]. In a clinical setting, this may be highly advantageous, since the toxicity benefit of CBD fusion does not fully depend on tumor burden. This may also be beneficial from a drug development point of view, as preclinical evaluation of toxicity is usually conducted in healthy animals. Thus, the accelerated clearance from the blood, paired with the prolonged pharmacodynamic effect in the tumor (as evidenced by intratumoral IFNγ elevation) is particularly attractive. Our toxicity studies demonstrate that CBD-IL-12 therapy is better tolerated than therapy with untargeted IL-12, which is encouraging for its clinical translation.

For clinical translation, one additional advantage is that CBD-IL-12 can target tumor stroma after i.v. injection, which is a common route for many clinical anticancer drugs. Other injection routes, such as intratumoral injection, have been applied to rIL-12[180,220] and plasmids encoding IL-12[221]. However, systemic injection of drugs is convenient, does not cause injection-site reactions and can target not only superficial tumours, but also inaccessible/metastatic tumors. Interestingly, we observed that i.v.-injected CBD-IL-12 was more efficacious than p.t.-administered CBD-IL-12. This may reflect more favourable accumulation of CBD-IL-12 within the tumor stroma by vascular distribution than along a needle track and associated interstitial dispersion[222] and thus greater availability of CBD-IL-12 to the immune cells.

IL-12 has also been engineered for systemic administration as a fusion protein with antibodies against components that are specifically expressed within the tumour microenvironment, such as those targeting the ED-B domain of tumour fibronectin[171] and necrosis-derived DNA[174]. These strategies are being tested in the clinic, showing promise for employing active targeting approaches[223]. A potential shortcoming in using antibody-fused cytokines, though, is that they can generate anti-drug antibody responses[224]. By our design of CBD-IL-12, a potential advantage lies in the use of a CBD protein that naturally exists in the blood, here the A3 domain from VWF, limiting the possibility of immune system recognition. The only possible immunogenic component in our design is the $(G_3S)_2$ linker connecting CBD to each of the subunits.

In conclusion, we have utilized a molecular engineering approach to improve IL-12 therapy in aspects of both efficacy and safety. CBD-IL-12 therapy induced a prolonged elevation in intratumoral IFNγ while demonstrating lower systemic IFNγ, compared to treatment with unmodified IL-12. CBD-IL-12 monotherapy eradicated immunologically cold tumors in the EMT6 breast cancer model by a single injection. Combination therapy with CPI induced regression of large and aggressive B16F10 tumors, stabilized the growth of the genetically-engineered $Braf^{V600E}/PTEN^{fl/fl}$ melanoma, and caused T cell infiltration in CPI-unresponsive $Braf^{V600E}/PTEN^{fl/fl}/\beta Cat^{STA}$ melanoma. CBD-IL-12 therapy is not antigen-specific, but capable of antigen-specific response induction. CBD-IL-12 therapy is simple and highly efficacious, holding a high translational promise.

2.5 Materials and Methods

2.5.1 Mice and Cancer Cell Lines

8 to 12-week-old C57Bl/6 female mice were purchased from Charles River Laboratory. 8 to 12-week-old Balb/c female mice were purchased from Jackson Laboratory. B16F10 and EMT6 breast cancer cell lines were obtained from ATCC and cultured according to instructions. *Tyr:Cre-ER^{+}/LSL-Braf^{V600E}/Pten$^{fl/fl}$* and *Tyr:Cre-ER^{+}/LSL-Braf^{V600E}/PTEN$^{fl/fl}$/βCat^{STA}* mice, ages 6 to 12 weeks were bred at the animal facility of the University of Chicago. All animal experiments performed in this work were approved by the Institutional Animal Care and Use Committee of the University of Chicago. Cell lines were routinely checked for mycoplasma contamination.

2.5.2 Production and Purification of Recombinant IL-12 and CBD-IL-12

For the production of wild-type IL-12, optimized sequences encoding murine p35 and p40 subunits were synthesized and subcloned into mammalian expression vector pcDNA3.1(+) by Genscript. A sequence encoding $(His)_6$ was added to the N-terminus of the p35 subunit to allow affinity-based protein purification. For the production of CBD-IL-12, sequence encoding the CBD protein (A3 domain of VWF[193]) was fused to the N-terminus of the murine p35 subunit via $(GGGS)_2$ linker and to the C-terminus of the murine p40 subunit via $(GGGS)_2$ linker. $(His)_6$ tag was added to the N-terminus of the CBD-p35 subunit. Sequences encoding CBD-p35 and p40-CBD were subcloned into mammalian expression vector pcDNA3.1(+) by Genscript. Suspension-adapted HEK-293F were maintained in serum-free Free Style 293 Expression Medium (Gibco). On the day of transfection, cells were inoculated into fresh medium at a concentration of 1×10^6 cells/mL. 500 μg/L p35 (or CBD-p35) plasmid DNA, 500 μg/L p40 (or p40-CBD) plasmid DNA were mixed with 2 mg/L linear 25 kDa polyethyleneimine (Polysciences) and co-transfected in

OptiPRO SFM medium (4% final volume). After 7 days of culture, supernatants were harvested, and purification was performed as described before[193,225]. Purified proteins were tested for endotoxin via HEK-Blue TLR4 reporter cell line and endotoxin levels were confirmed to be less than 0.01 EU/mL. Protein purity was assessed by SDS-PAGE as described previously[193,226]. Protein concentration was determined through absorbance at 280 nm using NanoDrop (Thermo Scientific).

2.5.3 MALDI-TOF MS Analysis of IL-12 and CBD-IL-12

IL-12 and CBD-IL-12 were analyzed by MALDI-TOF MS using Bruker Ultraflextreme MALDI-TOF/TOF instrument. All spectra were collected with acquisition software Bruker flexControl™ and processed with analysis software Bruker flexAnalysis™. First, a saturated solution of the matrix, α-cyano-4-hydroxycinnamic acid (Sigma-Aldrich), was prepared in 50:50 (v/v) acetonitrile:(1% TFA in water). The analyte in PBS (5 µL, 0.1 mg/mL) and the matrix solution (25 µL) were then mixed and the mixture centrifuged for 2 min (myFUGE by Benchmark). The supernatant (1 µL) was then deposited on the MTP 384 ground steel target plate. The drop was dried rapidly in a nitrogen gas flow, which resulted in the formation of uniform sample/matrix co-precipitate. All samples were analysed using high mass linear positive mode method with 5000 laser shots at a laser intensity of 75%. The measurements were externally calibrated at three points with a mix of carbonic anhydrase, phosphorylase B, and bovine serum albumin.

2.5.4 Analysis of STAT4 Phosphorylation by Flow Cytometry

Mouse $CD8^+$ T cells were purified from spleens of C57BL/6 mice using EasySep mouse $CD8^+$ T cell isolation kit (Stem Cell). Purified $CD8^+$ T cells (10^6 cells/mL) were activated in six-

well plates precoated with 2 μg/mL α-CD3 (clone 17A2, Bioxcell) and supplemented with soluble 5 μg/mL α-CD28 (clone 37.51, BioLegend) and 30 ng/mL mouse IL-2 (Peprotech) for 3 days. Culture medium was IMDM (Gibco) containing 10% heat-inactivated FBS, 1% Penicillin/Streptomycin and 50 μM 2-mercaptoethanol (Sigma Aldrich). After 3 days of culture, activated $CD8^+$ T cells were rested for 6 hrs in fresh culture medium and were transferred into 96-well plates (50,000 cells/well). Indicated amounts of IL-12 or CBD-IL-12 were applied to $CD8^+$ T cells for 20 min at 37 °C to induce STAT4 phosphorylation. Cells were fixed immediately using BD Phosflow Lyse/Fix buffer for 10 min at 37 °C and then permeabilized with BD Phosflow Perm Buffer III for 30 min on ice. Cells were stained with Alexa Fluor (AF) 647-conjugated antibody against pSTAT4 (clone 38, BD) recognizing phosphorylation of Tyr693. Staining was performed for 1 hr at room temperature (RT) in the dark. Cells were acquired on BD LSR and data were analysed using FlowJo (Treestar). Mean Fluorescence Intensity (MFI) of $pSTAT4^+$ population was plotted against cytokine concentration. Dose-response curve was fitted using Prism (v8, GraphPad).

2.5.5 Splenocyte Activation Test

To assess *in vitro* bioactivity of produced IL-12 and CBD-IL-12, splenocytes were isolated from C57Bl/6 mice, plated in 96-well plates at 5×10^5 cells/well. CBD-IL-12 or IL-12 were added to the wells at indicated concentrations. 48 h later, cell supernatants were assayed using IFNγ ELISA (Invitrogen). Culture medium was RPMI (Gibco) supplemented with 10% heat inactivated FBS, 1% Penicillin/Streptomycin, 5 mM HEPES (Gibco) and 10 ng/mL mouse IL-2 (Peprotech). Dose-response curve was fitted using Prism (v8, GraphPad).

2.5.6 Surface Plasmon Resonance (SPR) Against Collagen I and III

SPR measurements were made with a Biacore X100 SPR system (GE Healthcare). Collagen I or collagen III (EMD Millipore) was immobilized via amine coupling on a CM5 chip (GE Healthcare) for ~1000 resonance units (RU) according to the manufacturer's instructions. CBD-IL-12 was flowed for 90 sec (for collagen I) and for 30 sec (for collagen III) at increasing concentrations in the running buffer at 30 μL/min. The sensor chip was regenerated with 50 mM NaOH for every cycle. Specific binding of CBD-IL-12 to collagen was calculated automatically using the response to a non-functionalized channel as a reference. Binding curves were fitted using BIAevaluation software (GE Healthcare). Binding results were fitted with Langmuir binding kinetics (1:1 binding with drifting baseline Rmax local).

2.5.7 Detection of IL-12 and CBD-IL-12 Binding to Human Melanoma Cryosections

Human melanoma cryosections were purchased from OriGene Technologies. Cryosections were first blocked with 2% BSA in PBS-T at RT. 50 μg of CBD-IL-12 (IL-12 molar basis) or IL-12 were added to sections and incubated for 2 hr at RT. Tissues were then stained with the following primary antibodies: rabbit anti-human collagen I antibody (Abcam, ab34710), mouse anti-human CD31 antibody (Abcam, ab119339) and rat anti-mouse IL-12p70 antibody (from mouse IL-12p70 ELISA kit, Invitrogen). Tissues were then stained with the following fluorescently-labelled secondary antibodies: Alexa 594-labeled donkey anti-rat IgG (Jackson Immunoresearch Labs, 712586153), Alexa 488-labeled donkey anti-mouse IgG (Jackson Immunoresearch Labs, 715546151), and Alexa 647-labeled donkey anti-rabbit IgG (Jackson Immunoresearch Labs, 711605152). Secondary antibody staining was performed for 1 hr. Sections were then covered with Prolong Gold Antifade Mountant containing DAPI (Thermo Fisher) and

sealed with a coverslip. Microscopy was performed using IX73 microscope (Olympus) and images were processed using ImageJ software (NIH).

2.5.8 Antitumor Efficacy of IL-12 and CBD-IL-12

For the primary tumour model of B16F10 melanoma, 5×10^5 B16F10 cells were inoculated intradermally on the back of the female C57Bl/6 mouse in 30 μL sterile PBS. For the EMT6 mammary carcinoma model, 5×10^5 EMT6 cells were injected into the left mammary fat pad of female Balb/c mice in 30 μL sterile PBS. For the secondary challenge of EMT6 carcinoma, 5×10^5 EMT6 cells were injected in the opposite mammary fat pad, 3 months after the primary challenge. Dose and schedule of the cytokines and antibodies are described in the figure legends. For i.v. routes, compounds were injected in 100 μL volume. For p.t. injection, compounds were administered in 30 μL volume. The volume of the tumour was calculated using the following formula: (height) × (width) × (thickness) × (π/6). Mice were sacrificed when the tumour volume reached 1000 mm^3 and/or based on humane end-point criteria.

2.5.9 Tumor Accumulation in EMT6-bearing Mice and Biodistribution in Tumor-free Mice

IL-12 or CBD-IL-12 protein was fluorescently labelled using DyLight 650 NHS ester (Thermo Fisher), and unreacted dye was removed by a Zebaspin spin column (Thermo Fisher) according to the manufacturer's instruction. For tumour accumulation experiments, total of 5×10^5 EMT6 cells re-suspended in 50 μL of PBS were injected subcutaneously into the mammary fat pad on the right side of each Balb/c mouse. When the tumour reached approximately 500 mm^3, 25 μg DyLight 650 labelled IL-12 or 25 μg (16.5 μg IL-12 basis) DyLight 650-labeled CBD-IL-12 was injected i.v. 1 hr after injection, mice were sacrificed, and tumours were extracted and imaged with the Xenogen IVIS Imaging System 100 (Xenogen) under the following

conditions: f/stop: 2; optical filter excitation 640 nm; emission 670 nm; exposure time: 0.5 sec; small binning. The protein amount in each tumour was calculated based on a standard dilution series of IL-12 or CBD-IL-12 labelled with DyLight650 and normalized to the weight of the tumour. Biodistribution experiment in tumour-free mice was performed similarly.

2.5.10 Pharmacokinetics of IL-12 and CBD-IL-12

Naïve C57Bl/6 mice received doses of 25 μg of IL-12 or 25 μg of CBD-IL-12 (IL-12 equimolar basis) i.v. (n = 3/group). 15 μL of blood was collected from the tail 10 min, 30 min, 60 min and 240 min after injection in EDTA-containing heparinized tubes. Plasma was separated and concentrations of IL-12 and CBD-IL-12 were measured by IL-12p70 ELISA (Invitrogen). Plasma was diluted 5000 times for 10, 30 and 60 min, and 1000 times for 240 min. In-house-produced IL-12 and CBD-IL-12 served as the standards for the ELISA. No endogenous IL-12 could be detected from PBS-injected mice. Plasma half-life was estimated assuming one phase decay model (v8, GraphPad Prism).

2.5.11 Serum IFNγ and Blood Chemistry Analysis

For assessment of serum IFNγ, mice were treated with either IL-12 or molar equivalent of CBD-IL-12. On indicated days, blood was collected in protein low-binding tubes (Eppendorf). Blood was allowed to clot overnight at 4°C. The next day, serum was obtained by centrifugation at 4000 × g for 10 min. IFNγ ELISA (Invitrogen) was performed on the sera (18x dilution) according to manufacturer's instructions. No endogenous IFNγ could be detected at this dilution from PBS-treated animals. Alanine aminotransferase (ALT) assay (Sigma-Aldrich) was performed using sera (4x dilution), according to manufacturer's instructions. Serum amylase, lipase, total

protein, total bilirubin, creatinine, and blood urea nitrogen were determined using Vet Axcel blood chemistry analyser (Alfa Wasserman).

2.5.12 Histological Assessment of Lungs and Kidney

5×10^5 B16F10 cells were inoculated intradermally on the back of the female C57Bl/6 mouse in 30 μL sterile PBS. Mice received doses of 25 μg of IL-12 or 25 μg of CBD-IL-12 (IL-12 equimolar basis) i.v. 7 days after inoculation. 3 days after cytokine treatment, lungs and kidneys were collected and fixed with 2% paraformaldehyde. After paraffin embedding, blocks were cut into 5 μm sections, followed by staining with hematoxylin and eosin. Slides were imaged by EVOS FL Auto (Life Technologies). Slides were blindly assessed for tissue damage.

2.5.13 Histological Analysis of EMT6 Tumors

5×10^5 EMT6 cells were injected into left mammary fat pad of Balb/c mice. 7 days later, mice were treated with either PBS or CBD-IL-12 (25 μg IL-12 basis). On day 10, tumors were collected and fixed with 2% paraformaldehyde. After paraffin embedding, blocks were cut into 5 μm sections, followed by staining with hematoxylin and eosin. After deparaffinization and rehydration, tissue sections were treated with target retrieval solution (S1699, DAKO) and heated in steamer for 20 min at temperature >95 C°. Tissue sections were incubated with anti-mouse CD8 antibody (clone 4SM15, eBioscience) for 1 hr incubation at RT in a humidity chamber. Following TBS wash, the tissue sections were incubated with biotinylated anti-rat IgG (10 μg/mL, Vector laboratories) for 30 min at RT. The antigen-antibody binding was detected by Elite kit (PK-6100, Vector Laboratories) and DAB (DAKO, K3468) system. Slides were imaged by EVOS FL Auto (Life Technologies).

2.5.14 Intratumoral IFNγ Kinetics and Intratumoral Cytokines/chemokines

Mice bearing day 7 B16F10 tumours were treated with either IL-12 or CBD-IL-12 and sacrificed on day 9, 10 and 11. Tumours were collected, snap frozen in liquid nitrogen and stored at -80°C. Tumours were then homogenized in Tissue Protein Extraction buffer (T-PER, Thermo Fisher). Protease inhibitor tablets (Roche) were added to the T-PER buffer. Tumours were placed in Lysing Matrix D tubes (MP Bio). Homogenization was performed using FastPrep tissue homogenizer (MP Bio). IFNγ was quantified using IFNγ ELISA (Invitrogen) and normalized by total protein content. Total protein content was measured using Pierce BCA Protein Assay (Thermo Fisher). Luminex assay was performed using Milliplex assay (Millipore Sigma) according to manufacturer's instructions.

2.5.15 Analysis of In Vivo IFNγ-producing Cells in B16F10 Melanoma

Protocol for identification of *in vivo* IFNγ-producing immune cells has been described previously[202]. 5×10^5 B16F10 cells were inoculated intradermally on the back of the female C57Bl/6 mouse in 30 μL sterile PBS. 6 days after tumour implantation, mice were treated with either PBS or CBD-IL-12. On day 10, mice were given 250 μg of brefeldin A (BFA) (Sigma Aldrich) in 500 μL via intraperitoneal (i.p.) injection. 5 hr after BFA injection, tumours were harvested and digested for 30 min at 37 °C. Digestion medium was DMEM (Gibco) supplemented with 5% FBS, 2.0 mg/mL Collagenase D (Sigma), 20 μg/mL DNAse I (Worthington Biochemical), 1.2 mM $CaCl_2$ and 10 μg/mL BFA. Single-cell suspensions were prepared using a 70 μm cell strainer (Fisher). 20 mg of tumour was plated per well. For antibodies against surface targets, the staining was done in PBS with 2% FBS. For intracellular targets, staining was performed according to the manufacturer's protocols (00-5523-00, Thermo Fisher Scientific).

Following anti-mouse antibodies were used: CD45 Allophycocyanine-Cy7 (APC-Cy7) (clone 30-F11, BioLegend), CD3ε BUV395 (clone 145-2C11, BD), CD4 Brilliant Violet (BV) 785 (clone RM4-5, BioLegend), CD8α BV510 (clone 53-6.7, BioLegend), Foxp3 PE (clone MF23, BD), CD11c PE-Cy7 (clone N418, BioLegend), NK1.1 BV605 (clone PK136, BioLegend), MHCII PerCP-Cy5.5 (clone, M5/114.15.2, BioLegend), CD11b BUV737 (clone M1/70, BD), IFNγ APC (clone XMG1.2, BioLegend), F4/80 AF488 (clone BM8, BioLegend), CD103 eFluor 450 (clone 2E7, ThermoFisher). Cell viability was determined using the fixable viability dye eFluor 455UV dye (65-0868-14, eBioscience). Cells were acquired on BD LSR and data were analysed using FlowJo (Treestar).

2.5.16 Pulmonary Metastatic Model of B16F10 Melanoma

For the pulmonary metastasis model of B16F10 melanoma, female C57Bl/6 mice were injected i.v. with 5×10^5 B16F10 cells in 100 μL volume. Mice received treatment 8 days after the challenge. On day 17, the lungs were perfused with PBS and imaged for quantification of the metastatic burden. To assess the metastatic burden, we quantified the total area of B16 nodules using ImageJ (NIH) and normalized it by the total area of the lung.

2.5.17 Generation of Single-cell Suspension from the Lungs for Flow Cytometry

Mice were perfused through the left ventricle of the heart with 10 mL of PBS. The lung lobes were then isolated and digested. Briefly, the lobes were cut into small pieces with a scissor and then digested in 5 mL DMEM (Gibco) with 5% FBS, 1 mg/mL Collagenase IV (Worthington Biochemical), 3.3 mg/mL Collagenase D (Sigma), 20 μg/mL DNAse I (Worthington Biochemical) and 1.2 mM $CaCl_2$ for 60 min at 37 °C on a shaker. After quenching the media with 5 mM EDTA (Gibco), single-cell suspensions were prepared using a 70 μm cell strainer (Fisher). Finally, red

blood cells were lysed with 1 mL ACK lysing buffer (Gibco) for 90 sec and neutralized with 10 mL DMEM media with 5% FBS.

2.5.18 Analysis of Immune Infiltrates in the Pulmonary Metastatic Model of B16F10 Melanoma

Single cell suspensions were counted after digestion and 2×10^6 live cells/well were plated for staining. For antibodies against surface targets, the staining was done in PBS with 2% FBS. For intracellular targets, staining was performed according to the manufacturer's protocols (00-5523-00, Thermo Fisher Scientific). The following anti-mouse antibodies were used for flow cytometry: CD45 APC-Cy7 (clone 30-F11, BioLegend), CD3ε BUV395 (clone 145-2C11, BD), Foxp3 AF647 (clone MF23, BD), CD8α AF488 (clone 53-6.7, BioLegend), CD4 BV785 (clone RM4-5, BioLegend), CD25 PE (clone PC61, BioLegend), CD44 PerCP-Cy5.5 (clone IM7, BioLegend), CD62L BUV737 (clone MEL-14, BD), NK1.1 BV421 (clone PK136, BD), CD103 PE (clone 2E7, BioLegend), CD86 BV510 (clone GL-1, BioLegend), F4/80 APC (clone A3-1, AbD Serotec), CD11c PE-Cy7 (clone N418, BioLegend), CD11b BV786 (clone M1/70, BD), CD80 BUV737 (clone 16-10A1, BD Biosciences), CD19 BUV395 (clone 1D3, BD), Ly6G FITC (clone 1A8-Ly6g, eBioscience), Ly6C BV605 (clone HK1.4, BioLegend), MHCII PerCP-Cy5.5 (clone, M5/114.15.2, BioLegend), CD8α PacBlue (53-6.7, BioLegend). Cell viability was determined using the fixable viability dye eFluor 455UV dye (65-0868-14, eBioscience).

2.5.19 Combination Therapy with Checkpoint Inhibitors (CPI)

In combination therapy studies, 5×10^5 B16F10 cells in 30 μL were injected intradermally on the back of the female C57Bl/6 mice. PBS, 25 μg CBD-IL-12 (IL-12 molar eq.) and CPI were administered on days 9 and 14 post B16F10 challenge. CPI stands for a combination of 100 μg α-

CTLA-4 (9H10, Bioxcell) and 100 μg α-PD-1 (29F.1A12, Bioxcell). CPI was administered via i.p. injection. CBD-IL-12 was administered via i.v. injection.

2.5.20 Induction of Autochthonous Braf^{V600E}/PTEN$^{fl/fl}$ and Braf^{V600E}/PTEN$^{fl/fl}$/βCat^{STA} Tumor Models, Analysis of Circulating T cells and Immunofluorescence

8-12-week old *Tyr:Cre-ER^{+}/LSL-Braf^{V600E}/Pten$^{fl/fl}$* mice were shaved on the back and 5 μL of 4-OH-tamoxifen was applied topically. 25 days after tamoxifen application, mice were divided into two groups. CPI-treated cohort received α-PD-1 and α-CTLA-4 i.p., 100 μg each. CBD-IL-12 + CPI-treated mice received 25 μg of CBD-IL-12 (IL-12 molar eq.) via i.v. injection and indicated amount of CPI via i.p. injection. The same treatment was given on days 30, 39 and 44 for a total of 4 treatments. Tumor size was measured using calipers and the tumor volume was calculated according to the following formula: (width) × (height) × (thickness) × π/4. For the analysis of circulating CD8^{+} T cells from Braf^{V600E}/PTEN$^{-/-}$ mice, mice were bled on day 50 post tamoxifen induction. Red blood cells were lysed with ACK lysing buffer (Gibco). Cell viability was assessed with the Fixable Viability Dye eFluor 455 UV from eBioscience. Antibodies used for flow cytometry included: CD45 APC-Cy7 (clone 30-F11, BioLegend), CD3 FITC (clone 145-2C11, BioLegend), CD8α PE-Cy7 (clone 53-6.7, BioLegend), CD62L BUV737 (clone MEL-14, BD), CD44 PerCP-Cy5.5 (clone IM7, BD) and PD-1 BV605 (clone 29F.1A12, BioLegend). Induction of melanoma in *Tyr:Cre-ER^{+}/LSL-Braf^{V600E}/Pten$^{fl/fl}$/βCat^{STA}* mice was performed similarly[227]. 25 days after tamoxifen application, mice received either CPI or CBD-IL-12 + CPI (dosed as mentioned above). Treatment was given every 5 days until day 45. On day 50, tumors were excised and fixed in formalin-free zinc fixative (BD) for 2 days. Tumors were placed in 15% sucrose (in TBS) for 2 days followed by 30% sucrose (in TBS) for additional 2 days. Tumors were

frozen and 7-μm sections were obtained. Cryosections were blocked with 0.5% casein in TB for 1 hr at RT. Sections were then incubated with rat anti-mouse CD8α (clone 53-6.7, BD) for 2 hr at RT. Slides were incubated with AF594-conjugated goat anti-rat (Jackson ImmunoResearch Labs) for 1 hr at RT. Sections were then covered with Prolong Gold Antifade Mountant containing DAPI (Thermo Fisher) and sealed with a coverslip. Microscopy was performed using IX73 microscope (Olympus). Image processing and $CD8^+$ T cell counting was performed using ImageJ software (NIH).

2.5.21 Antigen Restimulation of Splenocytes

Spleens were harvested from mice that cured B16F10 melanoma by CBD-IL-12 + CPI immunotherapy or from age-matched naïve mice. Splenocytes were plated at a density of 10^6/well in 200 μL of DMEM (Gibco) supplemented with 10% heat-inactivated FBS and 1% Penicillin/Streptomycin. Peptides used in restimulation assays were synthesized by Genscript and the sequences were as follows: gp100 (KVPRNQDWL), Trp1 (CRPGWRGAACNQKI), Trp2 (SVYDFFVWL), kif18b (PSKPSFQEFVDWE**N**VSPELNSTDQPFLP, mutation K739N), cps3fl (EFKHIKAFDRTFA**N**NPGPMVVFATPGML, mutation D314N). Bold amino acid represents the mutation. pMel (SILV) protein was purchased from Abnova. Peptides were used at a concentration of 2 μg/mL, pMel protein was used at 5 μg/mL. B16 exosomes were produced in-house and used at 50 μg/mL. All samples were run in duplicate. Cells were cultured for 72 hr. Cell culture supernatants were collected and immediately assayed for IL-2 and IFNγ by ELISA (Invitrogen).

2.5.22 Statistical Analysis

Statistical analysis between groups was performed using Prism software (v8, GraphPad). For multiple comparisons of means, one-way ANOVA followed by Tukey's post hoc test was used

if the data were found to be parametric by Brown-Forsythe test. For nonparametric data with multiple groups, Kruskal-Wallis test followed by Dunn's multiple comparison test was used. For comparison between two groups, a two-tailed Student's t-test with Welch's correction was used. For nonparametric data with two groups (determined by F test), Mann-Whitney test was used. Survival curves between two groups were analyzed using the log-rank (Mantel-Cox) test.

2.6 Author Contributions

Aslan Mansurov, Jun Ishihara, Melody A. Swartz, and Jeffrey A. Hubbell designed the experiments and wrote the manuscript. Aslan Mansurov and Jun Ishihara performed the experiments. Peyman Hosseinchi assisted with the pulmonary metastasis model. Lambert Potin assisted with the autochthonous melanoma model. Tiffany M. Marchell assisted with the antigen restimulation experiment and prepared B16F10 exosomes. Ako Ishihara blindly evaluated histological sections. John-Michael Williford and L. Taylor Gray assisted with tumour experiments. Aaron T. Alpar assisted with blood chemistry analysis. Michal M. Raczy assisted with and analysed MALDI-TOF data.

2.7 Funding

This work was funded by the Chicago Immunoengineering Innovation Center (CIIC), University of Chicago.

2.8 Conflict of Interest

J.I., A.I., M.A.S., J.A.H., are inventors on U.S. Provisional Patent applications 62/638,520, 28/984,351, and 62/727,156. J.I., A.I., M.A.S., J.A.H. are founders and shareholders in Arrow

Immune Inc., which is developing the technology presented in this report, and M.A.S., J.A.H. have leadership roles in that company. Other authors declare no competing of interests.

2.9 Acknowledgments

I would like to thank all the members of the Hubbell and Swartz laboratories for helpful discussions and suggestions. I would like to thank Suzana Gomes for taking care of all the cancer cell lines used in this study. I would like to thank Ani Solanki from University of Chicago's Animal Resource Center for performing tail-vein injections. I would like to thank University of Chicago's Flow Cytometry Core, particularly David Leclerc for maintaining the instruments as well as his help with Luminex Assay.

CHAPTER 3:

ELIMINATING THE IMMUNOTOXICITY OF INTERLEUKIN-12 THROUGH PROTEASE-SENSITIVE MASKING

3.1 Abstract

Checkpoint inhibitor (CPI) immunotherapy demonstrates modest efficacy against immunologically 'cold' or immune-excluded tumors. Although interleukin-12 (IL-12) is a powerful antitumor cytokine that enables activation and recruitment of immune cells into tumors, its widespread use in the clinic has been hindered due to severe immune-related adverse events (irAEs). An ideal IL-12 therapy would restrict the proinflammatory effects of IL-12 to the tumor site, while limiting its exposure in the periphery. Here, we solved the IL-12 toxicity challenge by exploiting the preferential overexpression of proteases in the tumor to engineer tumor-selective, masked IL-12. A receptor-based masking domain was fused to IL-12 via a protease-cleavable linker and prevented IL-12 from signaling systemically, whereas proteolytic cleavage of the linker domain by tumor-associated enzymes restored the biological activity of IL-12. We demonstrate that intravenously (i.v.) administered, masked IL-12 produces strong therapeutic effects through remodeling the immune-suppressive microenvironment and renders CPI-resistant tumors responsive, while systemic irAEs are eliminated, boosting the therapeutic index of this promising cytokine.

3.2 Introduction

CPI therapies, such as anti-programmed death 1 (αPD-1) antibodies, have demonstrated tremendous success in the treatment of certain cancer types; yet increasing evidence suggests that these therapies are largely ineffective in immunologically 'cold' tumors due to a lack of sufficiently primed $CD8^+$ T cells[228,229]. The immunosuppressive tumor microenvironment (TME) is dominated by regulatory T (T_{reg}) cells and protumorigenic macrophages (i.e., M2-like macrophages)[230]. Patients who respond well to CPI therapies tend to exhibit a T helper 1- (Th1)-biased TME, driven by the expression of interferon-γ (IFNγ) and IFNγ-related genes[231,232]. An approach that can safely transform immunologically cold tumors into inflamed tumors would both increase the proportion of patients responding to CPI therapies and offer alternative treatment options for CPI non-responders. Remodeling of such an immunosuppressive TME can be achieved by proinflammatory cues that induce Th1 cytokine and chemokine profiles.

Immunostimulatory agents, including proinflammatory cytokines, may overcome $CD8^+$ T cell exclusion by triggering a wide array of inflammatory responses, leading to infiltration and activation of antitumor $CD8^+$ T cells[233]. IL-12 is an attractive cytokine that stimulates both the innate and the adaptive immune system and is able to activate antigen-presenting cells (APCs)[138]. We have previously seen potency of an engineered IL-12 in multiple murine cancer models including complete remissions, which, in our hands, was stronger than other clinically-approved immunotherapies such as CPIs or IL-2[234]. The antitumor effects of IL-12 are mostly mediated by IFNγ, a direct downstream molecule that is secreted by T and natural killer (NK) cells[235].

Despite these strong therapeutic effects, clinical trials examining recombinant IL-12 have failed due to dose-limiting irAEs[123], as anticancer activity was observed at or above the maximum

tolerated dose[169]. Numerous attempts of IL-12 clinical translation have been made for over three decades, yet no IL-12 products have been approved in the clinic. Therefore, solving the challenge presented by IL-12-induced irAEs is crucial to translate this powerful antitumor cytokine to the clinic.

After IL-12 administration, cytokine release syndrome and liver damage have been observed in clinical trials[123]. A high concentration of circulating IFNγ mediates these side effects, as evidenced by studies conducted in mice lacking the IFNγ receptor[162] and by administration of neutralizing antibodies against IFNγ[159,160]. Yet IFNγ is indispensable for antitumor efficacy of IL-12 therapy[235], signifying the importance of developing an engineered IL-12 that would localize the therapeutic effects to the tumor site while sparing healthy tissues and the circulation.

Here, we designed a protein engineering approach as a solution for IL-12's toxicity and remodeling the cold TME. We describe a strategy to block the signaling activity of IL-12 by masking the receptor binding site of IL-12 with a fused receptor domain, attached via a tumor protease-cleavable linker, so that the activity is selectively restored upon proteolytic cleavage in the TME.

3.3 Results

3.3.1 In Vitro Activation of Masked IL-12 Leads to Fully Restored IL-12 Bioactivity

Latency can be conferred to cytokines upon fusion of domains that inhibit cytokine-receptor interaction[236,237]. We hypothesized that fusion of the first two fibronectin type-III domains of the mouse IL-12 receptor β1 (IL12Rβ1; Q20-A261, referred to herein as the mask, "M") to IL-12 would render it inactive (Fig. 16a and Fig. 17a).

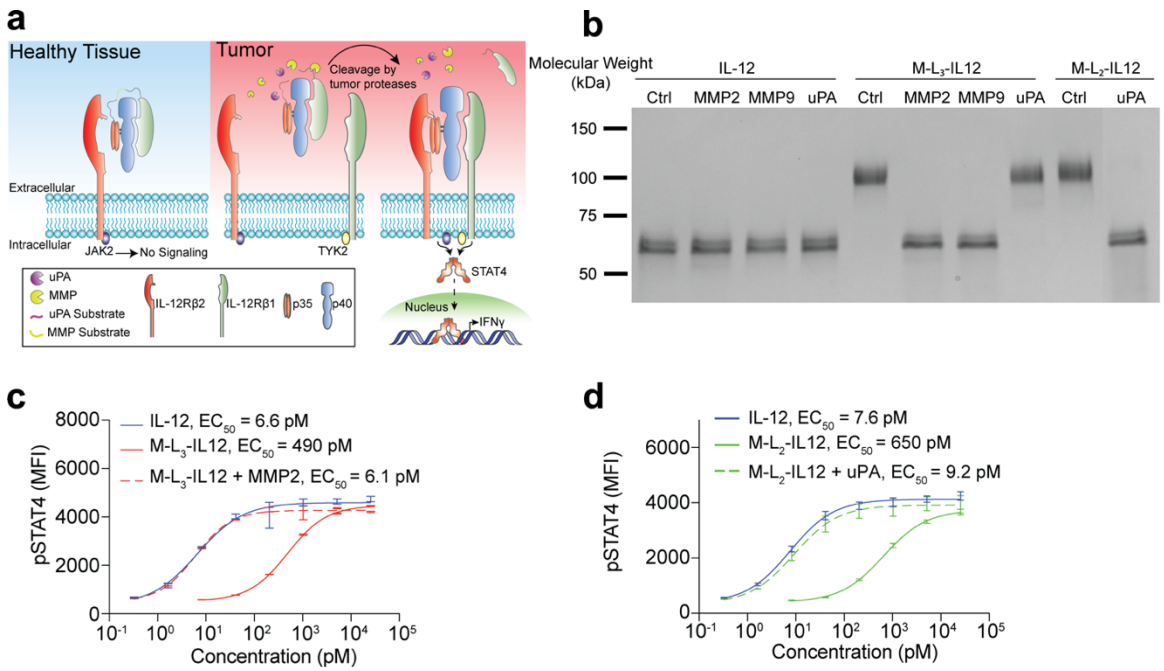

Figure 16. Masked IL-12 fully regains activity upon treatment with recombinant proteases. a, Schematic of masked IL-12 in healthy tissues (no signaling) and in the tumor, with the mask being cleaved by various tumor-associated proteases. b, SDS-PAGE analysis of the cleavage of masked IL-12 variants by recombinant proteases. IL-12 (50 μg/ml; 0.84 μM), M-L_3-IL12 (0.84 μM) or M-L_2-IL12 (0.84 μM) were incubated with activated MMP2 (2 μg/ml), MMP9 (5 μg/ml) for 30 min at 37°C or with uPA (10 μg/ml) for 2.5 hr at 37°C. c,d, Dose-response relationship of phosphorylated STAT4 (pY693) with MMP2-treated M-L_3-IL12 (c) and uPA-treated M-L_2-IL12 (d) in preactivated primary mouse $CD8^+$ T cells (n=2 per condition, technical duplicates). Data are mean ± s.e.m. Experiments were performed at least twice, with similar results. Representative data are shown.

By exploiting the heterodimeric structure of IL-12, we fused the mask to the N-terminus of p35 subunit and co-transfected it with p40, with the idea that the mask would engage p40[238]. By varying the distance between M and p35, we determined that the optimal length of the linker that prevented aggregation/dimerization is approximately 45 amino acids (Fig. 17b-d).

We then expressed several masked IL-12 variants with various linker substrates (L_n, where n refers to linker ID) that can be cleaved by different tumor proteases (Table 1).

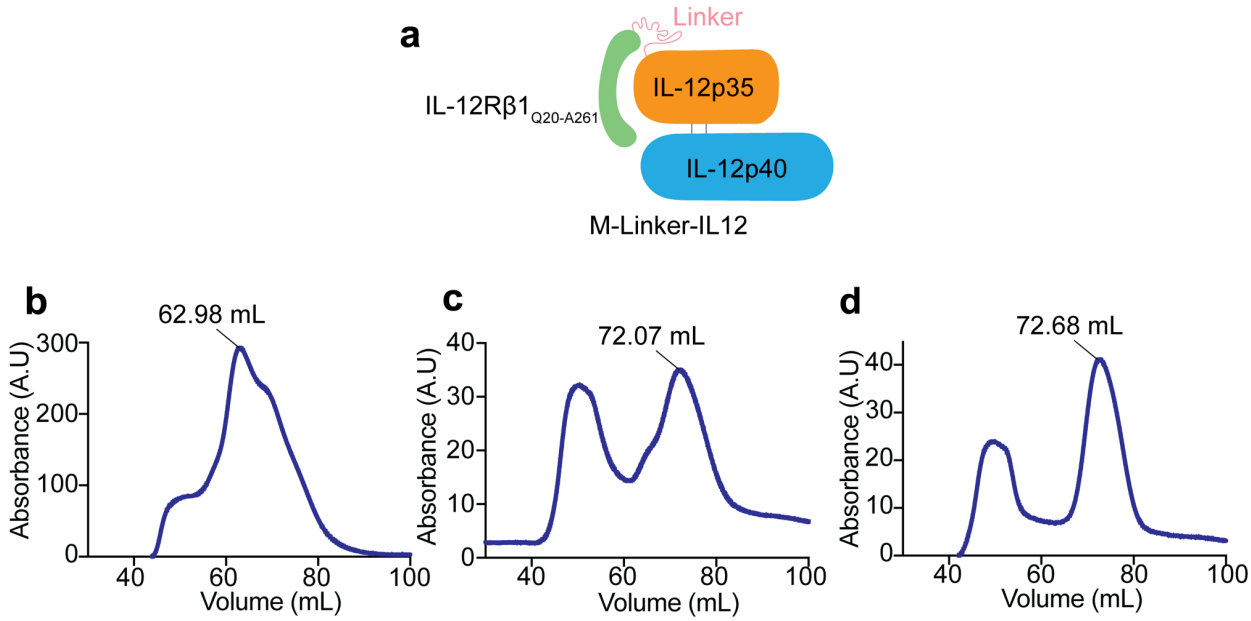

Figure 17. Size exclusion chromatograms of affinity-purified masked IL-12 constructs. a, Molecular schematic of masked IL-12. $(His)_6$-tagged masked IL-12 constructs containing $(G_3S)_2$ (b), $(G_3S)_5$ (c), and $(G_3S)_{11}$ (d) linkers between the mask and the p35 were expressed in HEK-293F cells and purified via Nickel-based affinity purification as described in the Materials and Methods. After elution, samples were loaded on size-exclusion columns to determine the optimal length between the mask and the p35 subunit. The masked IL-12 molecule in (b) was mostly eluted in aggregates and dimers. The masked IL-12 molecule in (c) still contained some dimer population at ~65 mL whereas the masked IL-12 containing $(G_3S)_{11}$ linker (d) was homogenous monomer.

We characterized proteolytic cleavage of masked IL-12 molecules, namely M-L_3-IL12 and M-L_2-IL12, by treating them with recombinant matrix metalloproteinase-2 (MMP2), MMP9 or urokinase-plasminogen activator (uPA), a serine protease (SP), and visualized the cleavage by SDS-polyacrylamide gel electrophoresis (SDS-PAGE) (Fig. 16b).

Table 1. Amino acid sequences of the linkers used. Cleavable domains are bolded.

Linker ID	Amino acid sequence	Cleaved by
L_1	$(GGGS)_2$(**HPVGLLAR**)$_3(GGGS)_2$	MMP2, MMP9
L_2	$(GGGS)_2$(SGL**LSGRSDNH**)$_3(GGGS)_2$	uPA, matriptase, legumain
L_3	$(GGGS)_2$(**VPLSLYSG**)$_3(GGGS)_2$	MMP2, MMP7, MMP9
L_4	$(GGGS)_2$(**VPLSLYSG**)$(GGGS)_2$(**LSGRSDNH**)$_2(GGGS)_2$	MMPs and SPs
L_6	(**HPVGLLARVPLSLYSG**)$_2$(**LSGRSDNH**)$(GGGS)_2$	MMPs and SPs

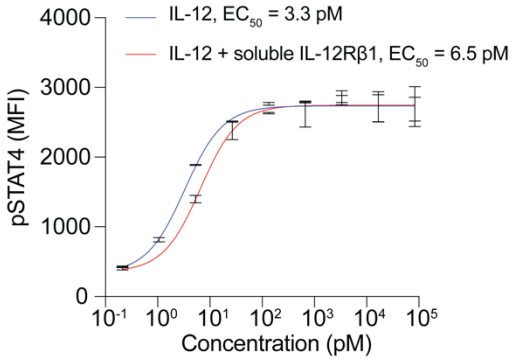

Figure 18. Soluble IL-12Rβ1 does not abrogate the IL-12 signaling when kept at equimolar ratio. IL-12 and extracellular portion of IL-12Rβ1 were incubated for 1 hr at 37 C° to allow for complex formation. Pre-activated primary mouse $CD8^+$ T cells were then treated for 15 min with either IL-12 alone or the preincubated complex of IL-12 and the IL-12Rβ1 (1:1 molar ratio, where the mixture of IL-12 + IL-12Rβ1 was serially diluted). Cells were fixed and stained for pSTAT4 as described in the Materials and Methods. Data are mean ± s.e.m; n = 2 per condition (technical duplicates); each dilution of cytokine or cytokine-receptor complex was assessed in duplicate. The experiment was performed twice, with similar results.

Proteolytic cleavage of MMP-sensitive M-L_3-IL12 (containing three repeats of $VPLSLYSG^{239}$) and SP-sensitive M-L_2-IL12 (containing three repeats of $LSGRSDNH^{240}$) yielded molecules corresponding to the molecular weight of IL-12. These proteases did not digest wild-type IL-12 itself. To test whether the cleaved molecules are bioactive, we stimulated preactivated mouse $CD8^+$ T cells with either latent or activated forms of masked IL-12 (Fig. 16c,d). The intact masked IL-12 variants were ~80-fold less active than the unmodified IL-12 as measured by phosphorylation of signal transducer and activator of transcription 4 (STAT4) in the absence of proteases, whereas proteolytic activation of engineered IL-12 fully restored the activity. To test if the mask does not associate with IL-12 after proteolytic cleavage, we incubated the soluble, extracellular portion of IL-12Rβ1 with IL-12 at 1:1 molar ratio and performed STAT4 stimulation assay (Fig. 18). Soluble IL-12Rβ1 only minimally affected IL-12 signaling, suggesting that the mask inhibits IL-12 bioactivity only when it is intact. Furthermore, the affinity of IL-12 for the full receptor complex

(IL-12Rβ1 + IL-12Rβ2) is much higher than for either subunit alone[241], suggesting that our mask's inhibitory activity will be insignificant after cleavage.

We investigated the cleavage of several linkers by MMP2 *in vitro* and found that HPVGLLAR[239] (substrate in M-L_1-IL12) is a more reactive substrate than VPLSLYSG[239] (substrate in M-L_3-IL12; Fig. 19) as visualized by SDS-PAGE analysis. Furthermore, cleavage efficiency was dependent on the number of substrate repeats, as the construct containing only one VPLSLYSG (M-L_4-IL12) was processed less efficiently than the construct containing three repeats of VPLSLYSG (M-L_3-IL12; Fig. 19). SP-sensitive M-L_2-IL12, containing three repeats of LSGRSDNH, was not cleaved by any of the MMPs tested (Fig. 20). Thus, we designed one additional linker, L_6, that contains two repeats each of both MMP substrates and one repeat of SP substrate. M-L_1-IL12 and M-L_6-IL12 exhibited similar reactivity against MMP-2 (Fig. 21).

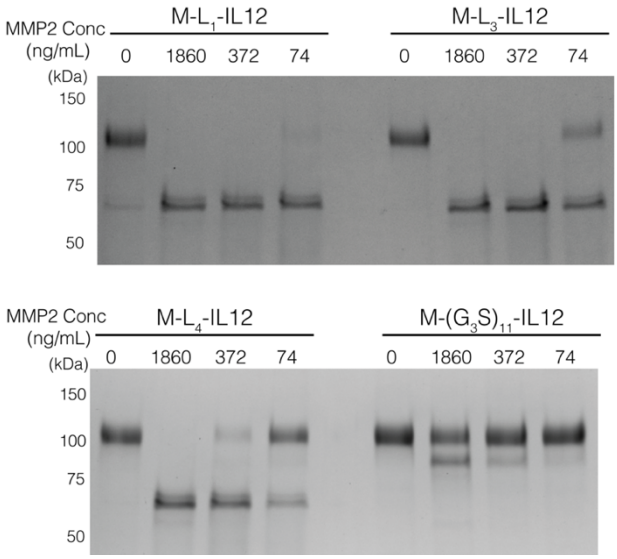

Figure 19. Protease substrates affect the efficiency of linker cleavage by MMP2. Masked IL-12 constructs were diluted to a final concentration of 75 μg/mL (or 0.83 μM) and incubated with the indicated concentration of activated MMP2 for 30 min at 37°C. Samples were then immediately denatured by boiling with non-reducing SDS-PAGE buffer and loaded for electrophoresis. MMP2 at 74 ng/mL (~1 nM) fully cleaves M-L_1-IL12, whereas some intact M-L_3-IL12 is present. M-L_4-IL12 contains only one MMP-responsive substrate, and thus, is only partially processed at that MMP2 concentration. Some degradation of M-$(G_3S)_{11}$-IL12 is observed, which may be due to nonspecific cleavage of IL-12Rβ1. The experiment was performed twice with similar results.

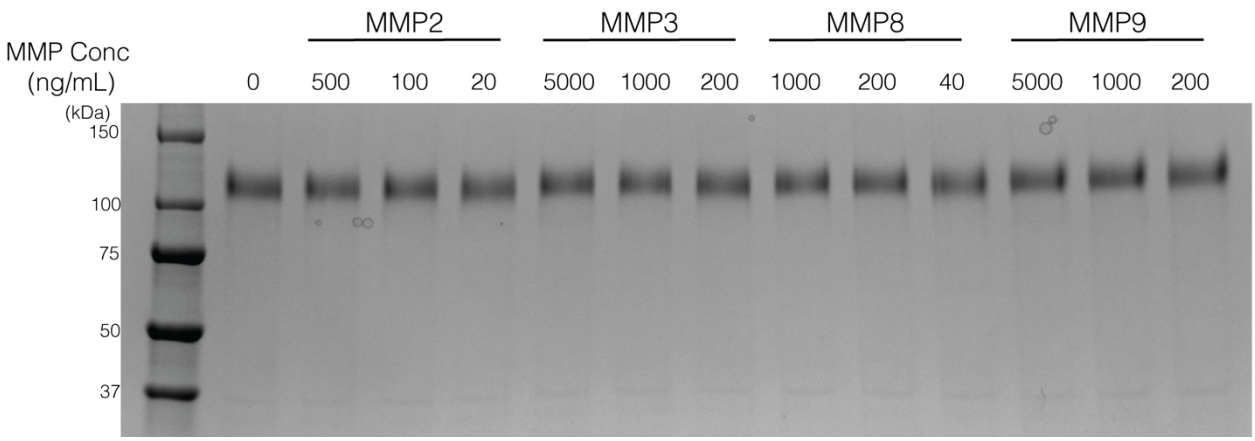

Figure 20. MMPs do not cleave SP-sensitive M-L_2-IL12. M-L_2-IL12, which contains three repeats of LSGRSDNH, was diluted to 45 μg/mL (or 0.5 μM) and incubated with indicated MMPs for 1 hr at 37 °C. Samples were then loaded on the gel and analyzed. Experiment was performed twice. with similar results.

3.3.2 Masked IL-12 Retains Antitumor Activity in Syngeneic Models and Causes Immunological Remodeling of TME

We then sought to examine the antitumor efficacy elicited by three masked IL-12 variants in the B16F10 mouse melanoma model to determine the optimal linker. MMP/SP-reactive M-L_6-IL12 induced a significantly stronger antitumor response compared to SP-only reactive M-L_2-IL12 and a slightly stronger response compared to M-L_4-IL12, which contained one MMP-sensitive substrate (VPLSLYSG) and two SP-sensitive substrates (Fig. 22a). This result suggests that the enzymatic sensitivity of the linker is a crucial design parameter for producing an adequate antitumor response[242], and thus we decided to perform further *in vivo* investigation of M-L_6-IL12.

We first compared the antitumor efficacy of M-L_6-IL12 to that of unmodified IL-12 in subcutaneous MC38 colon adenocarcinoma. In this immunogenic model, both molecules exhibited high efficacy, achieving a 100% complete response (CR) rate (Fig. 22b). We then assessed the antitumor efficacy of M-L_6-IL12 in the CPI-unresponsive, orthotopic EMT6 triple-negative breast cancer model, which is characterized by transforming growth factor β signature and T cell

exclusion[243]. Treatment with M-L_6-IL12, but not αPD-1 antibody, led to significant extension of survival with 8 CR out of 9 mice when compared to saline-treated mice (Fig. 22c). To investigate the efficacy of the combination of M-L_6-IL12 and αPD-1, we treated mice bearing established orthotopic B16F10 melanomas, a cold model, with either αPD-1, M-L_6-IL12 or combination of the two (Fig. 22d). Addition of αPD-1 to M-L_6-IL12 resulted in significantly extended survival when compared to either treatment alone. αPD-1 treatment alone had no major effect on the survival of these mice, consistent with previous observations[234].

To study the mechanism behind the therapeutic action of M-L_6-IL12, we characterized immunological responses in B16F10 melanoma, a model that displays low basal inflammation. We collected the tumors from treated mice for intratumoral cytokine/chemokine profiling and lymphocyte infiltration analysis. IFNγ, which is the direct downstream molecule and main mediator of antitumor activity of IL-12[244], was equally upregulated in the TME in both treatment groups (Fig. 23a). Tumor necrosis factor-α (TNFα), which supports cancer cell cycle arrest[245], was also equally expressed between the two groups (Fig. 23b).

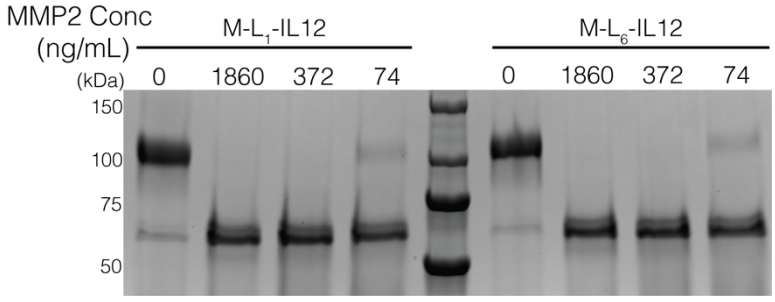

Figure 21. M-L_1-IL12 and M-L_6-IL12 are equally cleaved by MMP2. Indicated amounts of activated MMP2 was incubated with 150 μg/mL (1.67 μM) of masked IL-12 constructs for 30 min at 37 °C. Molecules were then loaded on the gel and analyzed. Experiment was performed twice with similar results.

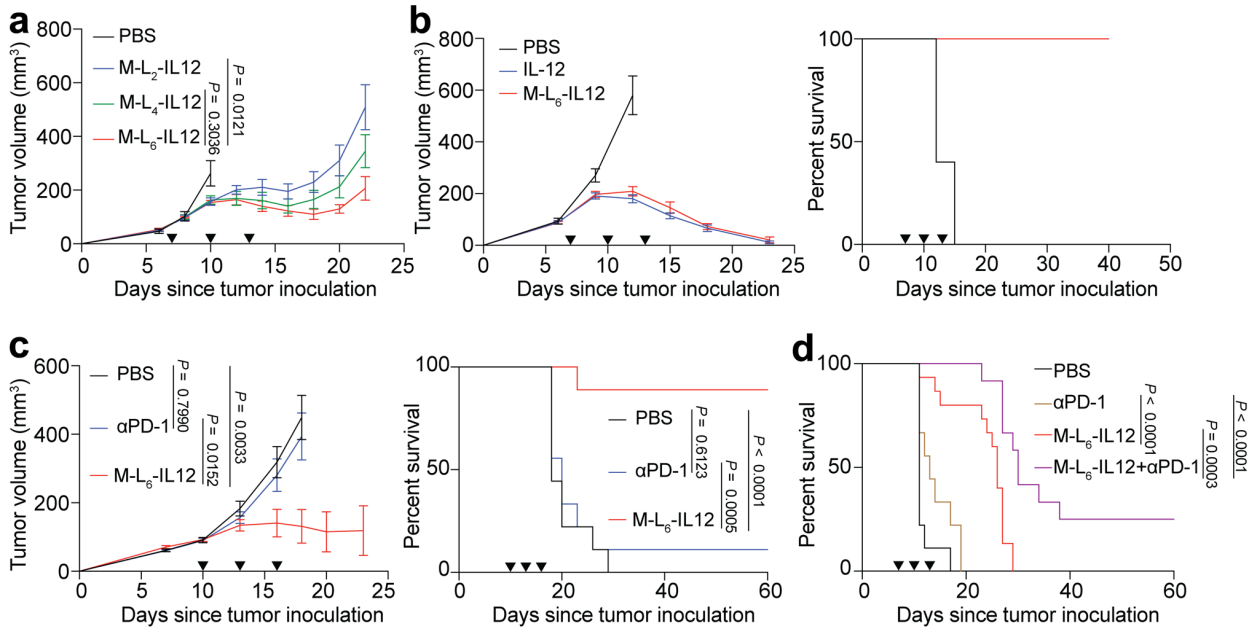

Figure 22. Masked IL-12 induces a strong antitumor response and potentiates CPI therapy. a, B16F10 melanoma-bearing mice were treated with PBS (n=6), or 250 pmol of M-L_2-IL12 (n=7), M-L_4-IL12 (n=8), M-L_6-IL12 (n=7) i.v. on days 7, 10 and 13 post tumor inoculation. Tumor growth curves are shown. b, Subcutaneous MC38 colon adenocarcinoma-bearing mice were treated with PBS (n=5), 5 µg (83.3 pmol) IL-12 (n=7) or 250 pmol of M-L_6-IL12 (n=7) i.v. on days 7, 10 and 13 post tumor inoculation. Tumor growth curves (left) and survival (right) are shown. c, Orthotopic EMT6 mammary carcinoma-bearing mice were treated with PBS (n=9), αPD-1 (n=9, 100 µg, i.p.) or M-L_6-IL12 (n=9, 250 pmol, i.v.) on days 10, 13 and 16 post tumor inoculation. Tumor growth curves (left) and survival (right) are shown. d, Orthotopic B16F10 melanoma-bearing mice were treated with PBS (n=9), αPD-1 (n=9, 100 µg, i.p.), M-L_6-IL12 (n=15, 250 pmol, i.v.) or M-L_6-IL12 + αPD-1 (n=12) on days 7, 10 and 13 post tumor inoculation. Survival curves are shown. Data are mean ± s.e.m. Arrowheads indicate times of treatment. Experiments in a,b,c were performed twice with similar results. Data in d were pooled from two independent experiments. Statistical analyses were performed using ordinary one-way ANOVA with Tukey's multiple comparison tests. For survival plots, Mantel-Cox test was used.

Significant production of granulocyte-macrophage colony-stimulating factor (GM-CSF), a maturation factor for antigen presenting cells (APCs)[246], was noted as well (Fig. 3c), demonstrating that masked IL-12 treatment activates the innate immune compartment. Upregulation of IL-1β and IL-1α (Fig. 23d,e) indicates Th1-biased TME remodeling[247,248].

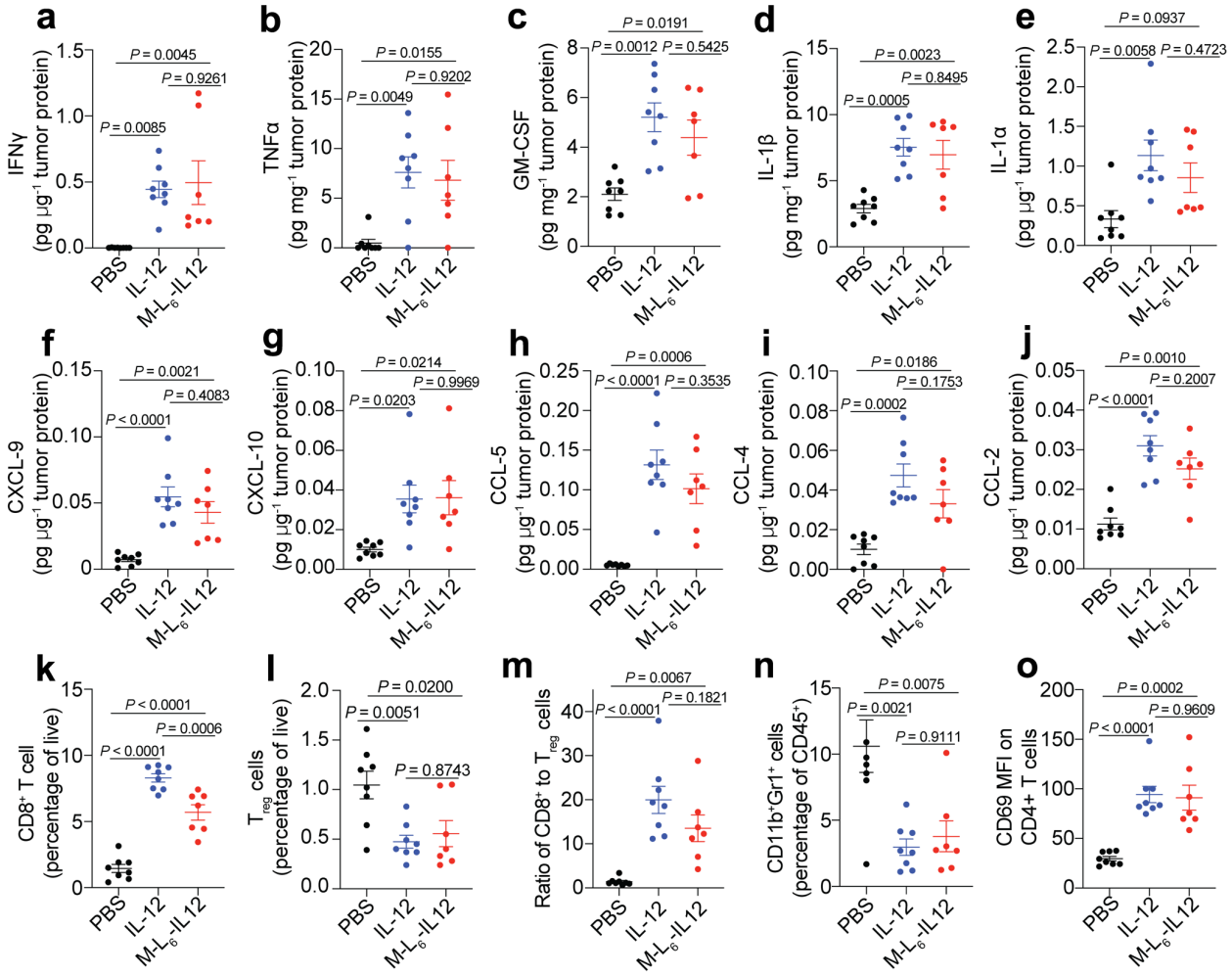

Figure 23. Masked IL-12 therapy elicits a wide range of inflammatory responses and causes immune cell infiltration in melanoma. Orthotopic B10F10 melanoma-bearing mice were treated with PBS (n=8), 5 µg (83.3 pmol) IL-12 (n=8) or 250 pmol of M-L_6-IL12 (n=7) i.v. on days 6 and 9 post tumor inoculation. Tumors were excised on day 11 and were homogenized for intratumoral cytokine/chemokine analysis (a-j) and processed for flow cytometric analysis (k-o). Intratumoral levels of IFNγ (a), TNFα (b), GM-CSF (c), IL-1β (d), IL-1α (e), CXCL-9 (f), CXCL-10 (g), CCL-5 (h), CCL-4 (i) and CCL-2 (j) were measured and normalized by total protein content. $CD8^+$ T cells as fraction of live cells (k), $CD4^+FoxP3^+$ T_{reg} cells as fraction of live cells (l), ratio of $CD8^+$ T cells to T_{reg} cells (m), $CD11b^+Gr1^+$ cells as fraction of $CD45^+$ cells (n), and CD69 MFI on $CD4^+Foxp3^-$ T cells (o). Data are mean ± s.e.m. Experiments were performed twice with similar results. Statistical analyses were performed using ordinary one-way ANOVA with Tukey's multiple comparison tests.

We also observed elevated expression of CXCL9, CXCL10, CCL5, and CCL4, chemokines that are associated with increased infiltration of $CD8^+$ T cells[249] (Fig. 23f-i).

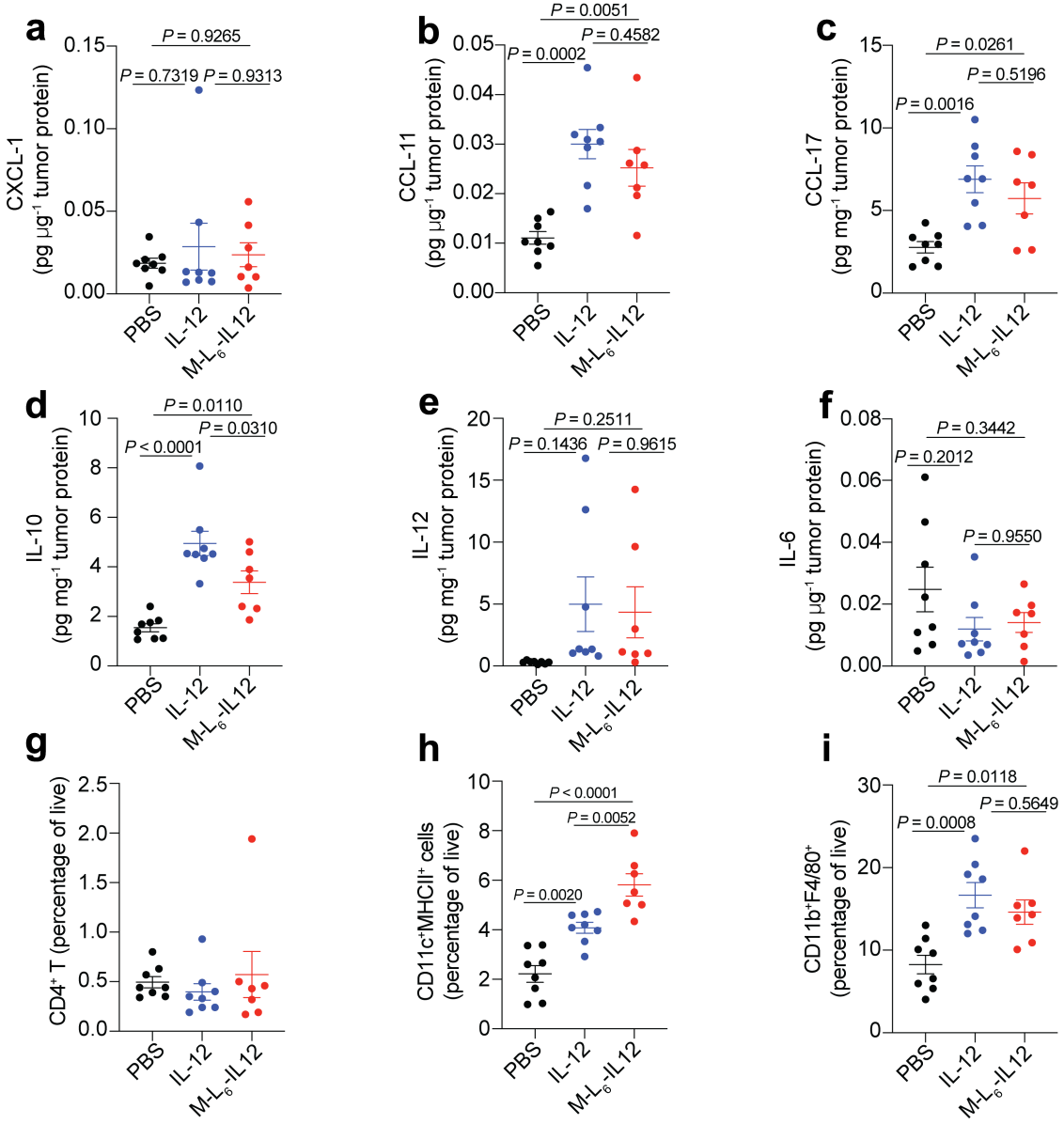

Figure 24. M-L$_6$-IL12 and unmodified IL-12 induce similar expression of proinflammatory markers and cell infiltration in B16F10 melanoma. Mice were treated as described in Fig. 23. Intratumoral levels of CXCL-1 (a), CCL-11 (b), CCL-17 (c), IL-10 (d), IL-12 (e), IL-6 (f) were quantified using a LEGENDPlex assay and normalized by total tumor protein content. Frequency of $CD3^+CD4^+Foxp3^-$ T cells (g), $CD11c^+MHCII^+$ dendritic cells (h), and $CD11b^+F4/80^+$ macrophages (i) as percentage of live cells are shown. PBS, n = 8; IL-12, n = 8; M-L$_6$-IL12, n = 7. Data are mean ± s.e.m. Statistical analyses were performed using ordinary one-way ANOVA with Tukey's multiple comparison test. Experiment was performed twice with similar results.

Other cytokines and chemokines (Fig. 24a-f) were expressed at similar levels in both unmodified IL-12- and M-L$_6$-IL12-treated groups.

These data show that masked IL-12 can potently activate the type II IFN pathway, which leads to secretion of wide variety of inflammatory molecules.

We then analyzed whether secretion of proinflammatory cytokines and chemokines led to infiltration of immune cells. Both treatments resulted in significant $CD8^+$ T infiltration as compared to saline-treated mice (Fig. 23k). Furthermore, we observed equal reduction in T_{reg} cells by both treatment groups (Fig. 23l). Importantly, the ratio of $CD8^+$ T cell to T_{reg} cells, which is considered as one of the main indicators of successful immunotherapy[95], was similarly upregulated in IL-12- and masked IL-12-treated animals (Fig. 23m). Both molecules reduced the percentages of suppressive $CD11b^+Gr\text{-}1^+$ cells[250] within the $CD45^+$ compartment (Fig. 23n). Although no major change was observed in the numbers of conventional $CD4^+$ T cells (Fig. 24g), M-L_6-IL12 treatment led to an increase in CD69 expression on these cells (Fig. 23o). Masked IL-12 caused dendritic cell (DC) and macrophage infiltration (Fig. 24h,i). These macrophages may be M1-polarized, as we have seen previously[234]. Together, these results demonstrate that M-L_6-IL12 and unmodified IL-12 exert comparable antitumor efficacy, causing profound immunological changes in the TME.

Given that cytokine/chemokine measurements and immune cell infiltration data were obtained from the same biological samples, we performed a correlation analysis to determine which cytokines/chemokines are associated with high $CD8^+$ T cell-to-T_{reg} ratios (Fig. 25). In the B16F10 melanoma model, the strongest positive correlation was observed for IFNγ, TNFα, and IL-1b, and chemokines CXCL-9/10, CCL-5, and CCL-4 (Fig. 25a-g). A weaker correlation with increased $CD8^+$ T cell-to-T_{reg} ratios was seen with IL-10 and IL-1a, whereas no significant correlation was noticed with intratumoral IL-6 and CXCL-1 (Fig. 25h-l). This analysis indicates that Th1-biased TME strongly correlates with therapeutic efficacy.

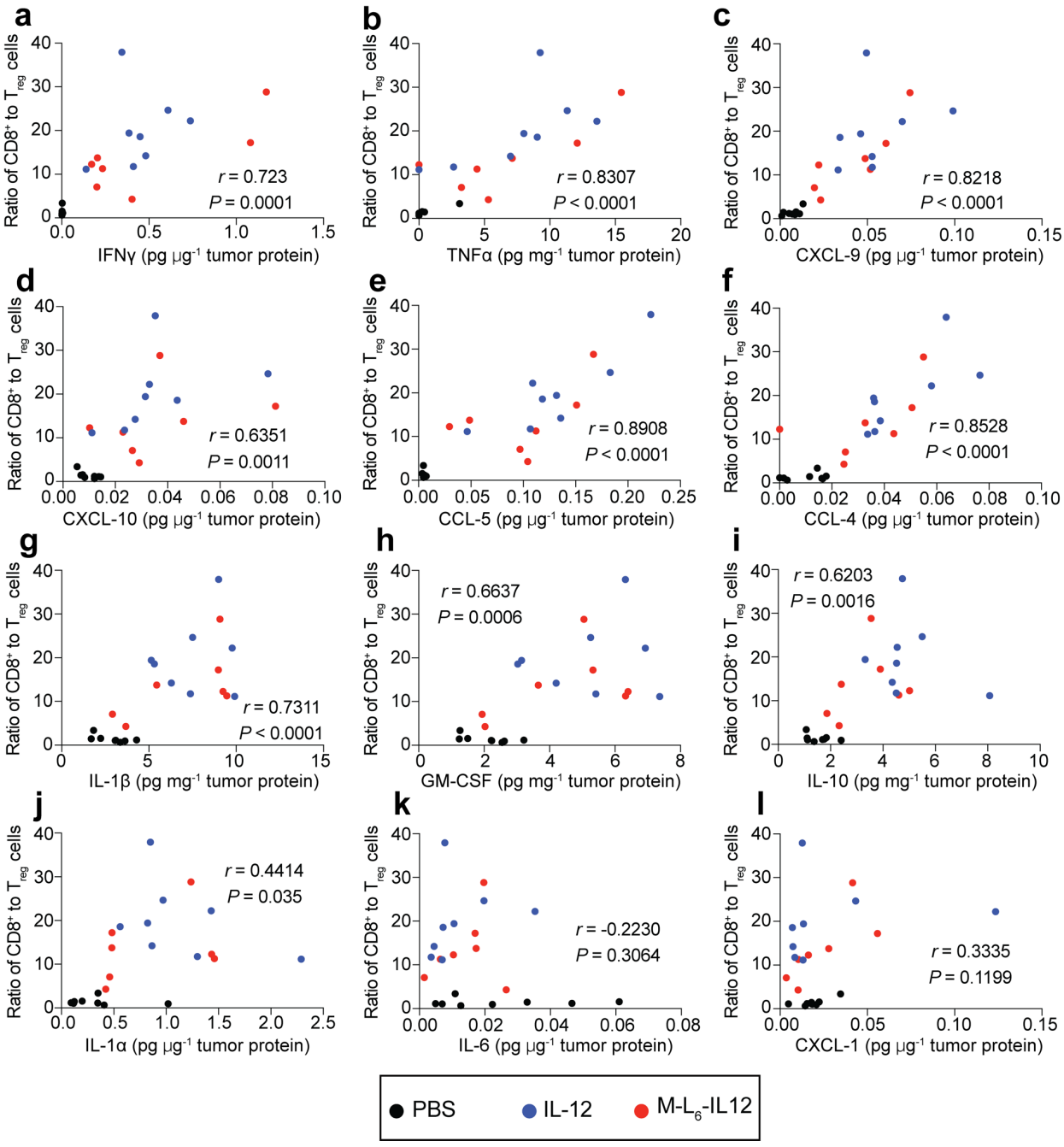

Figure 25. Correlation analysis between various cytokines/chemokines and CD8$^+$-to-Treg ratio. a-l, Pearson correlation analysis was performed on the data set presented in Fig. 23 and Fig. 24. Two-tailed *P* value and *r* value were obtained using Pearson correlation analysis on Prism GraphPad.

3.3.3 Treatment with Protease-sensitive IL-12 Minimizes irAEs

We next investigated whether the decreased *in vitro* bioactivity of masked IL-12 translates to fewer systemic irAEs. We treated healthy C3H/HeJ mice, a strain that is highly sensitive to low amounts of recombinant IL-12[160], daily with either 0.5 μg IL-12 or 3-fold molar dose of M-L_6-IL12 and monitored body weight change (Fig. 26a). Unmodified IL-12 induced marked body weight loss compared to saline-treated mice, whereas masked IL-12-treated mice maintained their body weight over the course of the study. In clinical trials, recombinant IL-12 administration led to significant elevation of IFNγ, the main contributor to the irAEs[160,162], and transaminases such as alanine aminotransferase (ALT) and aspartate aminotransferase (AST)[123] activities in blood, markers of hepatotoxicity. We administered either unmodified IL-12 or masked IL-12 three times, every three days to healthy C57BL/6 mice and quantified inflammatory biomarkers in the blood. Fusion of the mask to IL-12 substantially reduced plasma IFNγ, IL-6, TNFα and CCL-2 concentrations (Fig. 26b-e). We also observed a significantly decreased amount of circulating IL-12 in mice receiving the engineered IL-12 (Fig. 27a). No significant upregulation of IL-10, IL-1α, IL-1β or IFNβ was observed at this time point (Fig. 27b-e). Liver damage measured by ALT and AST activities, as well as pancreas damage measured by amylase activity in serum was also significantly decreased by fusing the mask to IL-12 (Fig. 26f-h). Albumin, blood urea nitrogen, and total protein levels were maintained among the groups (Fig. 27f-h).

Another common side effect of recombinant IL-12 therapy observed in the clinic is the decrease of circulating white blood cells, such as neutrophils and lymphocytes[165]. Treatment with unmodified IL-12, but not M-L_6-IL12, induced significant leukopenia, neutropenia and lymphopenia compared to healthy controls (Fig. 26i-k).

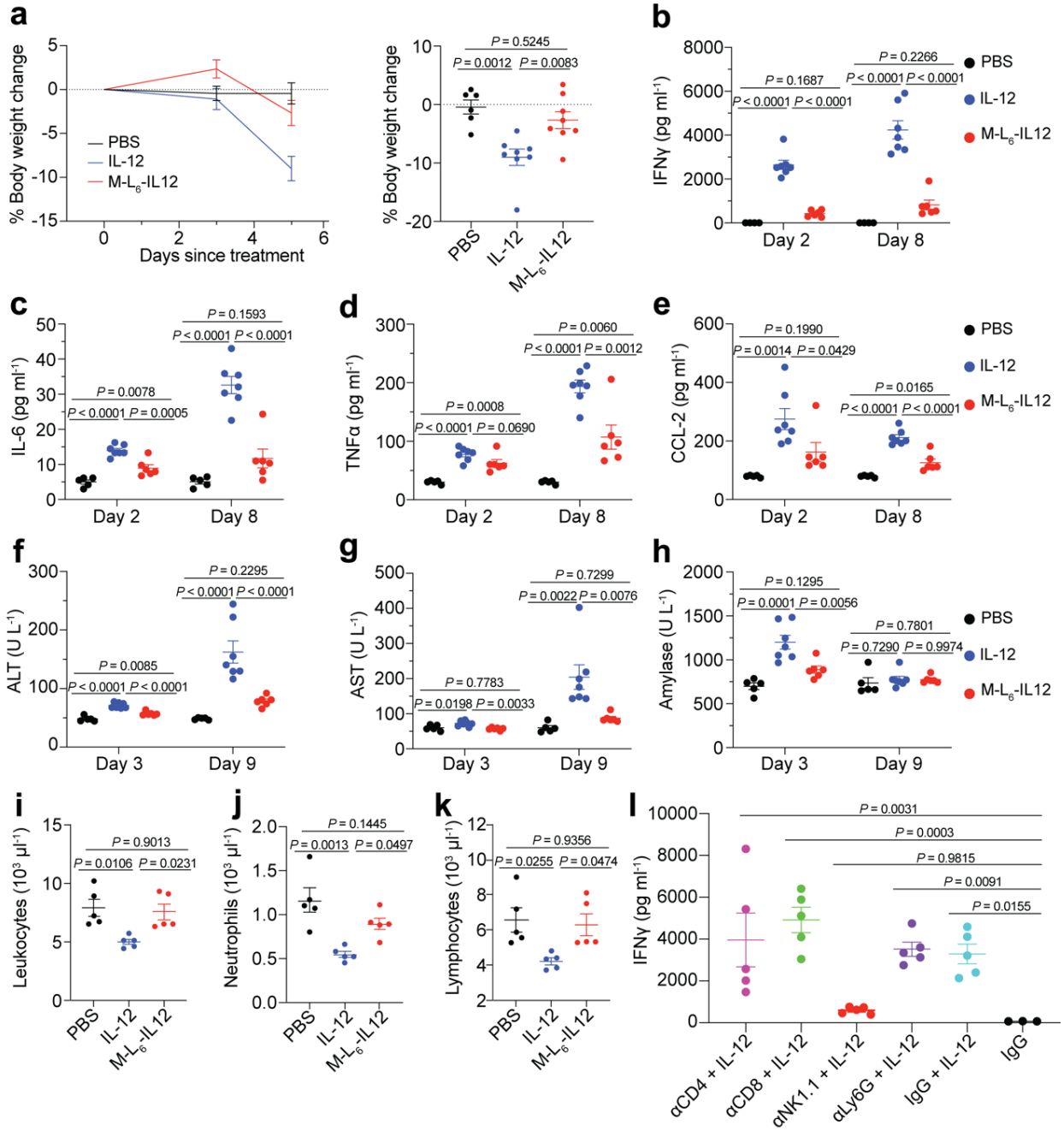

Figure 26. Masked IL-12 eliminates side effects associated with IL-12 therapy in healthy animals. a, Healthy C3H/HeJ mice were dosed daily (starting from day 0) with PBS (n=6), 0.5 µg (8.3 pmol) of IL-12 (n=8) or 25 pmol of M-L_6-IL12 (n=8) s.c. 6 times. Body weight change (left) and day 5 comparison (right) are shown. b-h, Healthy C57BL/6 mice were treated with PBS (n=5), 5 µg (83.3 pmol) IL-12 (n=7) or 250 pmol M-L_6-IL12 (n=6) i.v. on days 0, 3 and 6. Mice were bled on days 2, 3, 8 and 9 for plasma cytokine analysis (b-e) and blood chemistry analysis (f-h). Plasma IFNγ (b), IL-6 (c), TNFα (d), CCL-2 (e), and serum ALT (f), AST (g) and amylase (h) are shown. i-k, Healthy C57BL/6 mice were treated with PBS (n=5), 5 µg (83.3 pmol) IL-12 (n=5) or 250 pmol M-L_6-IL12 (n=5) i.v. and bled 4 days later for quantification of circulating leukocytes (i), neutrophils (j) and lymphocytes (k) using hematology analyzer. (Continued on the following page.)

Figure 26, continued. Masked IL-12 eliminates side effects associated with IL-12 therapy in healthy animals. l, Healthy C57BL/6 mice were administered neutralizing antibodies (400 μg, n=5 per group) on days 0 and 3. On day 4, mice were treated i.v. with 5 μg (83.3 pmol) IL-12 and bled on day 6 for plasma IFNγ measurement Data are mean ± s.e.m. Experiments were performed twice with similar results. Statistical analyses were performed using ordinary one-way ANOVA with Tukey's multiple comparison tests.

We next evaluated the effect of administration of neutralizing antibodies on systemic IFNγ production upon IL-12 injection (Fig. 26l). We found that depletion of NK cells had a major impact on IFNγ production, whereas depletion of $CD4^+$, $CD8^+$ or $LyG6^+$ cells did not reduce systemic IFNγ. This result suggests that NK cells are the main producers of IFNγ in response to IL-12, corroborating recent findings[238].

We then sought to verify our findings of reduced toxicity in tumor-bearing mice (Fig. 28). As in tumor-free mice, masked IL-12 injection significantly decreased plasma IFNγ concentration compared to IL-12 (Fig. 28a). The concentration of IL-12 protein in the blood, which may include some of the injected protein as well as *de novo* IL-12, was also decreased to the level of saline-treated mice (Fig. 28b). We did not observe significant upregulation in plasma IL-1α at the timepoint tested (Fig. 28c). IL-12 reportedly induces infiltration of myeloid cells into the spleen[251] and decreases systemic hematopoiesis[252]. Administration of unmodified IL-12 led to decreased $CD45^+$ cells, increased percentages of splenic $CD11b^+Gr\text{-}1^+$ and $CD11b^+Gr\text{-}1^-$ cells compared to saline-treated mice, whereas masked IL-12 did not (Fig. 28k-m). Significant reduction in numbers of splenic $CD8^+$ and $CD4^+$ T cells was noted upon treatment with IL-12 but not masked IL-12 (Fig. 28g,h), indicating diminished peripheral activity of masked IL-12. These data demonstrate that our masking approach significantly reduces the irAEs induced by IL-12 in both healthy and tumor-bearing mice, down to the level of saline injections.

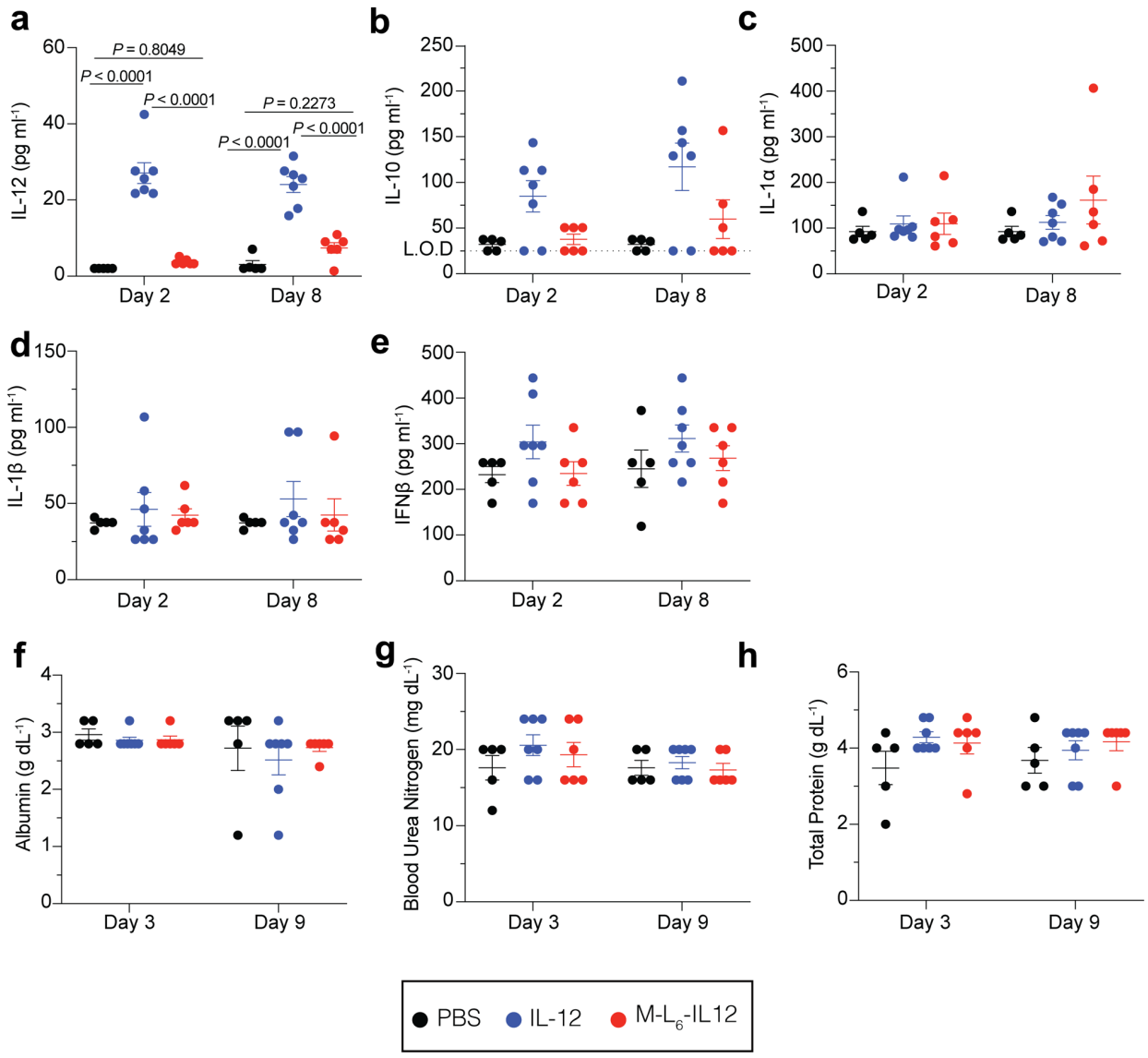

Figure 27. Masked IL-12 minimizes systemic inflammatory response. Mice were treated and analyzed as described in Fig. 26b-h. Plasma levels of IL-12 (a), IL-10 (b), IL-1α (c), IL-1β (d), and IFNβ (e) were quantified using a LEGENDPlex assay. Serum levels of albumin (f), blood urea nitrogen (g), and total protein (h) were quantified using a blood chemistry analyzer. PBS, n = 5; IL-12, n = 7; M-L_6-IL12, n = 6. Data are mean ± s.e.m. Statistical analyses were performed using ordinary one-way ANOVA with Tukey's multiple comparison test. Experiments were performed twice with similar results. L.O.D = limit of detection.

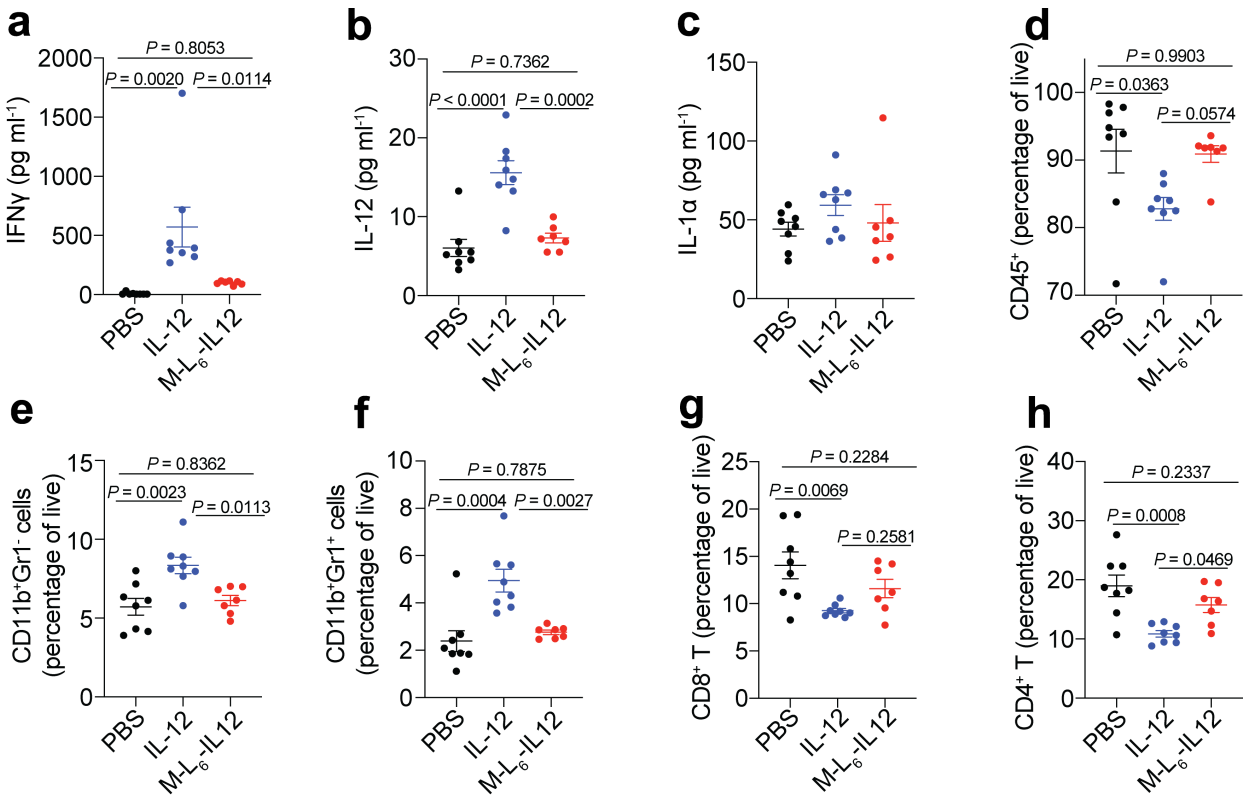

Figure 28. Treatment of melanoma-bearing mice with masked IL-12 does not generate systemic irAEs. Orthotopic B10F10 melanoma-bearing mice were treated with PBS (n=8), 83.3 pmol IL-12 (n=8) or 250 pmol M-L$_6$-IL12 (n=7) i.v. on days 6 and 9 post tumor inoculation. On day 11, mice were bled for plasma cytokine quantification (a-c) and spleens were excised for flow cytometric analysis (d-h). Plasma IFNγ (a), IL-12 (b) and IL-1α (c) were quantified using LEGENDPlex. CD45$^+$ cells (d), CD11b$^+$Gr1$^-$ cells (e), CD11b$^+$Gr1$^+$ cells (f), CD8$^+$ T cells (g) and CD4$^+$ T cells as fraction of live cells (h) are shown. Data are mean ± s.e.m. Experiments were performed twice with similar results. Statistical analyses were performed using ordinary one-way ANOVA with Tukey's multiple comparison tests.

3.3.4 Ex Vivo Cleavage by Human Tumors Activates Masked IL-12

Expression of various proteases is increased in human solid tumors[35], and thus we sought to investigate whether masked IL-12 can be activated by a human tumor lysate. To test this, we obtained a flash frozen human breast cancer biopsy (stage IIA infiltrating lobular carcinoma), as well as a biopsy of the adjacent normal tissue (ANT) from the same patient. We homogenized both tissues and incubated the homogenate with M-L$_6$-IL12 and performed the STAT4 phosphorylation

assay (Fig. 29a). Incubation of M-L_6-IL12 with the tumor lysate, but not the ANT lysate, resulted in full activation of masked IL-12. Incubation of masked IL-12 with ANT resulted in minor activation as compared to masked IL-12 incubated with buffer only, which is perhaps due to nonspecific cleavage of the linker by intracellular proteases.

To demonstrate that our approach can be applied to engineer human IL-12 as well, we generated human masked IL-12, in which the mask was derived from human IL-12Rβ1$_{C24\text{-}E234}$. This fusion protein was expressed at high yields and a two-step purification led to a homogenous monomer (Fig. 29b). Human masked IL-12 exhibited ~35-fold decreased bioactivity compared to human IL-12 (Fig. 29c), confirming the applicability of human IL-12Rβ1 as the masking domain.

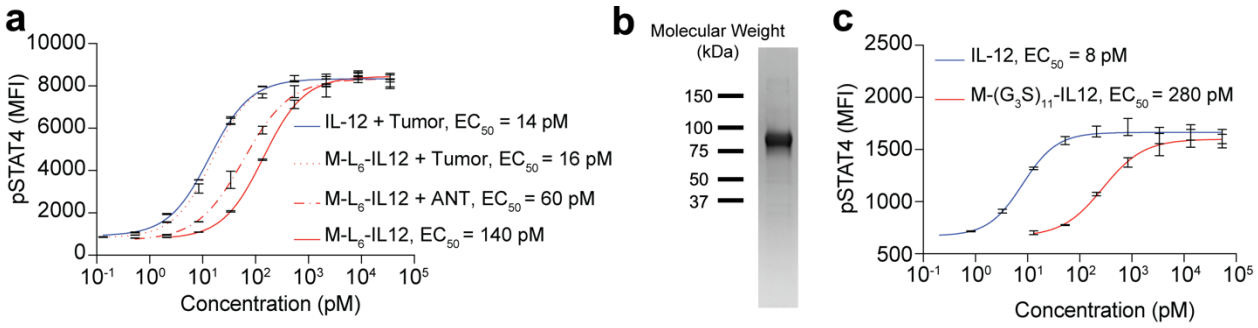

Figure 29. Cleavage of the mask by human tumors and generation of human masked IL-12. a, Cleavage of M-L_6-IL12 by human breast tumor homogenate. IL-12 or M-L_6-IL12 (at 0.84 μM) were mixed with either tumor homogenate or adjacent normal tissue (ANT) lysate (2 mg/mL) and incubated overnight at 37°C. Samples were then diluted and applied on pre-activated mouse $CD8^+$ T cells and MFI of pSTAT4 was measured via flow cytometry (n=2 per condition, technical duplicates). b, SDS-PAGE analysis of purified human M-$(G_3S)_{11}$-IL12 under nonreducing conditions. c, Recombinant human IL-12 or human M-$(G_3S)_{11}$-IL12 were applied to pre-activated human $CD8^+$ T cells and MFI of pSTAT4 was measured via flow cytometry (n=2 per condition, technical duplicates). Data are mean ± s.e.m.; EC_{50}, half-maximum effective concentration. Experiments were performed at least twice, with similar results. Representative data are shown.

3.4 Discussion

Recent engineering strategies aimed at reducing the incidence of irAEs upon IL-12 therapy have relied on targeting IL-12 to tumor matrix[234,253,254] and tumor necrosis[255], biasing IL-12 mutein to preferentially activate $CD8^+$ T cells versus NK cells[238], and delivering IL-12 gene directly to tumors[181,182,256]. Despite encouraging preclinical and clinical results, the route of administration, exposure of IL-12 to circulating lymphocytes and subsequent toxicity may limit the broad use of this cytokine. Masked IL-12 produces minimal systemic side effects yet is capable of driving profound inflammation selectively within the tumor. Masked IL-12 can be administered either i.v. or subcutaneously (s.c.), both of which are highly preferred routes in the clinic.

Our data show that NK cells are the main source of systemic IFNγ, which leads to undesired effects. Avoiding the NK cell binding in circulation would be critical for reducing IL-12 side effects. Our results reveal that the masking approach eliminates irAEs even after repeated administration of M-L_6-IL12. This is encouraging given that in clinical trials, recombinant IL-12 was administered multiple times.

In contrast to very little IFNγ in the blood, masked IL-12 induced strong intratumoral IFNγ expression. IFNγ induces chemokine expression, and these chemokines likely induced effector $CD8^+$ T cell infiltration. The activation of $CD8^+$ T cells and reduction of T_{reg} cells are via secretion of IFNγ from T cells, as we previously reported[234]. We tested EMT6 and B16F10 melanoma, which are immunologically cold, CPI-unresponsive tumors. Our data clearly demonstrate that masked IL-12 remodels the immunosuppressive, cold TME, and bears potential to synergize with CPI therapies.

We selected the cytokine binding domain of the extracellular IL-12Rβ1 as the mask because the binding affinity (K_D) of IL-12 for the full receptor (IL-12Rβ1 and β2) is in the pM range while the K_D for IL-12Rβ1 alone is in the nM range[241]. Thus, once cleaved, the soluble mask will not inhibit IL-12 binding to the IL-12R, due to ~1000-fold difference in affinity between the full complex and a single subunit. Additionally, since IL-12Rβ1 naturally exists in the body, it is unlikely that the fusion protein will be immunogenic, and thus is more advantageous compared to other possible non-endogenous masking domains.

Designing biologics that are sensitive to proteolytic cleavage by tumor-associated enzymes is a promising strategy to localize therapeutic effects to the disease site. Various proteases, such as MMPs and SPs, are aberrantly overexpressed in the TME[35], yet their expression in the periphery is tightly regulated. This feature has been exploited to engineer protease-sensitive nanoparticles[257,258], antibodies[240,259], and certain cytokines[236,260]. Protease-sensitive masked checkpoint inhibitor (CPI) antibodies have already demonstrated encouraging early clinical trial results[261]. We have previously investigated antitumor efficacies of tumor matrix-binding chemokine[262], CPI[263], IL-2[263], IL-12[234], doxorubicin[264], and anti-CD40 antibody[265]. Among these important antitumor agents, tumor-targeted IL-12 has shown the strongest antitumor efficacy in multiple tumor models, including complete remission of cold tumors. In this study, we show that masking approach for IL-12, one of the most toxic cytokines, can be successfully applied, transforming it into a potential therapeutic.

Collectively, our results reveal that systemic administration of masked IL-12 induces a potent antitumor effect, resulting in eradication of established colon tumors and immune-excluded orthotopic breast tumors; yet fusion of a masking domain abrogates IL-12-induced peripheral toxicity, as evidenced by a variety of systemic inflammatory markers. We also report that *ex vivo*

patient tumor lysate fully activates masked IL-12, highlighting the translatability of our approach to patients with advanced oncologic diseases.

3.5 Materials and Methods

3.5.1 Mice and Cancer Cell Lines

8 to 12-week-old C57BL/6 female mice were purchased from Charles River Laboratory. 8 to 12-week-old BALB/c female mice and 8 to 12-week-old C3H/HeJ female mice were purchased from Jackson Laboratory. B16F10 melanoma, EMT6 breast and MC38 colon cancer cell lines were obtained from ATCC and cultured according to instructions. All animal experiments performed in this work were approved by the Institutional Animal Care and Use Committee of the University of Chicago. Cell lines were routinely checked for mycoplasma contamination.

3.5.2 Production and Purification of Recombinant IL-12 and Masked IL-12

For the production of wild-type IL-12, optimized sequences encoding mouse p35 and p40 subunits were synthesized and subcloned into the mammalian expression vector pcDNA3.1(+) by Genscript. A sequence encoding $(His)_6$ was added to the N-terminus of the p35 subunit to allow affinity-based protein purification. For the production of masked IL-12, a sequence encoding the mask protein ($IL\text{-}12R\beta1_{Q20\text{-}A261}$) was fused to the N-terminus of the murine p35 subunit via various linkers described in the study (Supplementary Table 1). A $(His)_6$ tag, followed by G_3S, was added to the N-terminus of the Mask-p35 subunit. Sequences encoding Mask-p35 and p40 were subcloned into mammalian expression vector pcDNA3.1(+) by Genscript. Suspension-adapted HEK-293F were maintained in serum-free Free Style 293 Expression Medium (Gibco). On the day of transfection, cells were inoculated into fresh medium at a concentration of 1×10^6 cells/mL. 500 μg/L p35 (or Mask-p35) plasmid DNA, 500 μg/L p40 plasmid DNA were mixed with 2 mg/L

linear 25 kDa polyethyleneimine (Polysciences) and co-transfected in OptiPRO SFM medium (4% final volume). After 4-5 days of culture, supernatants were harvested, and purification was performed as described previously[234]. Purified proteins were tested for endotoxin via HEK-Blue TLR4 reporter cell line, and endotoxin levels were confirmed to be less than 0.01 EU/mL. Protein purity was assessed by SDS-PAGE as described previously. Protein concentration was determined through absorbance at 280 nm using NanoDrop (Thermo Scientific). To produce recombinant human IL-12, optimized sequences encoding human p35 and p40 were synthesized and subcloned into mammalian expression vector pcDNA3.1(+) by Genscript. To produce recombinant human masked IL-12, a sequence encoding the human mask (derived from human IL-12Rβ1$_{C24\text{-}E234}$) was fused to the N-terminus of human p35 via a $(G_3S)_{11}$ linker and was subcloned into the mammalian expression vector pcDNA3.1(+) by Genscript. Human p40 plasmid was also synthesized by and subcloned into the mammalian expression vector pcDNA3.1(+) by Genscript. Co-transfection and purification of human IL-12 (or human masked IL-12) was performed similarly to the mouse analog.

3.5.3 Cleavage of Masked IL-12 by Recombinant Proteases

Recombinant mouse MMP2, MMP3, MMP8, MMP9 and recombinant human urokinase plasminogen activator (uPA) were purchased from R&D Systems. Recombinant MMPs were supplied in their inactive form and were activated using 1 mM *p*-aminophenylmercuric acetate (APMA, Sigma) as indicated in the product datasheet of each MMP. Following activation, MMPs and cytokines were diluted in an assay buffer containing 150 mM NaCl, 50 mM Tris, 10 mM $CaCl_2$, 0.05% Brij-35 at pH = 7.5. Final concentrations of the proteases and cytokines are mentioned in figure legends. Samples were then analyzed via gel electrophoresis. Cleavage assays

using uPA, which was supplied as an active enzyme, was conducted according to manufacturer's protocol.

3.5.4 Analysis of STAT4 Phosphorylation via Flow Cytometry

Mouse $CD8^+$ T cells were purified from spleens of C57BL/6 mice using EasySep mouse $CD8^+$ T cell isolation kit (Stem Cell). Purified $CD8^+$ T cells (10^6 cells/mL) were activated in six-well plates precoated with 5 μg/mL α-CD3 (clone 17A2, Bioxcell) and supplemented with soluble 5 μg/mL α-CD28 (clone 37.51, Biolegend) and 50 ng/mL mouse IL-2 (Peprotech) for 3 days. Culture medium was IMDM (Gibco) containing 10% heat-inactivated FBS, 1% Penicillin/Streptomycin and 50 μM 2-mercaptoethanol (Sigma Aldrich). After 3 days of culture, activated $CD8^+$ T cells were rested for 6 hr in fresh culture medium and were transferred into 96-well plates (50,000 cells/well). Indicated amounts of IL-12 or (cleaved or intact) masked IL-12 were applied to $CD8^+$ T cells for 15 min at 37°C to induce STAT4 phosphorylation. Cells were fixed immediately using BD Phosflow Lyse/Fix buffer for 10 min at 37°C and then permeabilized with BD Phosflow Perm Buffer III for 30 min on ice. Cells were stained with AF647-conjugated antibody against pSTAT4 (clone 38, BD) recognizing phosphorylation of Tyr693. Staining was performed for 1 hr at room temperature (RT) in the dark. When assessing the inhibitory effect of extracellular domain of recombinant mouse IL-12Rβ1 (R & D), mouse IL-12 was incubated with IL-12Rβ1 at 1:1 molar ratio and applied to pre-activated mouse $CD8^+$ T cells. For the analysis of STAT4 phosphorylation in human cells, human $CD8^+$ T cells were magnetically sorted from frozen PBMCs using EasySep human $CD8^+$ T Cell Isolation Kit (Stem Cell). Sorted human $CD8^+$ T cells were activated in six-well plates precoated with 5 μg/mL α-CD3 (clone OKT3, BioLegend) and supplemented with soluble 5 μg/mL α-CD28 (clone CD28.2, BioLegend) and 50 ng/mL human IL-2 (Peprotech) for 3 days. pSTAT4 assay was performed as described above. Cells were acquired

on BD LSR and data were analyzed using FlowJo (Treestar). Mean Fluorescence Intensity (MFI) of $pSTAT4^+$ population was plotted against cytokine concentration. Dose-response curve was fitted using Prism (v8, GraphPad).

3.5.5 Cleavage of Masked IL-12 by Human Tumors

Flash-frozen human breast cancer biopsy and the adjacent normal tissue (ANT) from the same patient were purchased from Cureline, Inc. (CA, USA). The patient was a 44 year-old female (Caucasian) and had stage IIA lobular infiltrating carcinoma. Surgery was performed in August of 2018 and samples were flash-frozen within 20 minutes of surgery. Tissues were placed in Lysing Matrix D tubes (MP Bio) along with the buffer containing 150 mM NaCl, 50 mM Tris, 10 mM $CaCl_2$, 0.05% Brij-35 at pH = 7.5. Homogenization was performed using FastPrep tissue homogenizer (MP Bio). Supernatant was harvested by centrifugation at 10,000 × g for 20 min. Total protein concentration in the supernatant was determined via Pierce BCA Protein Assay kit (Thermo Fisher). Supernatants were stored in -80 °C. For the cleavage experiment, tissue lysate was incubated with masked IL-12 overnight at 37 °C and the mixture was further diluted in cell media for pSTAT4 assay.

3.5.6 Antitumor Efficacy of IL-12 and Masked IL-12

For the primary tumor model of B16F10 melanoma, 5×10^5 B16F10 cells were inoculated intradermally on the back of female C57BL/6 mice in 30 μL sterile PBS. For the EMT6 mammary carcinoma model, 5×10^5 EMT6 cells were injected into the left mammary fat pad of female BALB/c mice in 30 μL sterile PBS. For the primary tumor model of MC38 colon adenocarcinoma, 5×10^5 MC38 cells were inoculated subcutaneously on the back of the female C57BL/6 mice in 30 μL sterile PBS. Dose and schedule of the cytokines and antibodies are described in the figure

legends. Cytokines were injected in 100 μL volume through tail-vein (intravenously, i.v.). For the experiments involving αPD-1 antibody (29 F.1A12, Bioxcell), antibody was administered intraperitoneally at 100 μg in PBS. The volume of the tumor was calculated using the following formula: (height) × (width) × (thickness) × (π/6). Mice were sacrificed when the tumor volume reached 1000 mm^3 and/or based on humane end-point criteria.

3.5.7 Body Weight Loss in C3H/HeJ Mice

8 to 12-week-old C3H/HeJ female mice were weighed on D0. After the initial weights, mice were injected with either PBS, IL-12 or M-L_6-IL12 subcutaneously in 100 μL. Injections and body weight measurements were performed daily until day 5. Percent body weight change was calculated according to the following formula: [(Current body weight) – (Initial body weight)]/(Initial body weight) × 100%.

3.5.8 Systemic Markers of Toxicity

For assessment of plasma cytokines, mice were treated with either IL-12 or masked IL-12 as indicated on the figure legends. On specified days, blood was collected in EDTA-coated tubes (Eppendorf). Blood was spun at 3000 × g for 15 min to obtain plasma. For proinflammatory cytokine analysis, LEGENDplex Mouse Inflammation Panel (13-plex) was used (BioLegend). Plasma was diluted in half using assay buffer provided in the kit. The assay was performed according to manufacturer's instructions. For blood chemistry analysis, mice were bled on indicated days and sera were obtained by spinning blood at 3000 × g for 15 min in in protein low-binding tubes (Eppendorf). Sera were diluted 4x in sterile water and serum ALT, AST amylase, total protein, total bilirubin, and albumin were determined using Vet Axcel blood chemistry analyzer (Alfa Wasserman). For the analysis of leukopenia, healthy C57BL/6 were injected i.v.

with either IL-12 or masked IL-12 as indicated. 4 days later, blood was collected in EDTA-coated tubes and analyzed using AcT 5diff CP (Beckman Coulter) hematology analyzer.

3.5.9 Analysis of Intratumoral Inflammatory Markers

Mice bearing B16F10 tumors were treated with either IL-12 or M-L_6-IL12 twice on days 6 and 9 post tumor inoculation. Mice were euthanized on day 11. Tumors were excised and cut approximately in half. One half was processed for flow cytometry (described below) and the other half was snap-frozen in liquid nitrogen and stored at −80 °C. Tumors were then homogenized in Tissue Protein Extraction buffer (T-PER, Thermo Fisher Scientific). Protease inhibitor tablets (Roche) were added to the T-PER buffer. Tumors were placed in Lysing Matrix D tubes (MP Bio). Homogenization was performed using FastPrep tissue homogenizer (MP Bio). Supernatant was harvested by centrifugation at 10,000 × g for 20 min. Intratumoral cytokines and chemokines were quantified using LEGENDplex Mouse Inflammation Panel (13-plex) and LEGENDplex Mouse Proinflammatory Chemokine Panel (13-plex) (both from BioLegend), respectively, and normalized by total protein content. Tumor samples were diluted in half using assay buffer provided in the kits.

3.5.10 Immune Cell Infiltrates in B16F10 Melanoma

B16F10 cells (5×10^5) were inoculated intradermally on the back of the female C57BL/6 mice in 30 μL sterile PBS. Then, 6 and 9 days after tumor implantation, mice were treated with either PBS, IL-12 or M-L_6-IL12. On day 11, tumors were collected and digested for 30 min at 37°C. Digestion medium was DMEM (Gibco) supplemented with 5% FBS, 2.0 mg mL^{-1} collagenase D (Sigma-Aldrich), 20 μg mL^{-1} DNase I (Worthington Biochemical), 1.2 mM $CaCl_2$ and 10 μg mL^{-1} BFA. Single-cell suspensions were prepared using a cell strainer (70 μm; Thermo

Fisher Scientific). Tumor (20 mg) was plated in each well. For antibodies against surface targets, staining was performed in PBS with 2% FBS. For intracellular targets, staining was performed according to the manufacturer's protocols (00-5523-00, Thermo Fisher Scientific). The following anti-mouse antibodies were used: CD45 Pacific Blue (clone 30-F11, BioLegend), CD3e BUV395 (clone 145-2C11, BD Biosciences), Foxp3 PE (clone MF23, BioLegend), CD8α BV510 (clone 53-6.7, BioLegend), CD4 BV785 (clone RM4-5, BioLegend), CD11b BUV737 (clone M1/70, BD Biosciences), CD69 AF647 (clone H1.2F3, BioLegend), CD103 BV605 (clone 2E7, BioLegend), F4/80 FITC (clone CI:A3-1, AbD Serotec), CD11c PE-Cy7 (clone N418, BioLegend), MHCII PerCP-Cy5.5 (clone, M5/114.15.2, BioLegend) and Gr-1 APC-Cy7 (clone RB6-8C5). Cell viability was determined using the fixable viability dye eFluor 455UV dye (65-0868-14, eBioscience).

3.5.11 Immune Cell Infiltrates in the Spleen

B16F10 cells (5×10^5) were inoculated intradermally on the back of the female C57BL/6 mice in 30 μL sterile PBS. Then, 6 and 9 days after tumor implantation, mice were treated with either PBS, IL-12 or M-L_6-IL12. On day 11, spleens were collected, and single-cell suspensions were prepared by mechanically disrupting the spleen through a cell strainer (70 μm; Thermo Fisher Scientific). 2×10^6 cells were plated in each well. For antibodies against surface targets, staining was performed in PBS with 2% FBS. For intracellular targets, staining was performed according to the manufacturer's protocols (00-5523-00, Thermo Fisher Scientific). The following anti-mouse antibodies were used: CD45 Pacific Blue (clone 30-F11, BioLegend), CD3e BUV395 (clone 145-2C11, BD Biosciences), Foxp3 PE (clone MF23, BioLegend), CD8α BV510 (clone 53-6.7, BioLegend), CD4 BV785 (clone RM4-5, BioLegend), CD11b BUV737 (clone M1/70, BD Biosciences), CD69 AF647 (clone H1.2F3, BioLegend), CD103 BV605 (clone 2E7, BioLegend),

F4/80 FITC (clone CI:A3-1, AbD Serotec), CD11c PE-Cy7 (clone N418, BioLegend), MHCII PerCP-Cy5.5 (clone, M5/114.15.2, BioLegend) and Gr-1 APC-Cy7 (clone RB6-8C5, BioLegend). Cell viability was determined using the fixable viability dye eFluor 455UV dye (65-0868-14, eBioscience).

3.5.12 Depletion Studies

Depletion of cellular subsets were performed by injecting antibodies against CD4 (GK1.5, Bioxcell, 400 μg), CD8α (2.43, Bioxcell, 400 μg), NK1.1 (PK136, Bioxcell, 400 μg), Ly6G (1A8, Bioxcell, 400 μg) or rat IgG isotype control (LTF-2, Bioxcell, 400 μg) on days 0 and 3. On day 4, mice were administered 5 μg IL-12 i.v. and bled on day 6 for quantification of IFNγ via LegendPLEX assay.

3.5.13 Statistical Analysis

Statistical analysis between groups was performed using Prism (v.8, GraphPad). For multiple comparisons, one-way analysis of variance followed by Tukey post hoc test was used. For survival plots, log-rank (Mantel–Cox) tests was used.

3.6 Author Contributions

Aslan Mansurov, Jun Ishihara, Melody A. Swartz, Juan L. Mendoza and Jeffrey A. Hubbell designed the experiments and wrote the manuscript. Aslan Mansurov performed the experiments. Peyman Hosseinchi assisted with the immune cell infiltrates in B16F10 melanoma. Abigail L. Lauterbach assisted with the STAT phosphorylation assays. L. Taylor Gray assisted with tumor experiments. Aaron T. Alpar assisted with blood chemistry analysis. Erica Budina assisted with protein production. Shijie Cao assisted with LEGEDNPlex assays. Ani Solanki performed tail-

vein injections. Suzana Gomes assisted with cancer cell line maintenance. John-Michael Williford assisted with protease cleavage experiments.

3.7 Funding

This work was funded by the Chicago Immunoengineering Innovation Center (CIIC), University of Chicago.

3.8 Conflict of Interest

A.M., J.I., J.L.M., and J.A.H are inventors on a patent application filed by the University of Chicago covering the technology described herein. They and M.A.S. hold equity in Arrow Immune, Inc., which is developing that technology, and J.A.H. is an officer of that company.

3.9 Acknowledgments

This work was funded by the Chicago Immunoengineering Innovation Center of the University of Chicago and NIH R01 CA219304 (to M.A.S.). We would like to thank University of Chicago's Cytometry and Antibody Technology facility, particularly D. Leclerc.

CHAPTER 4:

DISCUSSION AND FUTURE DIRECTIONS

The main objective of this thesis was to improve the therapeutic index of IL-12, one of the most promising cytokines for cancer immunotherapy. Insufficient therapeutic index is a challenge that is common to all proinflammatory cytokines. The immune cells in our body have evolved to secrete cytokines in a localized manner and respond to them at relatively low concentrations (~pg). However, in a therapeutic setting, patients are administered much higher doses of cytokines (~μg), which leads to severe immunotoxicity. We believe that only a significant enhancement of the therapeutic index (5-10-fold) could lead to the successful translation of cytokines in immunotherapy. We pursued this goal via molecular engineering of recombinant IL-12. However, it is important to mention that other approaches such as virus-mediated and gene-mediated (DNA or mRNA) delivery strategies are being developed as well for several inflammatory cytokines. In this Chapter, we provide brief conclusions of the two engineering approaches, namely collagen-binding IL-12 and protease-sensitive masked IL-12 and describe their limitations and discuss future directions.

4.1 Discussion and Future Directions in Collagen Targeting

In Chapter 2, we demonstrate the development of collagen-targeting IL-12, which upon i.v. administration, actively targets the disordered tumor stroma through collagen affinity and enhances local inflammation. CBD-IL-12 induced a significantly greater intratumoral response than the unmodified IL-12 and reduced the inflammation in the periphery. One potential limitation of this strategy is that it relies on the aberrant expression of collagen in solid tumors and their exposure to the bloodstream, which has not been scrutinized in human disease. The extent of

'leakiness' of human solid tumors may heavily depend on factors such as tumor stage, location in the body and whether the malignancy is a primary site or metastatic site. Although, in our mouse studies, we used metastatic and spontaneously arising tumor models, differences between species may be significant.

The route of administration in the clinical setting is another source of concern. In our studies, we examined the i.v. and peritumoral (p.t.) routes, of which, the i.v. route was superior. We believe that, upon p.t. administration, much of the injected cytokine drains to the lymph node, decreasing the effective concentration within the tumor. We did not, however, investigate the intratumoral (i.t.) route, which may potentially be more advantageous than the i.v. route. One challenge with the i.v. route is that the concentration of IL-12 spikes in the blood at the time of injection, whereas s.c. or i.t. routes lead to a more transient increase in concentration. In case of CBD-IL-12, s.c. administration is not viable, as the drug would not be delivered to the tumor site but rather stick to the collagen in the skin, whereas i.t. administration seems appealing. Traditionally, intralesional therapy has not been regarded as a feasible route due to difficulties in accessing visceral tumors, patient compliance, and potential risk of causing cancer cells to enter the bloodstream because of needle puncture. For that reason, cytotoxic small molecule drugs have been administered either orally or i.v. For agonistic immunotherapeutics, though, intralesional administration may indeed be more attractive[266]. In fact, the first ever intratumoral therapy approved by the FDA was talimogene laherparepvec (T-VEC) in 2015, an oncolytic virus encoding GM-CSF. Advancements in interventional radiology for local immunotherapy may provide certain solutions to the above-mentioned problems[267].

As for the i.v. administration, we believe that the decrease in toxicity is due to shorter residence time of CBD-IL-12 in the blood when compared to IL-12 (supported by our observation

that CBD-IL-12 is less toxic in tumor-free mice as well). Given that circulating NK cells express the IL-12R complex, systemic IFNγ storm is a direct result of IL-12 binding to NK cells (as we demonstrate in Chapter 3). Decreased half-life, however, leads to the question of the biodistribution of CBD-IL-12 after i.v. administration and whether it has a significant impact on IL-12 toxicity. Shorter half-life suggests that CBD-IL-12 is being accumulated in other organs, perhaps with relatively high level of microvascular permeability, such as kidneys or liver. Whether such accumulation of CBD-IL-12 causes liver- or kidney-specific toxicity depends solely on the presence of IL-12R-expressing immune cells in those tissues. One way to get insights into more detailed biodistribution, without relying on sophisticated techniques such as radiolabeling, is to simply compare the levels of phosphorylated STAT4 in the tissues of concern after injection of IL-12 or CBD-IL-12 (perhaps via western blotting). Since STAT4 is immediately phosphorylated following IL-12 binding to IL-12R, this transcription factor is an ideal target to study the biodistribution from a pharmacodynamic perspective. Plainly studying the presence of CBD-IL-12 in various tissues (as would be performed in traditional biodistribution experiments) might be misleading, as the expression of IL-12R is restricted to certain cells in our body: if a particular tissue has negligible IL-12R expression, presence of CBD-IL-12 in that tissue will, presumably, not generate local inflammation. This feature makes IL-12 different from other cytokines such as IL-2, IL-15 or IFNs, the receptors for which are widely expressed throughout the body.

Another concern that needs to be raised with regards to the i.v. administration involves patients with chronic inflammation. Chronic inflammation in the tissue causes activation and increased infiltration of immune cells, which may worsen the symptoms of patients undergoing any cancer immunotherapy. With CBD-IL-12, such adverse effects may be amplified as the

inflamed tissues are likely to be infiltrated by IL-12R-expressing immune cells and tend to exhibit a leakier ECM around the blood vessels. This, however, is beyond the focus of this thesis.

4.2 Discussion and Future Directions in Protease-sensitive IL-12

In Chapter 3, we report the development of a protease-sensitive masked IL-12, which is conditionally activated in the presence of tumor-associated proteases. This approach dramatically decreased the systemic side effects associated with IL-12 therapy, while retaining potent antitumor activity. This technology is different from the one presented in Chapter 2, yet it also comes with its own complexity and nuances. Perhaps the major limitation of protease-sensitive masked IL-12 is the variable expression of tumor-associated enzymes among cancers. First, the expression of proteases is dependent on the tumor stage and location, as later stage tumors and metastatic sites express higher levels of proteases than early malignancies in the primary site[42]. Furthermore, the secretion of particular proteases varies significantly across tumor types[268], making it difficult to construct a single linker with broad reactivity against distinct tumors. We tried to address this issue by combining substrates that are reactive to MMPs and SPs, and we indeed demonstrate that linker sequence has significant impact on the antitumor control. Yet, to perform such optimization for a clinical application, one would need to screen a broad range of tumor tissues or manufacture tumor type-specific immunotherapeutics (a personalized approach). On the contrary, constructing a linker with an exceedingly broad reactivity against enzymes might induce irAEs due to excessive cleavage in circulation. Thus, the balance between linker reactivity and selectivity must be carefully optimized.

Another crucial design parameter of this technology is the affinity of the masking domain to IL-12. A mask with a very high affinity (K_D = ~pM) would still inhibit IL-12 interaction with the native receptor after cleavage. We addressed this problem by showing that the binding of IL-

12 to the endogenous receptor is not inhibited by the soluble mask. We have not, though, investigated how the affinity of the masking domain affects the antitumor efficacy and toxicity. This could be studied by introducing mutations to our masking domain (IL-12Rβ1) that either increase or decrease the affinity to IL-12. Such information would be valuable for the optimization of other protease-activatable biologics.

During our studies, production and purification process of masked IL-12 also posed some challenges. This is due to the partial cleavage of the mask in HEK293 culture. In fact, one of the linkers that we had previously tested, (PLGVRGK) was almost completely cleaved in the culture process and thus we were not able to purify the masked molecule (the product we obtained was simply IL-12 itself, without a masking domain). Other recombinant protein expression systems, such as insect cells or other mammalian cells, that may contain fewer proteases in the culture would result in higher yield of the target molecule.

4.3 Understanding the Clinical Indications for IL-12

The two technologies presented in this thesis rely on different tumor-specific phenomena, namely the hyperpermeability of blood vasculature and overexpression of proteases. Yet it is also important to discuss the potential challenges in using IL-12 as the active agent. One challenge is the tachyphylaxis that was observed in the clinic associated with repeated administration of IL-12. Continued loss of responsiveness to IL-12 is a result of specific pSTAT4 degradation[161], which translates to diminished IFNγ production by T and NK cells over time. One corollary to this phenomenon is that perhaps IL-12 should not be administered at the same dosing regimen as other cytokines (which do not display tachyphylaxis). Due to progressive loss of responsiveness, chronic

administration of IL-12 does not seem very meaningful. Furthermore, chronic inflammation may, in fact, stimulate tumor growth, a phenomenon which has been described for certain cytokines[269].

Exploring the right combination strategies for IL-12 therapy is another direction that could further advance this research. In mice, combination with αPD-1/PD-L1 and αCTLA-4 have been extensively studied. Given the substantial species difference between human and mouse IL-12, it is possible that other, potentially less investigated, immunoregulatory mechanisms exist in humans. Thus, identifying such targets and designing the right combination therapies would increase the effectivness of IL-12 therapy. Investigating the direct interaction between IL-12 and APCs would also add significant benefit.

For successful translation of IL-12-based immunotherapies, we should also deepen our understanding of which tumor types are most likely to respond to IL-12 therapy. In mouse models, we have seen strong potency of IL-12 in B16F10 melanoma and EMT6 triple negative mammary carcinoma, both of which are poorly infiltrated tumors. Yet we did not observe significant antitumor effect in 4T1 triple-negative breast cancer model (data not shown). Understanding the immunological differences among these tumor models and translating this knowledge into human disease may inform us about the most suitable cancer types for IL-12 therapy.

4.4 Conclusion

In conclusion, this work describes two fundamentally different approaches to engineer recombinant IL-12 to enhance its therapeutic index. With a correctly defined dosing regimen, tumor type and the right combination strategy, these technologies may have a clinically meaningful impact.

References

1 Hanahan, D. & Folkman, J. Patterns and emerging mechanisms of the angiogenic switch during tumorigenesis. *Cell* **86**, 353-364, doi:10.1016/s0092-8674(00)80108-7 (1996).

2 Folkman, J. Tumor angiogenesis: therapeutic implications. *N Engl J Med* **285**, 1182-1186, doi:10.1056/nejm197111182852108 (1971).

3 Lugano, R., Ramachandran, M. & Dimberg, A. Tumor angiogenesis: causes, consequences, challenges and opportunities. *Cell Mol Life Sci* **77**, 1745-1770, doi:10.1007/s00018-019-03351-7 (2020).

4 Apte, R. S., Chen, D. S. & Ferrara, N. VEGF in Signaling and Disease: Beyond Discovery and Development. *Cell* **176**, 1248-1264, doi:10.1016/j.cell.2019.01.021 (2019).

5 Guo, P. *et al.* Platelet-derived growth factor-B enhances glioma angiogenesis by stimulating vascular endothelial growth factor expression in tumor endothelia and by promoting pericyte recruitment. *Am J Pathol* **162**, 1083-1093, doi:10.1016/s0002-9440(10)63905-3 (2003).

6 Horsman, M. R. & Vaupel, P. Pathophysiological Basis for the Formation of the Tumor Microenvironment. *Frontiers in Oncology* **6**, doi:10.3389/fonc.2016.00066 (2016).

7 Sceneay, J., Smyth, M. J. & Möller, A. The pre-metastatic niche: finding common ground. *Cancer Metastasis Rev* **32**, 449-464, doi:10.1007/s10555-013-9420-1 (2013).

8 Chen, L., Endler, A. & Shibasaki, F. Hypoxia and angiogenesis: regulation of hypoxia-inducible factors via novel binding factors. *Experimental & Molecular Medicine* **41**, 849-857, doi:10.3858/emm.2009.41.12.103 (2009).

9 Rankin, E. B. & Giaccia, A. J. Hypoxic control of metastasis. *Science* **352**, 175-180, doi:10.1126/science.aaf4405 (2016).

10 Kaplan, R. N. *et al.* VEGFR1-positive haematopoietic bone marrow progenitors initiate the pre-metastatic niche. *Nature* **438**, 820-827, doi:10.1038/nature04186 (2005).

11 Wong, C. C. *et al.* Hypoxia-inducible factor 1 is a master regulator of breast cancer metastatic niche formation. *Proc Natl Acad Sci U S A* **108**, 16369-16374, doi:10.1073/pnas.1113483108 (2011).

12 Matsumura, Y. & Maeda, H. A new concept for macromolecular therapeutics in cancer chemotherapy: mechanism of tumoritropic accumulation of proteins and the antitumor agent smancs. *Cancer Res* **46**, 6387-6392 (1986).

13 Maeda, H., Wu, J., Sawa, T., Matsumura, Y. & Hori, K. Tumor vascular permeability and the EPR effect in macromolecular therapeutics: a review. *J Control Release* **65**, 271-284, doi:10.1016/s0168-3659(99)00248-5 (2000).

14 Fang, J., Nakamura, H. & Maeda, H. The EPR effect: Unique features of tumor blood vessels for drug delivery, factors involved, and limitations and augmentation of the effect. *Adv Drug Deliv Rev* **63**, 136-151, doi:10.1016/j.addr.2010.04.009 (2011).

15 Anselmo, A. C. & Mitragotri, S. Nanoparticles in the clinic: An update. *Bioeng Transl Med* **4**, e10143, doi:10.1002/btm2.10143 (2019).

16 Wilhelm, S. *et al.* Analysis of nanoparticle delivery to tumours. *Nature Reviews Materials* **1**, 16014, doi:10.1038/natrevmats.2016.14 (2016).

17 Mouw, J. K., Ou, G. & Weaver, V. M. Extracellular matrix assembly: a multiscale deconstruction. *Nat Rev Mol Cell Biol* **15**, 771-785, doi:10.1038/nrm3902 (2014).

18 Pozzi, A., Yurchenco, P. D. & Iozzo, R. V. The nature and biology of basement membranes. *Matrix Biol* **57-58**, 1-11, doi:10.1016/j.matbio.2016.12.009 (2017).

19 Provenzano, P. P. *et al.* Collagen density promotes mammary tumor initiation and progression. *BMC Med* **6**, 11, doi:10.1186/1741-7015-6-11 (2008).

20 Conti, J. A. *et al.* The desmoplastic reaction surrounding hepatic colorectal adenocarcinoma metastases aids tumor growth and survival via alphav integrin ligation. *Clin Cancer Res* **14**, 6405-6413, doi:10.1158/1078-0432.Ccr-08-0816 (2008).

21 Schober, M. *et al.* Desmoplasia and chemoresistance in pancreatic cancer. *Cancers (Basel)* **6**, 2137-2154, doi:10.3390/cancers6042137 (2014).

22 Liang, Y., Diehn, M., Bollen, A. W., Israel, M. A. & Gupta, N. Type I collagen is overexpressed in medulloblastoma as a component of tumor microenvironment. *J Neurooncol* **86**, 133-141, doi:10.1007/s11060-007-9457-5 (2008).

23 Banyard, J., Bao, L. & Zetter, B. R. Type XXIII collagen, a new transmembrane collagen identified in metastatic tumor cells. *J Biol Chem* **278**, 20989-20994, doi:10.1074/jbc.M210616200 (2003).

24 Peyrol, S. *et al.* Lysyl oxidase gene expression in the stromal reaction to in situ and invasive ductal breast carcinoma. *Am J Pathol* **150**, 497-507 (1997).

25 Erler, J. T. *et al.* Lysyl oxidase is essential for hypoxia-induced metastasis. *Nature* **440**, 1222-1226, doi:10.1038/nature04695 (2006).

26 Dooley, S. & ten Dijke, P. TGF-β in progression of liver disease. *Cell Tissue Res* **347**, 245-256, doi:10.1007/s00441-011-1246-y (2012).

27 Xu, S. *et al.* The role of collagen in cancer: from bench to bedside. *Journal of Translational Medicine* **17**, 309, doi:10.1186/s12967-019-2058-1 (2019).

28 Pećina-Slaus, N. Tumor suppressor gene E-cadherin and its role in normal and malignant cells. *Cancer Cell Int* **3**, 17, doi:10.1186/1475-2867-3-17 (2003).

29 Kirkland, S. C. Type I collagen inhibits differentiation and promotes a stem cell-like phenotype in human colorectal carcinoma cells. *Br J Cancer* **101**, 320-326, doi:10.1038/sj.bjc.6605143 (2009).

30 Eikenes, L., Bruland Ø, S., Brekken, C. & Davies Cde, L. Collagenase increases the transcapillary pressure gradient and improves the uptake and distribution of monoclonal antibodies in human osteosarcoma xenografts. *Cancer Res* **64**, 4768-4773, doi:10.1158/0008-5472.Can-03-1472 (2004).

31 Fischer, A. Mechanism of the Proteolytic Activity of Malignant Tissue Cells. *Nature* **157**, 442-442, doi:10.1038/157442c0 (1946).

32 Kessenbrock, K., Plaks, V. & Werb, Z. Matrix metalloproteinases: regulators of the tumor microenvironment. *Cell* **141**, 52-67, doi:10.1016/j.cell.2010.03.015 (2010).

33 Ulisse, S., Baldini, E., Sorrenti, S. & D'Armiento, M. The urokinase plasminogen activator system: a target for anti-cancer therapy. *Curr Cancer Drug Targets* **9**, 32-71, doi:10.2174/156800909787314002 (2009).

34 Uhland, K. Matriptase and its putative role in cancer. *Cell Mol Life Sci* **63**, 2968-2978, doi:10.1007/s00018-006-6298-x (2006).

35 Winkler, J., Abisoye-Ogunniyan, A., Metcalf, K. J. & Werb, Z. Concepts of extracellular matrix remodelling in tumour progression and metastasis. *Nat Commun* **11**, 5120, doi:10.1038/s41467-020-18794-x (2020).

36 Ardi, V. C., Kupriyanova, T. A., Deryugina, E. I. & Quigley, J. P. Human neutrophils uniquely release TIMP-free MMP-9 to provide a potent catalytic stimulator of angiogenesis. *Proc Natl Acad Sci U S A* **104**, 20262-20267, doi:10.1073/pnas.0706438104 (2007).

37 Nakamura, E. S., Koizumi, K., Kobayashi, M. & Saiki, I. Inhibition of lymphangiogenesis-related properties of murine lymphatic endothelial cells and lymph node metastasis of lung cancer by the matrix metalloproteinase inhibitor MMI270. *Cancer Sci* **95**, 25-31, doi:10.1111/j.1349-7006.2004.tb03166.x (2004).

38 Liu, S. C. *et al.* Relationships between the level of matrix metalloproteinase-2 and tumor size of breast cancer. *Clin Chim Acta* **371**, 92-96, doi:10.1016/j.cca.2006.02.026 (2006).

39 Schmalfeldt, B. *et al.* Increased expression of matrix metalloproteinases (MMP)-2, MMP-9, and the urokinase-type plasminogen activator is associated with progression from benign to advanced ovarian cancer. *Clin Cancer Res* **7**, 2396-2404 (2001).

40 Werle, B. *et al.* Cathepsin B, plasminogenactivator-inhibitor (PAI-1) and plasminogenactivator-receptor (uPAR) are prognostic factors for patients with non-small cell lung cancer. *Anticancer Res* **24**, 4147-4161 (2004).

41 Remacle, A., Murphy, G. & Roghi, C. Membrane type I-matrix metalloproteinase (MT1-MMP) is internalised by two different pathways and is recycled to the cell surface. *Journal of Cell Science* **116**, 3905-3916, doi:10.1242/jcs.00710 (2003).

42 Cui, G., Cai, F., Ding, Z. & Gao, L. MMP14 predicts a poor prognosis in patients with colorectal cancer. *Hum Pathol* **83**, 36-42, doi:10.1016/j.humpath.2018.03.030 (2019).

43 Winer, A., Adams, S. & Mignatti, P. Matrix Metalloproteinase Inhibitors in Cancer Therapy: Turning Past Failures Into Future Successes. *Mol Cancer Ther* **17**, 1147-1155, doi:10.1158/1535-7163.Mct-17-0646 (2018).

44 Coley, W. B. The treatment of malignant tumors by repeated inoculations of erysipelas. With a report of ten original cases. 1893. *Clin Orthop Relat Res*, 3-11 (1991).

45 Wiemann, B. & Starnes, C. O. Coley's toxins, tumor necrosis factor and cancer research: a historical perspective. *Pharmacol Ther* **64**, 529-564, doi:10.1016/0163-7258(94)90023-x (1994).

46 Knowlton, E. *et al.* Professional antigen presenting cells in human herpesvirus 8 infection. *Frontiers in Immunology* **3**, doi:10.3389/fimmu.2012.00427 (2013).

47 Guo, F. F. & Cui, J. W. The Role of Tumor-Infiltrating B Cells in Tumor Immunity. *Journal of Oncology* **2019**, 2592419, doi:10.1155/2019/2592419 (2019).

48 Ribot, J. C., deBarros, A. & Silva-Santos, B. Searching for “signal 2”: costimulation requirements of γδ T cells. *Cellular and Molecular Life Sciences* **68**, 2345-2355, doi:10.1007/s00018-011-0698-2 (2011).

49 Spellberg, B. & Edwards, J. E., Jr. Type 1/Type 2 Immunity in Infectious Diseases. *Clinical Infectious Diseases* **32**, 76-102, doi:10.1086/317537 (2001).

50 Nishimura, T. *et al.* The critical role of Th1-dominant immunity in tumor immunology. *Cancer Chemother Pharmacol* **46 Suppl**, S52-61, doi:10.1007/pl00014051 (2000).

51 Tosolini, M. *et al.* Clinical Impact of Different Classes of Infiltrating T Cytotoxic and Helper Cells (Th1, Th2, Treg, Th17) in Patients with Colorectal Cancer. *Cancer Research* **71**, 1263-1271, doi:10.1158/0008-5472.Can-10-2907 (2011).

52 Bindea, G. *et al.* Spatiotemporal dynamics of intratumoral immune cells reveal the immune landscape in human cancer. *Immunity* **39**, 782-795, doi:10.1016/j.immuni.2013.10.003 (2013).

53 Ng, S. L., Teo, Y. J., Setiagani, Y. A., Karjalainen, K. & Ruedl, C. Type 1 Conventional CD103+ Dendritic Cells Control Effector CD8+ T Cell Migration, Survival, and Memory Responses During Influenza Infection. *Frontiers in Immunology* **9**, doi:10.3389/fimmu.2018.03043 (2018).

54 Böttcher, J. P. & Reis e Sousa, C. The Role of Type 1 Conventional Dendritic Cells in Cancer Immunity. *Trends Cancer* **4**, 784-792, doi:10.1016/j.trecan.2018.09.001 (2018).

55 Roberts, E. W. *et al.* Critical Role for CD103(+)/CD141(+) Dendritic Cells Bearing CCR7 for Tumor Antigen Trafficking and Priming of T Cell Immunity in Melanoma. *Cancer Cell* **30**, 324-336, doi:10.1016/j.ccell.2016.06.003 (2016).

56 Merad, M., Sathe, P., Helft, J., Miller, J. & Mortha, A. The dendritic cell lineage: ontogeny and function of dendritic cells and their subsets in the steady state and the inflamed setting. *Annu Rev Immunol* **31**, 563-604, doi:10.1146/annurev-immunol-020711-074950 (2013).

57 Spranger, S., Dai, D., Horton, B. & Gajewski, T. F. Tumor-Residing Batf3 Dendritic Cells Are Required for Effector T Cell Trafficking and Adoptive T Cell Therapy. *Cancer cell* **31**, 711-723.e714, doi:10.1016/j.ccell.2017.04.003 (2017).

58 Lou, Y. *et al.* Plasmacytoid dendritic cells synergize with myeloid dendritic cells in the induction of antigen-specific antitumor immune responses. *J Immunol* **178**, 1534-1541, doi:10.4049/jimmunol.178.3.1534 (2007).

59 Liu, C. *et al.* Plasmacytoid dendritic cells induce NK cell-dependent, tumor antigen-specific T cell cross-priming and tumor regression in mice. *J Clin Invest* **118**, 1165-1175, doi:10.1172/jci33583 (2008).

60 Labidi-Galy, S. I. *et al.* Plasmacytoid dendritic cells infiltrating ovarian cancer are associated with poor prognosis. *Oncoimmunology* **1**, 380-382, doi:10.4161/onci.18801 (2012).

61 Ostuni, R., Kratochvill, F., Murray, P. J. & Natoli, G. Macrophages and cancer: from mechanisms to therapeutic implications. *Trends Immunol* **36**, 229-239, doi:10.1016/j.it.2015.02.004 (2015).

62 Cortez-Retamozo, V. *et al.* Origins of tumor-associated macrophages and neutrophils. *Proc Natl Acad Sci U S A* **109**, 2491-2496, doi:10.1073/pnas.1113744109 (2012).

63 Woo, S. R., Corrales, L. & Gajewski, T. F. Innate immune recognition of cancer. *Annu Rev Immunol* **33**, 445-474, doi:10.1146/annurev-immunol-032414-112043 (2015).

64 Najafi, M. *et al.* Macrophage polarity in cancer: A review. *J Cell Biochem* **120**, 2756-2765, doi:10.1002/jcb.27646 (2019).

65 Jarosz-Biej, M. *et al.* M1-like macrophages change tumor blood vessels and microenvironment in murine melanoma. *PLoS One* **13**, e0191012, doi:10.1371/journal.pone.0191012 (2018).

66 Doedens, A. L. *et al.* Macrophage expression of hypoxia-inducible factor-1 alpha suppresses T-cell function and promotes tumor progression. *Cancer Res* **70**, 7465-7475, doi:10.1158/0008-5472.Can-10-1439 (2010).

67 Medrek, C., Pontén, F., Jirström, K. & Leandersson, K. The presence of tumor associated macrophages in tumor stroma as a prognostic marker for breast cancer patients. *BMC Cancer* **12**, 306, doi:10.1186/1471-2407-12-306 (2012).

68 Nahrendorf, M. & Swirski, F. K. Abandoning M1/M2 for a Network Model of Macrophage Function. *Circ Res* **119**, 414-417, doi:10.1161/circresaha.116.309194 (2016).

69 Orecchioni, M., Ghosheh, Y., Pramod, A. B. & Ley, K. Macrophage Polarization: Different Gene Signatures in M1(LPS+) vs. Classically and M2(LPS-) vs. Alternatively Activated Macrophages. *Front Immunol* **10**, 1084, doi:10.3389/fimmu.2019.01084 (2019).

70 Cerwenka, A. & Lanier, L. L. Natural killer cell memory in infection, inflammation and cancer. *Nat Rev Immunol* **16**, 112-123, doi:10.1038/nri.2015.9 (2016).

71 Paul, S. & Lal, G. The Molecular Mechanism of Natural Killer Cells Function and Its Importance in Cancer Immunotherapy. *Frontiers in Immunology* **8**, doi:10.3389/fimmu.2017.01124 (2017).

72 Martínez-Lostao, L., Anel, A. & Pardo, J. How Do Cytotoxic Lymphocytes Kill Cancer Cells? *Clin Cancer Res* **21**, 5047-5056, doi:10.1158/1078-0432.Ccr-15-0685 (2015).

73 Martín-Fontecha, A. *et al.* Induced recruitment of NK cells to lymph nodes provides IFN-gamma for T(H)1 priming. *Nat Immunol* **5**, 1260-1265, doi:10.1038/ni1138 (2004).

74 Gonzalez, H., Hagerling, C. & Werb, Z. Roles of the immune system in cancer: from tumor initiation to metastatic progression. *Genes Dev* **32**, 1267-1284, doi:10.1101/gad.314617.118 (2018).

75 Jenkins, M. K., Chu, H. H., McLachlan, J. B. & Moon, J. J. On the composition of the preimmune repertoire of T cells specific for peptide–major histocompatibility complex ligands. *Annual review of immunology* **28**, 275-294 (2009).

76 Mason, D. A very high level of crossreactivity is an essential feature of the T-cell receptor. *Immunology today* **19**, 395-404 (1998).

77 de Greef, P. C. *et al.* The naive T-cell receptor repertoire has an extremely broad distribution of clone sizes. *Elife* **9**, doi:10.7554/eLife.49900 (2020).

78 Chen, D. S. & Mellman, I. Oncology meets immunology: the cancer-immunity cycle. *Immunity* **39**, 1-10, doi:10.1016/j.immuni.2013.07.012 (2013).

79 Marzo, A. L. *et al.* Tumor antigens are constitutively presented in the draining lymph nodes. *J Immunol* **162**, 5838-5845 (1999).

80 Sautès-Fridman, C., Petitprez, F., Calderaro, J. & Fridman, W. H. Tertiary lymphoid structures in the era of cancer immunotherapy. *Nature Reviews Cancer* **19**, 307-325, doi:10.1038/s41568-019-0144-6 (2019).

81 Voskoboinik, I., Whisstock, J. C. & Trapani, J. A. Perforin and granzymes: function, dysfunction and human pathology. *Nature Reviews Immunology* **15**, 388-400 (2015).

82 Shankaran, V. *et al.* IFNγ and lymphocytes prevent primary tumour development and shape tumour immunogenicity. *Nature* **410**, 1107-1111, doi:10.1038/35074122 (2001).

83 Pardoll, D. M. & Topalian, S. L. The role of CD4+ T cell responses in antitumor immunity. *Curr Opin Immunol* **10**, 588-594, doi:10.1016/s0952-7915(98)80228-8 (1998).

84 Janssen, E. M. *et al.* CD4+ T cells are required for secondary expansion and memory in CD8+ T lymphocytes. *Nature* **421**, 852-856 (2003).

85 Spitzer, M. H. *et al.* Systemic immunity is required for effective cancer immunotherapy. *Cell* **168**, 487-502. e415 (2017).

86 Kambayashi, T. & Laufer, T. M. Atypical MHC class II-expressing antigen-presenting cells: can anything replace a dendritic cell? *Nature Reviews Immunology* **14**, 719-730 (2014).

87 Johnson, D. B. *et al.* Melanoma-specific MHC-II expression represents a tumour-autonomous phenotype and predicts response to anti-PD-1/PD-L1 therapy. *Nature communications* **7**, 1-10 (2016).

88 Park, I. A. *et al.* Expression of the MHC class II in triple-negative breast cancer is associated with tumor-infiltrating lymphocytes and interferon signaling. *PLoS One* **12**, e0182786 (2017).

89 Roemer, M. G. *et al.* Major histocompatibility complex class II and programmed death ligand 1 expression predict outcome after programmed death 1 blockade in classic Hodgkin lymphoma. *Journal of Clinical Oncology* **36**, 942 (2018).

90 Li, Z., Li, D., Tsun, A. & Li, B. FOXP3+ regulatory T cells and their functional regulation. *Cellular & Molecular Immunology* **12**, 558-565, doi:10.1038/cmi.2015.10 (2015).

91 Chen, M.-L. *et al.* Regulatory T cells suppress tumor-specific CD8 T cell cytotoxicity through TGF-β signals in vivo. *Proceedings of the National Academy of Sciences of the United States of America* **102**, 419-424, doi:10.1073/pnas.0408197102 (2005).

92 Shevach, E. M. Foxp3+ T Regulatory Cells: Still Many Unanswered Questions—A Perspective After 20 Years of Study. *Frontiers in Immunology* **9**, doi:10.3389/fimmu.2018.01048 (2018).

93 Uhlig, H. H. *et al.* Characterization of Foxp3+ CD4+ CD25+ and IL-10-secreting CD4+ CD25+ T cells during cure of colitis. *The Journal of Immunology* **177**, 5852-5860 (2006).

94 Grosso, J. F. & Jure-Kunkel, M. N. CTLA-4 blockade in tumor models: an overview of preclinical and translational research. *Cancer Immunity Archive* **13** (2013).

95 Waldman, A. D., Fritz, J. M. & Lenardo, M. J. A guide to cancer immunotherapy: from T cell basic science to clinical practice. *Nature Reviews Immunology* **20**, 651-668, doi:10.1038/s41577-020-0306-5 (2020).

96 Speiser, D. E., Ho, P. C. & Verdeil, G. Regulatory circuits of T cell function in cancer. *Nat Rev Immunol* **16**, 599-611, doi:10.1038/nri.2016.80 (2016).

97 Hornyák, L. *et al.* The Role of Indoleamine-2,3-Dioxygenase in Cancer Development, Diagnostics, and Therapy. *Frontiers in Immunology* **9**, doi:10.3389/fimmu.2018.00151 (2018).

98 Grzywa, T. M. *et al.* Myeloid Cell-Derived Arginase in Cancer Immune Response. *Frontiers in Immunology* **11**, doi:10.3389/fimmu.2020.00938 (2020).

99 Walker, L. S. K. & Sansom, D. M. The emerging role of CTLA4 as a cell-extrinsic regulator of T cell responses. *Nature Reviews Immunology* **11**, 852-863, doi:10.1038/nri3108 (2011).

100 Collins, A. V. *et al.* The interaction properties of costimulatory molecules revisited. *Immunity* **17**, 201-210 (2002).

101 Takahashi, T. *et al.* Immunologic Self-Tolerance Maintained by Cd25+Cd4+Regulatory T Cells Constitutively Expressing Cytotoxic T Lymphocyte–Associated Antigen 4. *Journal of Experimental Medicine* **192**, 303-310, doi:10.1084/jem.192.2.303 (2000).

102 Chuang, E. *et al.* The CD28 and CTLA-4 receptors associate with the serine/threonine phosphatase PP2A. *Immunity* **13**, 313-322, doi:10.1016/s1074-7613(00)00031-5 (2000).

103 Marengère, L. E. *et al.* Regulation of T cell receptor signaling by tyrosine phosphatase SYP association with CTLA-4. *Science* **272**, 1170-1173, doi:10.1126/science.272.5265.1170 (1996).

104 Francisco, L. M., Sage, P. T. & Sharpe, A. H. The PD-1 pathway in tolerance and autoimmunity. *Immunol Rev* **236**, 219-242, doi:10.1111/j.1600-065X.2010.00923.x (2010).

105 Hui, E. *et al.* T cell costimulatory receptor CD28 is a primary target for PD-1-mediated inhibition. *Science* **355**, 1428-1433, doi:10.1126/science.aaf1292 (2017).

106 Wei, S. C. *et al.* Distinct Cellular Mechanisms Underlie Anti-CTLA-4 and Anti-PD-1 Checkpoint Blockade. *Cell* **170**, 1120-1133.e1117, doi:10.1016/j.cell.2017.07.024 (2017).

107 Mimura, K. *et al.* PD-L1 expression is mainly regulated by interferon gamma associated with JAK-STAT pathway in gastric cancer. *Cancer Sci* **109**, 43-53, doi:10.1111/cas.13424 (2018).

108 Chen, J. *et al.* Interferon-γ-induced PD-L1 surface expression on human oral squamous carcinoma via PKD2 signal pathway. *Immunobiology* **217**, 385-393, doi:10.1016/j.imbio.2011.10.016 (2012).

109 Spranger, S., Bao, R. & Gajewski, T. F. Melanoma-intrinsic β-catenin signalling prevents anti-tumour immunity. *Nature* **523**, 231-235, doi:10.1038/nature14404 (2015).

110 Duan, Q., Zhang, H., Zheng, J. & Zhang, L. Turning Cold into Hot: Firing up the Tumor Microenvironment. *Trends Cancer* **6**, 605-618, doi:10.1016/j.trecan.2020.02.022 (2020).

111 Fellner, C. Ipilimumab (yervoy) prolongs survival in advanced melanoma: serious side effects and a hefty price tag may limit its use. *P t* **37**, 503-530 (2012).

112 Alsaab, H. O. *et al.* PD-1 and PD-L1 Checkpoint Signaling Inhibition for Cancer Immunotherapy: Mechanism, Combinations, and Clinical Outcome. *Frontiers in Pharmacology* **8**, doi:10.3389/fphar.2017.00561 (2017).

113 Liu, B., Song, Y. & Liu, D. Recent development in clinical applications of PD-1 and PD-L1 antibodies for cancer immunotherapy. *Journal of Hematology & Oncology* **10**, 174, doi:10.1186/s13045-017-0541-9 (2017).

114 Michot, J. M. *et al.* Immune-related adverse events with immune checkpoint blockade: a comprehensive review. *Eur J Cancer* **54**, 139-148, doi:10.1016/j.ejca.2015.11.016 (2016).

115 Martins, F. *et al.* Adverse effects of immune-checkpoint inhibitors: epidemiology, management and surveillance. *Nature Reviews Clinical Oncology* **16**, 563-580, doi:10.1038/s41571-019-0218-0 (2019).

116 Postow, M. A. *et al.* Nivolumab and ipilimumab versus ipilimumab in untreated melanoma. *N Engl J Med* **372**, 2006-2017, doi:10.1056/NEJMoa1414428 (2015).

117 Qin, S. *et al.* Novel immune checkpoint targets: moving beyond PD-1 and CTLA-4. *Molecular Cancer* **18**, 155, doi:10.1186/s12943-019-1091-2 (2019).

118 Fyfe, G. *et al.* Results of treatment of 255 patients with metastatic renal cell carcinoma who received high-dose recombinant interleukin-2 therapy. *J Clin Oncol* **13**, 688-696, doi:10.1200/jco.1995.13.3.688 (1995).

119 Atkins, M. B. *et al.* High-dose recombinant interleukin 2 therapy for patients with metastatic melanoma: analysis of 270 patients treated between 1985 and 1993. *J Clin Oncol* **17**, 2105-2116, doi:10.1200/jco.1999.17.7.2105 (1999).

120 Golomb, H. M. *et al.* Alpha-2 interferon therapy of hairy-cell leukemia: a multicenter study of 64 patients. *J Clin Oncol* **4**, 900-905, doi:10.1200/jco.1986.4.6.900 (1986).

121 Groopman, J. E. *et al.* Recombinant alpha-2 interferon therapy for Kaposi's sarcoma associated with the acquired immunodeficiency syndrome. *Ann Intern Med* **100**, 671-676, doi:10.7326/0003-4819-100-5-671 (1984).

122 Lee, S. & Margolin, K. Cytokines in cancer immunotherapy. *Cancers (Basel)* **3**, 3856-3893, doi:10.3390/cancers3043856 (2011).

123 Atkins, M. B. *et al.* Phase I evaluation of intravenous recombinant human interleukin 12 in patients with advanced malignancies. *Clin Cancer Res* **3**, 409-417 (1997).

124 Dutcher, J. P. *et al.* High dose interleukin-2 (Aldesleukin) - expert consensus on best management practices-2014. *J Immunother Cancer* **2**, 26, doi:10.1186/s40425-014-0026-0 (2014).

125 Shuford, W. W. *et al.* 4-1BB costimulatory signals preferentially induce CD8+ T cell proliferation and lead to the amplification in vivo of cytotoxic T cell responses. *J Exp Med* **186**, 47-55, doi:10.1084/jem.186.1.47 (1997).

126 Wen, T., Bukczynski, J. & Watts, T. H. 4-1BB ligand-mediated costimulation of human T cells induces CD4 and CD8 T cell expansion, cytokine production, and the development of cytolytic effector function. *J Immunol* **168**, 4897-4906, doi:10.4049/jimmunol.168.10.4897 (2002).

127 Segal, N. H. *et al.* Results from an Integrated Safety Analysis of Urelumab, an Agonist Anti-CD137 Monoclonal Antibody. *Clin Cancer Res* **23**, 1929-1936, doi:10.1158/1078-0432.Ccr-16-1272 (2017).

128 Weiner, L. M., Surana, R. & Wang, S. Monoclonal antibodies: versatile platforms for cancer immunotherapy. *Nat Rev Immunol* **10**, 317-327, doi:10.1038/nri2744 (2010).

129 PENTO, J. T. Monoclonal Antibodies for the Treatment of Cancer. *Anticancer Research* **37**, 5935-5939 (2017).

130 Rosenberg, S. A., Restifo, N. P., Yang, J. C., Morgan, R. A. & Dudley, M. E. Adoptive cell transfer: a clinical path to effective cancer immunotherapy. *Nature Reviews Cancer* **8**, 299-308, doi:10.1038/nrc2355 (2008).

131 Mohanty, R. *et al.* CAR T cell therapy: A new era for cancer treatment (Review). *Oncol Rep* **42**, 2183-2195, doi:10.3892/or.2019.7335 (2019).

132 Brudno, J. N. & Kochenderfer, J. N. Toxicities of chimeric antigen receptor T cells: recognition and management. *Blood* **127**, 3321-3330, doi:10.1182/blood-2016-04-703751 (2016).

133 Levy, D. E. & Darnell, J. E., Jr. Stats: transcriptional control and biological impact. *Nat Rev Mol Cell Biol* **3**, 651-662, doi:10.1038/nrm909 (2002).

134 Meyer, T. & Vinkemeier, U. STAT nuclear translocation: potential for pharmacological intervention. *Expert Opin Ther Targets* **11**, 1355-1365, doi:10.1517/14728222.11.10.1355 (2007).

135 Ruggiero, A. *et al.* Paradoxical glomerular filtration of carbon nanotubes. *Proc Natl Acad Sci U S A* **107**, 12369-12374, doi:10.1073/pnas.0913667107 (2010).

136 Kobayashi, M. *et al.* Identification and purification of natural killer cell stimulatory factor (NKSF), a cytokine with multiple biologic effects on human lymphocytes. *J Exp Med* **170**, 827-845, doi:10.1084/jem.170.3.827 (1989).

137 Wolf, S. F. *et al.* Cloning of cDNA for natural killer cell stimulatory factor, a heterodimeric cytokine with multiple biologic effects on T and natural killer cells. *J Immunol* **146**, 3074-3081 (1991).

138 Langrish, C. L. *et al.* IL-12 and IL-23: master regulators of innate and adaptive immunity. *Immunol Rev* **202**, 96-105, doi:10.1111/j.0105-2896.2004.00214.x (2004).

139 Teng, M. W. *et al.* IL-12 and IL-23 cytokines: from discovery to targeted therapies for immune-mediated inflammatory diseases. *Nat Med* **21**, 719-729, doi:10.1038/nm.3895 (2015).

140 Sakkas, L. I., Mavropoulos, A., Perricone, C. & Bogdanos, D. P. IL-35: a new immunomodulator in autoimmune rheumatic diseases. *Immunol Res* **66**, 305-312, doi:10.1007/s12026-018-8998-3 (2018).

141 Carl, J. W. & Bai, X. F. IL27: its roles in the induction and inhibition of inflammation. *Int J Clin Exp Pathol* **1**, 117-123 (2008).

142 Presky, D. H. *et al.* A functional interleukin 12 receptor complex is composed of two beta-type cytokine receptor subunits. *Proc Natl Acad Sci U S A* **93**, 14002-14007, doi:10.1073/pnas.93.24.14002 (1996).

143 Zhang, G. X. *et al.* Role of IL-12 receptor beta 1 in regulation of T cell response by APC in experimental autoimmune encephalomyelitis. *J Immunol* **171**, 4485-4492, doi:10.4049/jimmunol.171.9.4485 (2003).

144 Szabo, S. J., Dighe, A. S., Gubler, U. & Murphy, K. M. Regulation of the interleukin (IL)-12R beta 2 subunit expression in developing T helper 1 (Th1) and Th2 cells. *J Exp Med* **185**, 817-824, doi:10.1084/jem.185.5.817 (1997).

145 Wu, C. Y., Gadina, M., Wang, K., O'Shea, J. & Seder, R. A. Cytokine regulation of IL-12 receptor beta2 expression: differential effects on human T and NK cells. *Eur J Immunol* **30**, 1364-1374, doi:10.1002/(sici)1521-4141(200005)30:5<1364::Aid-immu1364>3.0.Co;2-u (2000).

146 Trinchieri, G., Pflanz, S. & Kastelein, R. A. The IL-12 family of heterodimeric cytokines: new players in the regulation of T cell responses. *Immunity* **19**, 641-644 (2003).

147 Grohmann, U. *et al.* IL-12 acts directly on DC to promote nuclear localization of NF-kappaB and primes DC for IL-12 production. *Immunity* **9**, 315-323, doi:10.1016/s1074-7613(00)80614-7 (1998).

148 Nagayama, H. *et al.* IL-12 responsiveness and expression of IL-12 receptor in human peripheral blood monocyte-derived dendritic cells. *J Immunol* **165**, 59-66, doi:10.4049/jimmunol.165.1.59 (2000).

149 Nastala, C. L. *et al.* Recombinant IL-12 administration induces tumor regression in association with IFN-gamma production. *J Immunol* **153**, 1697-1706 (1994).

150 Wang, L. L. *et al.* CXC-chemokine-ligand-10 gene therapy efficiently inhibits the growth of cervical carcinoma on the basis of its anti-angiogenic and antiviral activity. *Biotechnology and applied biochemistry* **53**, 209-216, doi:10.1042/ba20090012 (2009).

151 Coughlin, C. M. *et al.* Tumor cell responses to IFNγ affect tumorigenicity and response to IL-12 therapy and antiangiogenesis. *Immunity* **9**, 25-34 (1998).

152 Kanegane, C. *et al.* Contribution of the CXC chemokines IP-10 and Mig to the antitumor effects of IL-12. *Journal of leukocyte biology* **64**, 384-392 (1998).

153 Voest, E. E. *et al.* Inhibition of angiogenesis in vivo by interleukin 12. *J Natl Cancer Inst* **87**, 581-586, doi:10.1093/jnci/87.8.581 (1995).

154 Eisenring, M., Vom Berg, J., Kristiansen, G., Saller, E. & Becher, B. IL-12 initiates tumor rejection via lymphoid tissue–inducer cells bearing the natural cytotoxicity receptor NKp46. *Nature immunology* **11**, 1030 (2010).

155 D'andrea, A. *et al.* Interleukin 10 (IL-10) inhibits human lymphocyte interferon gamma-production by suppressing natural killer cell stimulatory factor/IL-12 synthesis in accessory cells. *The Journal of experimental medicine* **178**, 1041-1048 (1993).

156 Du, C. & Sriram, S. Mechanism of inhibition of LPS-induced IL-12p40 production by IL-10 and TGF-β in ANA-1 cells. *Journal of leukocyte biology* **64**, 92-97 (1998).

157 Brunda, M. J. *et al.* Antitumor and antimetastatic activity of interleukin 12 against murine tumors. *J Exp Med* **178**, 1223-1230, doi:10.1084/jem.178.4.1223 (1993).

158 Cohen, J. IL-12 deaths: explanation and a puzzle. *Science* **270**, 908, doi:10.1126/science.270.5238.908a (1995).

159 Sacco, S. *et al.* Protective effect of a single interleukin-12 (IL-12) predose against the toxicity of subsequent chronic IL-12 in mice: role of cytokines and glucocorticoids. *Blood* **90**, 4473-4479 (1997).

160 Leonard, J. P. *et al.* Effects of single-dose interleukin-12 exposure on interleukin-12-associated toxicity and interferon-gamma production. *Blood* **90**, 2541-2548 (1997).

161 Wang, K. S., Zorn, E. & Ritz, J. Specific down-regulation of interleukin-12 signaling through induction of phospho-STAT4 protein degradation. *Blood* **97**, 3860-3866, doi:10.1182/blood.v97.12.3860 (2001).

162 Ryffel, B. Interleukin-12: role of interferon-gamma in IL-12 adverse effects. *Clin Immunol Immunopathol* **83**, 18-20, doi:10.1006/clin.1996.4306 (1997).

163 van Herpen, C. M. *et al.* Intratumoral administration of recombinant human interleukin 12 in head and neck squamous cell carcinoma patients elicits a T-helper 1 profile in the locoregional lymph nodes. *Clinical Cancer Research* **10**, 2626-2635 (2004).

164 van Herpen, C. M. *et al.* Intratumoral rhIL-12 administration in head and neck squamous cell carcinoma patients induces B cell activation. *International journal of cancer* **123**, 2354-2361 (2008).

165 Portielje, J. E. *et al.* Phase I study of subcutaneously administered recombinant human interleukin 12 in patients with advanced renal cell cancer. *Clinical cancer research* **5**, 3983-3989 (1999).

166 Ohno, R. *et al.* A dose-escalation and pharmacokinetic study of subcutaneously administered recombinant human interleukin 12 and its biological effects in Japanese patients with advanced malignancies. *Clinical cancer research* **6**, 2661-2669 (2000).

167 Bajetta, E. *et al.* Pilot study of subcutaneous recombinant human interleukin 12 in metastatic melanoma. *Clin Cancer Res* **4**, 75-85 (1998).

168 Little, R. F. *et al.* Activity of subcutaneous interleukin-12 in AIDS-related Kaposi sarcoma. *Blood* **107**, 4650-4657 (2006).

169 Gollob, J. A. *et al.* Phase I trial of concurrent twice-weekly recombinant human interleukin-12 plus low-dose IL-2 in patients with melanoma or renal cell carcinoma. *Journal of Clinical Oncology* **21**, 2564-2573 (2003).

170 Alatrash, G. *et al.* Clinical and immunologic effects of subcutaneously administered interleukin-12 and interferon alfa-2b: phase I trial of patients with metastatic renal cell carcinoma or malignant melanoma. *J Clin Oncol* **22**, 2891-2900, doi:10.1200/jco.2004.10.045 (2004).

171 Halin, C. *et al.* Enhancement of the antitumor activity of interleukin-12 by targeted delivery to neovasculature. *Nat Biotechnol* **20**, 264-269, doi:10.1038/nbt0302-264 (2002).

172 Pasche, N., Wulhfard, S., Pretto, F., Carugati, E. & Neri, D. The antibody-based delivery of interleukin-12 to the tumor neovasculature eradicates murine models of cancer in combination with paclitaxel. *Clin Cancer Res* **18**, 4092-4103, doi:10.1158/1078-0432.Ccr-12-0282 (2012).

173 Kim, H., Gao, W. & Ho, M. Novel immunocytokine IL12-SS1 (Fv) inhibits mesothelioma tumor growth in nude mice. *PLoS One* **8**, e81919, doi:10.1371/journal.pone.0081919 (2013).

174 Fallon, J. *et al.* The immunocytokine NHS-IL12 as a potential cancer therapeutic. *Oncotarget* **5**, 1869-1884, doi:10.18632/oncotarget.1853 (2014).

175 Strauss, J. *et al.* First-in-Human Phase I Trial of a Tumor-Targeted Cytokine (NHS-IL12) in Subjects with Metastatic Solid Tumors. *Clin Cancer Res* **25**, 99-109, doi:10.1158/1078-0432.Ccr-18-1512 (2019).

176 Lan, Y. *et al.* Enhanced preclinical antitumor activity of M7824, a bifunctional fusion protein simultaneously targeting PD-L1 and TGF-β. *Sci Transl Med* **10**, doi:10.1126/scitranslmed.aan5488 (2018).

177 Lo, K. M. *et al.* huBC1-IL12, an immunocytokine which targets EDB-containing oncofetal fibronectin in tumors and tumor vasculature, shows potent anti-tumor activity in human tumor models. *Cancer Immunol Immunother* **56**, 447-457, doi:10.1007/s00262-006-0203-1 (2007).

178 Rudman, S. M. *et al.* A phase 1 study of AS1409, a novel antibody-cytokine fusion protein, in patients with malignant melanoma or renal cell carcinoma. *Clin Cancer Res* **17**, 1998-2005, doi:10.1158/1078-0432.Ccr-10-2490 (2011).

179 Jung, K. *et al.* Heterodimeric Fc-fused IL12 shows potent antitumor activity by generating memory CD8(+) T cells. *Oncoimmunology* **7**, e1438800, doi:10.1080/2162402x.2018.1438800 (2018).

180 Momin, N. *et al.* Anchoring of intratumorally administered cytokines to collagen safely potentiates systemic cancer immunotherapy. *Sci Transl Med* **11**, doi:10.1126/scitranslmed.aaw2614 (2019).

181 Algazi, A. P. *et al.* Phase II Trial of IL-12 Plasmid Transfection and PD-1 Blockade in Immunologically Quiescent Melanoma. *Clinical Cancer Research* **26**, 2827-2837, doi:10.1158/1078-0432.Ccr-19-2217 (2020).

182 Hewitt, S. L. *et al.* Intratumoral IL12 mRNA Therapy Promotes TH1 Transformation of the Tumor Microenvironment. *Clinical Cancer Research* **26**, 6284-6298 (2020).

183 Chiocca, E. A. *et al.* Regulatable interleukin-12 gene therapy in patients with recurrent high-grade glioma: Results of a phase 1 trial. *Science Translational Medicine* **11**, eaaw5680, doi:10.1126/scitranslmed.aaw5680 (2019).

184 Larkin, J. *et al.* Combined Nivolumab and Ipilimumab or Monotherapy in Untreated Melanoma. *The New England journal of medicine* **373**, 23-34, doi:10.1056/NEJMoa1504030 (2015).

185 Sharma, P. & Allison, J. P. The future of immune checkpoint therapy. *Science* **348**, 56-61, doi:10.1126/science.aaa8172 (2015).

186 Rosenberg, S. A., Yang, J. C. & Restifo, N. P. Cancer immunotherapy: moving beyond current vaccines. *Nature medicine* **10**, 909-915, doi:10.1038/nm1100 (2004).

187 McHeyzer-Williams, M. G. *et al.* Antigen-specific immunity. *Immunologic Research* **22**, 223-236, doi:10.1385/ir:22:2-3:223 (2000).

188 Fallarino, F., Ashikari, A., Boon, T. & Gajewski, T. F. Antigen-specific regression of established tumors induced by active immunization with irradiated IL-12- but not B7-1-transfected tumor cells. *Int Immunol* **9**, 1259-1269, doi:10.1093/intimm/9.9.1259 (1997).

189 Rogge, L. *et al.* Selective expression of an interleukin-12 receptor component by human T helper 1 cells. *The Journal of experimental medicine* **185**, 825-831 (1997).

190 Tugues, S. *et al.* New insights into IL-12-mediated tumor suppression. *Cell Death Differ* **22**, 237-246, doi:10.1038/cdd.2014.134 (2015).

191 Lasek, W., Zagozdzon, R. & Jakobisiak, M. Interleukin 12: still a promising candidate for tumor immunotherapy? *Cancer immunology, immunotherapy : CII* **63**, 419-435, doi:10.1007/s00262-014-1523-1 (2014).

192 Kerkar, S. P. *et al.* IL-12 triggers a programmatic change in dysfunctional myeloid-derived cells within mouse tumors. *The Journal of clinical investigation* **121**, 4746-4757, doi:10.1172/jci58814 (2011).

193 Ishihara, J. *et al.* Targeted antibody and cytokine cancer immunotherapies through collagen affinity. *Sci Transl Med* **11**, doi:10.1126/scitranslmed.aau3259 (2019).

194 Bekaii-Saab, T. S. *et al.* A phase I trial of paclitaxel and trastuzumab in combination with interleukin-12 in patients with HER2/neu-expressing malignancies. *Mol Cancer Ther* **8**, 2983-2991, doi:10.1158/1535-7163.Mct-09-0820 (2009).

195 Gollob, J. A. *et al.* Phase I trial of concurrent twice-weekly recombinant human interleukin-12 plus low-dose IL-2 in patients with melanoma or renal cell carcinoma. *J Clin Oncol* **21**, 2564-2573, doi:10.1200/jco.2003.12.119 (2003).

196 Mariathasan, S. *et al.* TGFbeta attenuates tumour response to PD-L1 blockade by contributing to exclusion of T cells. *Nature* **554**, 544-548, doi:10.1038/nature25501 (2018).

197 Zhang, Y., Li, N., Suh, H. & Irvine, D. J. Nanoparticle anchoring targets immune agonists to tumors enabling anti-cancer immunity without systemic toxicity. *Nat Commun* **9**, 6, doi:10.1038/s41467-017-02251-3 (2018).

198 Joyce, J. A. & Fearon, D. T. T cell exclusion, immune privilege, and the tumor microenvironment. *Science* **348**, 74-80, doi:10.1126/science.aaa6204 (2015).

199 Gollob, J. A. *et al.* Phase I trial of twice-weekly intravenous interleukin 12 in patients with metastatic renal cell cancer or malignant melanoma: ability to maintain IFN-gamma induction is associated with clinical response. *Clinical cancer research : an official journal of the American Association for Cancer Research* **6**, 1678-1692 (2000).

200 Ayers, M. *et al.* IFN-gamma-related mRNA profile predicts clinical response to PD-1 blockade. *The Journal of clinical investigation* **127**, 2930-2940, doi:10.1172/jci91190 (2017).

201 Ghiringhelli, F. *et al.* Activation of the NLRP3 inflammasome in dendritic cells induces IL-1beta-dependent adaptive immunity against tumors. *Nature medicine* **15**, 1170-1178, doi:10.1038/nm.2028 (2009).

202 Liu, F. & Whitton, J. L. Cutting edge: re-evaluating the in vivo cytokine responses of CD8+ T cells during primary and secondary viral infections. *Journal of immunology (Baltimore, Md. : 1950)* **174**, 5936-5940, doi:10.4049/jimmunol.174.10.5936 (2005).

203 Neri, D. Antibody-Cytokine Fusions: Versatile Products for the Modulation of Anticancer Immunity. *Cancer Immunol Res* **7**, 348-354, doi:10.1158/2326-6066.Cir-18-0622 (2019).

204 Zhou, F. Molecular mechanisms of IFN-gamma to up-regulate MHC class I antigen processing and presentation. *Int Rev Immunol* **28**, 239-260, doi:10.1080/08830180902978120 (2009).

205 Clatza, A., Bonifaz, L. C., Vignali, D. A. & Moreno, J. CD40-induced aggregation of MHC class II and CD80 on the cell surface leads to an early enhancement in antigen presentation. *Journal of immunology (Baltimore, Md. : 1950)* **171**, 6478-6487 (2003).

206 Ho, P. C. *et al.* Immune-based antitumor effects of BRAF inhibitors rely on signaling by CD40L and IFNgamma. *Cancer research* **74**, 3205-3217, doi:10.1158/0008-5472.Can-13-3461 (2014).

207 Pan, D. *et al.* A major chromatin regulator determines resistance of tumor cells to T cell-mediated killing. *Science* **359**, 770-775, doi:10.1126/science.aao1710 (2018).

208 Boross, P. *et al.* Anti-tumor activity of human IgG1 anti-gp75 TA99 mAb against B16F10 melanoma in human FcgammaRI transgenic mice. *Immunol Lett* **160**, 151-157, doi:10.1016/j.imlet.2014.02.005 (2014).

209 Castle, J. C. *et al.* Exploiting the mutanome for tumor vaccination. *Cancer research* **72**, 1081-1091, doi:10.1158/0008-5472.Can-11-3722 (2012).

210 Dankort, D. *et al.* Braf(V600E) cooperates with Pten loss to induce metastatic melanoma. *Nat Genet* **41**, 544-552, doi:10.1038/ng.356 (2009).

211 Ishihara, J. *et al.* Matrix-binding checkpoint immunotherapies enhance antitumor efficacy and reduce adverse events. *Sci Transl Med* **9**, doi:10.1126/scitranslmed.aan0401 (2017).

212 Gros, A. *et al.* PD-1 identifies the patient-specific CD8(+) tumor-reactive repertoire infiltrating human tumors. *The Journal of clinical investigation* **124**, 2246-2259, doi:10.1172/jci73639 (2014).

213 Spranger, S., Bao, R. & Gajewski, T. F. Melanoma-intrinsic beta-catenin signalling prevents anti-tumour immunity. *Nature* **523**, 231-235, doi:10.1038/nature14404 (2015).

214 Drake, C. G., Lipson, E. J. & Brahmer, J. R. Breathing new life into immunotherapy: review of melanoma, lung and kidney cancer. *Nat Rev Clin Oncol* **11**, 24-37, doi:10.1038/nrclinonc.2013.208 (2014).

215 Moynihan, K. D. *et al.* Eradication of large established tumors in mice by combination immunotherapy that engages innate and adaptive immune responses. *Nature medicine* **22**, 1402-1410, doi:10.1038/nm.4200 (2016).

216 Garris, C. S. *et al.* Successful Anti-PD-1 Cancer Immunotherapy Requires T Cell-Dendritic Cell Crosstalk Involving the Cytokines IFN-gamma and IL-12. *Immunity* **49**, 1148-1161.e1147, doi:10.1016/j.immuni.2018.09.024 (2018).

217 Coughlin, C. M. *et al.* Tumor cell responses to IFNgamma affect tumorigenicity and response to IL-12 therapy and antiangiogenesis. *Immunity* **9**, 25-34 (1998).

218 Nagy, J. A., Chang, S. H., Dvorak, A. M. & Dvorak, H. F. Why are tumour blood vessels abnormal and why is it important to know? *Br J Cancer* **100**, 865-869, doi:10.1038/sj.bjc.6604929 (2009).

219 Grigorian, A. & O'Brien, C. B. Hepatotoxicity Secondary to Chemotherapy. *J Clin Transl Hepatol* **2**, 95-102, doi:10.14218/jcth.2014.00011 (2014).

220 van Herpen, C. M. *et al.* Intratumoral recombinant human interleukin-12 administration in head and neck squamous cell carcinoma patients modifies locoregional lymph node architecture and induces natural killer cell infiltration in the primary tumor. *Clinical cancer research : an official journal of the American Association for Cancer Research* **11**, 1899-1909, doi:10.1158/1078-0432.Ccr-04-1524 (2005).

221 Mahvi, D. M. *et al.* Intratumoral injection of IL-12 plasmid DNA--results of a phase I/IB clinical trial. *Cancer Gene Ther* **14**, 717-723, doi:10.1038/sj.cgt.7701064 (2007).

222 Swartz, M. A. & Lund, A. W. Lymphatic and interstitial flow in the tumour microenvironment: linking mechanobiology with immunity. *Nat Rev Cancer* **12**, 210-219, doi:10.1038/nrc3186 (2012).

223 Strauss, J. *et al.* First-in-Human Phase I Trial of a Tumor-Targeted Cytokine (NHS-IL12) in Subjects with Metastatic Solid Tumors. *Clinical cancer research : an official journal of the American Association for Cancer Research* **25**, 99-109, doi:10.1158/1078-0432.Ccr-18-1512 (2019).

224 Hank, J. A. *et al.* Immunogenicity of the Hu14.18-IL2 Immunocytokine Molecule in Adults With Melanoma and Children With Neuroblastoma. *Clinical Cancer Research* **15**, 5923-5930, doi:10.1158/1078-0432.Ccr-08-2963 (2009).

225 Williford, J. M. *et al.* Recruitment of CD103(+) dendritic cells via tumor-targeted chemokine delivery enhances efficacy of checkpoint inhibitor immunotherapy. *Sci Adv* **5**, eaay1357, doi:10.1126/sciadv.aay1357 (2019).

226 Sasaki, K. *et al.* Engineered collagen-binding serum albumin as a drug conjugate carrier for cancer therapy. *Sci Adv* **5**, eaaw6081, doi:10.1126/sciadv.aaw6081 (2019).

227 Ishihara, J. *et al.* Improving Efficacy and Safety of Agonistic Anti-CD40 Antibody Through Extracellular Matrix Affinity. *Mol Cancer Ther* **17**, 2399-2411, doi:10.1158/1535-7163.Mct-18-0091 (2018).

228 Zou, W., Wolchok, J. D. & Chen, L. PD-L1 (B7-H1) and PD-1 pathway blockade for cancer therapy: Mechanisms, response biomarkers, and combinations. *Sci Transl Med* **8**, 328rv324, doi:10.1126/scitranslmed.aad7118 (2016).

229 Kalbasi, A. & Ribas, A. Tumour-intrinsic resistance to immune checkpoint blockade. *Nature Reviews Immunology* **20**, 25-39, doi:10.1038/s41577-019-0218-4 (2020).

230 Vitale, I., Shema, E., Loi, S. & Galluzzi, L. Intratumoral heterogeneity in cancer progression and response to immunotherapy. *Nature medicine* **27**, 212-224 (2021).

231 Gocher, A. M., Workman, C. J. & Vignali, D. A. A. Interferon-γ: teammate or opponent in the tumour microenvironment? *Nature Reviews Immunology*, doi:10.1038/s41577-021-00566-3 (2021).

232 Ayers, M. *et al.* IFN-γ-related mRNA profile predicts clinical response to PD-1 blockade. *J Clin Invest* **127**, 2930-2940, doi:10.1172/jci91190 (2017).

233 Ackerman, S. E. *et al.* Immune-stimulating antibody conjugates elicit robust myeloid activation and durable antitumor immunity. *Nature Cancer* **2**, 18-33, doi:10.1038/s43018-020-00136-x (2021).

234 Mansurov, A. *et al.* Collagen-binding IL-12 enhances tumour inflammation and drives the complete remission of established immunologically cold mouse tumours. *Nature Biomedical Engineering* **4**, 531-543, doi:10.1038/s41551-020-0549-2 (2020).

235 Nguyen, K. G. *et al.* Localized Interleukin-12 for Cancer Immunotherapy. *Frontiers in Immunology* **11**, doi:10.3389/fimmu.2020.575597 (2020).

236 Adams, G., Vessillier, S., Dreja, H. & Chernajovsky, Y. Targeting cytokines to inflammation sites. *Nat Biotechnol* **21**, 1314-1320, doi:10.1038/nbt888 (2003).

237 Gerspach, J. *et al.* Restoration of membrane TNF-like activity by cell surface targeting and matrix metalloproteinase-mediated processing of a TNF prodrug. *Cell Death Differ* **13**, 273-284, doi:10.1038/sj.cdd.4401735 (2006).

238 Glassman, C. R. *et al.* Structural basis for IL-12 and IL-23 receptor sharing reveals a gateway for shaping actions on T versus NK cells. *Cell* **184**, 983-999. e924 (2021).

239 Turk, B. E., Huang, L. L., Piro, E. T. & Cantley, L. C. Determination of protease cleavage site motifs using mixture-based oriented peptide libraries. *Nat Biotechnol* **19**, 661-667, doi:10.1038/90273 (2001).

240 Desnoyers, L. R. *et al.* Tumor-Specific Activation of an EGFR-Targeting Probody Enhances Therapeutic Index. *Science Translational Medicine* **5**, 207ra144-207ra144, doi:10.1126/scitranslmed.3006682 (2013).

241 Presky, D. H. *et al.* Analysis of the multiple interactions between IL-12 and the high affinity IL-12 receptor complex. *J Immunol* **160**, 2174-2179 (1998).

242 Vasiljeva, O., Menendez, E., Nguyen, M., Craik, C. S. & Michael Kavanaugh, W. Monitoring protease activity in biological tissues using antibody prodrugs as sensing probes. *Sci Rep* **10**, 5894, doi:10.1038/s41598-020-62339-7 (2020).

243 Mariathasan, S. *et al.* TGFβ attenuates tumour response to PD-L1 blockade by contributing to exclusion of T cells. *Nature* **554**, 544-548, doi:10.1038/nature25501 (2018).

244 Tugues, S. *et al.* New insights into IL-12-mediated tumor suppression. *Cell Death & Differentiation* **22**, 237-246, doi:10.1038/cdd.2014.134 (2015).

245 Wu, X. *et al.* TNF-α sensitizes chemotherapy and radiotherapy against breast cancer cells. *Cancer Cell International* **17**, 13, doi:10.1186/s12935-017-0382-1 (2017).

246 Kim, K.-J. *et al.* Antitumor effects of IL-12 and GM-CSF co-expressed in an engineered oncolytic HSV-1. *Gene Therapy* **28**, 186-198, doi:10.1038/s41434-020-00205-x (2021).

247 Pan, J. *et al.* Interferon-gamma is an autocrine mediator for dendritic cell maturation. *Immunol Lett* **94**, 141-151, doi:10.1016/j.imlet.2004.05.003 (2004).

248 Von Stebut, E. *et al.* Interleukin 1alpha promotes Th1 differentiation and inhibits disease progression in Leishmania major-susceptible BALB/c mice. *J Exp Med* **198**, 191-199, doi:10.1084/jem.20030159 (2003).

249 Dangaj, D. *et al.* Cooperation between Constitutive and Inducible Chemokines Enables T Cell Engraftment and Immune Attack in Solid Tumors. *Cancer Cell* **35**, 885-900.e810, doi:10.1016/j.ccell.2019.05.004 (2019).

250 Yang, L., Edwards, C. M. & Mundy, G. R. Gr-1+CD11b+ myeloid-derived suppressor cells: formidable partners in tumor metastasis. *J Bone Miner Res* **25**, 1701-1706, doi:10.1002/jbmr.154 (2010).

251 Car, B. D. *et al.* Role of interferon-gamma in interleukin 12-induced pathology in mice. *Am J Pathol* **147**, 1693-1707 (1995).

252 Eng, V. M. *et al.* The stimulatory effects of interleukin (IL)-12 on hematopoiesis are antagonized by IL-12-induced interferon gamma in vivo. *J Exp Med* **181**, 1893-1898, doi:10.1084/jem.181.5.1893 (1995).

253 Puca, E. *et al.* The antibody-based delivery of interleukin-12 to solid tumors boosts NK and CD8+ T cell activity and synergizes with immune checkpoint inhibitors. *International Journal of Cancer* **146**, 2518-2530, doi:https://doi.org/10.1002/ijc.32603 (2020).

254 Momin, N. *et al.* Anchoring of intratumorally administered cytokines to collagen safely potentiates systemic cancer immunotherapy. *Science Translational Medicine* **11**, eaaw2614, doi:10.1126/scitranslmed.aaw2614 (2019).

255 Strauss, J. *et al.* First-in-Human Phase I Trial of a Tumor-Targeted Cytokine (NHS-IL12) in Subjects with Metastatic Solid Tumors. *Clinical Cancer Research* **25**, 99-109, doi:10.1158/1078-0432.Ccr-18-1512 (2019).

256 Li, Y. *et al.* Multifunctional oncolytic nanoparticles deliver self-replicating IL-12 RNA to eliminate established tumors and prime systemic immunity. *Nature Cancer* **1**, 882-893 (2020).

257 Yao, Q., Kou, L., Tu, Y. & Zhu, L. MMP-Responsive 'Smart' Drug Delivery and Tumor Targeting. *Trends Pharmacol Sci* **39**, 766-781, doi:10.1016/j.tips.2018.06.003 (2018).

258 Kwon, E. J., Dudani, J. S. & Bhatia, S. N. Ultrasensitive tumour-penetrating nanosensors of protease activity. *Nat Biomed Eng* **1**, doi:10.1038/s41551-017-0054 (2017).

259 Trang, V. H. *et al.* A coiled-coil masking domain for selective activation of therapeutic antibodies. *Nature Biotechnology* **37**, 761-765, doi:10.1038/s41587-019-0135-x (2019).

260 Puskas, J. *et al.* Development of an attenuated interleukin-2 fusion protein that can be activated by tumour-expressed proteases. *Immunology* **133**, 206-220, doi:10.1111/j.1365-2567.2011.03428.x (2011).

261 Autio, K. A., Boni, V., Humphrey, R. W. & Naing, A. Probody Therapeutics: An Emerging Class of Therapies Designed to Enhance On-Target Effects with Reduced Off-Tumor Toxicity for Use in Immuno-Oncology. *Clin Cancer Res* **26**, 984-989, doi:10.1158/1078-0432.Ccr-19-1457 (2020).

262 Williford, J.-M. *et al.* Recruitment of CD103+ dendritic cells via tumor-targeted chemokine delivery enhances efficacy of checkpoint inhibitor immunotherapy. *Science advances* **5**, eaay1357 (2019).

263 Ishihara, J. *et al.* Targeted antibody and cytokine cancer immunotherapies through collagen affinity. *Science translational medicine* **11** (2019).

264 Sasaki, K. *et al.* Engineered collagen-binding serum albumin as a drug conjugate carrier for cancer therapy. *Science advances* **5**, eaaw6081 (2019).

265 Ishihara, J. *et al.* Improving efficacy and safety of agonistic anti-CD40 antibody through extracellular matrix affinity. *Molecular cancer therapeutics* **17**, 2399-2411 (2018).

266 Melero, I., Castanon, E., Alvarez, M., Champiat, S. & Marabelle, A. Intratumoural administration and tumour tissue targeting of cancer immunotherapies. *Nature Reviews Clinical Oncology*, 1-19 (2021).

267 Tselikas, L. *et al.* Interventional radiology for local immunotherapy in oncology. *Clinical Cancer Research* **27**, 2698-2705 (2021).

268 Dudani, J. S., Warren, A. D. & Bhatia, S. N. Harnessing protease activity to improve cancer care. *Annual Review of Cancer Biology* **2**, 353-376 (2018).

269 Liu, C. & Gao, A. C. IFNγ, a Double-Edged Sword in Cancer Immunity and Metastasis. *Cancer Research* **79**, 1032-1033, doi:10.1158/0008-5472.Can-19-0083 (2019).